

**University of Alberta**

Experimental and Numerical Studies  
on Multiple Well Pairs SAGD Performance

by

**Xinkui Wang**

A thesis submitted to the Faculty of Graduate Studies and Research  
in partial fulfillment of the requirements for the degree of

**Master of Science**

in

Petroleum Engineering

Department of Civil and Environmental Engineering

©Xinkui Wang

Fall 2010

Edmonton, Alberta

Permission is hereby granted to the University of Alberta Libraries to reproduce single copies of this thesis and to lend or sell such copies for private, scholarly or scientific research purposes only. Where the thesis is converted to, or otherwise made available in digital form, the University of Alberta will advise potential users of the thesis of these terms.

The author reserves all other publication and other rights in association with the copyright in the thesis and, except as herein before provided, neither the thesis nor any substantial portion thereof may be printed or otherwise reproduced in any material form whatsoever without the author's prior written permission.

## **Examining Committee**

Dr. Rick Chalaturnyk, Department of Civil and Environment Engineering  
(Supervisor)

Dr. Haibo Huang, Alberta Research Council (part of Alberta Innovates –  
Technology Futures)  
(Co-Supervisor)

Dr. William McCaffrey, Department of Chemical Engineering

Dr. Alireza Nouri, Department of Civil and Environment Engineering

In Memory Of My Parents:

FuGuang Jiang

And

GenShou Wang

## **ABSTRACT**

A laboratory experiment and a numerical simulation of a dual well pair SAGD process with live bitumen were conducted to examine operating strategies on the recovery performance of a multiple well pair SAGD process.

The experiment was successfully carried out under such operation strategies as injecting steam into one well pair while producing from both producers after chambers mergence to sweep the oil between the two well pairs. The experimental results showed high oil recovery from the transition region between the two well pairs with these operation strategies. Numerical simulation matched reasonably well experimental results, which indicated that the numerical model captured the key mechanisms of the dual well pairs experiment. The improved SAGD process behaviour and performance was demonstrated in terms of faster oil production, enhanced solution gas production, and accelerated adjacent chambers communication in the experimental and numerical studies.

These operation strategies could be applied in the multiple well pairs SAGD and enhance SAGD performance after steam chambers merge between adjacent well pairs.

## **ACKNOWLEDGEMENTS**

I would like to express my sincere thanks to Professors Rick Chalaturnyk and Marcel Polikar for their supervision and guidance, and Dr. Haibo Huang for his coordination and co-supervision during my master's degree.

The financial support from the Alberta Research Council (now part of Alberta Innovates – Technology Futures) is gratefully acknowledged. I am also grateful to Dr. Doug Lillico, the Heavy Oil and Oil Sands Business Unit manager and AERI/ARC/Core/Industry Research (AACI) Program manager for granting permission to work on this project as part of the M.Sc. thesis study.

Special thanks go to Dr. Xiaohui Deng, the project leader, for his technical guidance specifically in the area of numerical simulation.

I am grateful for the technical assistance and support of my colleagues within the Heavy Oil and Oil Sands Business Unit of the Alberta research Council.

Last but not least, I would like to extend my love and appreciation to my wife Li Zhang, and my sons Jason RuoChen and Albert RuoYu for supporting me in every step of my thesis study and being so incredibly patient and understanding.

# TABLE OF CONTENTS

*ABSTRACT*

*ACKNOWLEDGEMENTS*

*TABLE OF CONTENTS*

*LIST OF TABLES*

*LIST OF FIGURES*

*LIST OF SYMBOLS AND ABBREVIATIONS*

<b>1</b>	<b><i>INTRODUCTION</i></b> .....	<b>1</b>
	1.1 Overview.....	1
	1.2 Statement of the Problem.....	2
	1.3 Research Objective.....	3
	1.4 Methodology and Scope of the Research.....	4
	1.5 Structure of the Thesis.....	4
<b>2</b>	<b><i>LITERATURE REVIEW</i></b> .....	<b>6</b>
	2.1 SAGD Process and Application.....	7
	2.2 Effect of Solution Gas on SAGD Performance.....	10
	2.3 Single Well Pair SAGD Performance Enhancement.....	11

2.3.1 Numerical Simulation Study.....	12
2.3.2 Experimental Observation .....	13
2.3.3 Field Observation.....	14
2.3.4 Integrated Studies: Non-Condensable Gas (NCG) Injection .....	14
<b>2.4 Multiple Well Pair Operating Strategy .....</b>	<b>17</b>
2.4.1 Numerical Simulation Study.....	18
2.4.2 Experimental Study on Dual Well Pair SAGD .....	19
2.4.3 Field Observation.....	19
2.4.4 Combination of Vertical and Horizontal Wells .....	20
<b>2.5 Summary .....</b>	<b>21</b>
<b>3    <i>EXPERIMENTAL DESIGN AND APPARATUS</i>.....</b>	<b>23</b>
<b>3.1 Experimental Objective .....</b>	<b>23</b>
<b>3.2 Experimental Design Criterion .....</b>	<b>23</b>
<b>3.3 Experimental Apparatus.....</b>	<b>26</b>
3.3.1 Dual Well Pair SAGD Test Model .....	26
3.3.2 Thermocouple Distribution.....	29
3.3.3 Pressure Transducer.....	31
3.3.4 Pressure Vessel .....	32
3.3.5 Production Station and Injection Station.....	34
3.3.6 Data Acquisition System.....	36
<b>3.4 Sand Pack Preparation .....</b>	<b>39</b>
<b>3.5 Leakage Test .....</b>	<b>41</b>
<b>3.6 Water Saturation .....</b>	<b>43</b>
<b>3.7 Live Oil Preparation.....</b>	<b>45</b>
<b>3.8 Live Oil Flooding .....</b>	<b>47</b>
<b>4    <i>EXPERIMENT</i> .....</b>	<b>48</b>
<b>4.1 Experimental Procedure .....</b>	<b>48</b>
<b>4.2 Steam Injection Rate .....</b>	<b>49</b>
<b>4.3 Production and Overburden Pressure.....</b>	<b>51</b>
<b>4.4 Liquid and Gas Production .....</b>	<b>51</b>

4.5 Chamber Temperature Reading .....	54
<b>5    RESULTS ANALYSIS AND DISCUSSION .....</b>	<b>57</b>
5.1 Production Pressure and Rate.....	57
5.2 Cumulative Production .....	61
5.3 Relationship between Steam Injection and Fluid Production .....	64
5.4 Steam Chamber Development.....	72
5.5 Residual Oil and Water Distribution.....	77
5.6 Well Production Behaviour .....	80
5.7 Steam Chamber Behaviour.....	80
5.8 Main Mechanisms in Dual Well Pair SAGD.....	82
5.9 Summary of Experimental Approach.....	84
<b>6    NUMERICAL SIMULATION .....</b>	<b>87</b>
6.1 Model Initialization .....	88
6.1.1 Grid Block .....	89
6.1.2 Initial Condition and Fluid Properties.....	90
6.1.3 Assumptions .....	94
6.2 Tuning Parameters.....	94
6.3 Numerical History Matching Results.....	97
6.4 Operating Strategy Analysis.....	105
6.4.1 Description of Operating Strategies.....	106
6.4.2 Comparison of Process Performance .....	106
6.4.3 Analysis and Discussion .....	109
6.5 Summary of Numerical Simulation Study .....	112
<b>7    SUMMARY.....</b>	<b>114</b>
<b>8    BIBLIOGRAPHY.....</b>	<b>117</b>

## LIST OF TABLES

TABLE 2-1	HEAVY OIL RESERVES AND PRODUCTION BY 2006 .....	6
TABLE 3-1	WELLS IN THE TEST CELL .....	28
TABLE 3-2	INITIAL CONDITION AND FLUID PROPERTIES .....	47
TABLE 4-1	EXPERIMENTAL SCHEME: OPERATING STRATEGIES .....	49
TABLE 6-1	WELL NAME AND LOCATION IN THE GRID .....	89
TABLE 6-2	INITIAL CONDITION IN EXPERIMENTAL AND NUMERICAL SIMULATION.....	90
TABLE 6-3	THERMAL CONDUCTIVITIES USED IN THE NUMERICAL MODEL .....	93
TABLE 6-4	FLUID PROPERTIES USED IN THE NUMERICAL MODEL .....	93
TABLE 6-5	STRATEGY STUDY - THREE CASES OF OPERATING STRATEGIES...	105

## LIST OF FIGURES

<b>FIGURE 2-1</b>	<b>VISCOSITIES AT DIFFERENT TEMPERATURE</b>	<b>7</b>
<b>FIGURE 2-2</b>	<b>SCHEMATIC OF SAGD PROCESS</b>	<b>8</b>
<b>FIGURE 2-3</b>	<b>STEAM CHAMBER GROWTH WITH OR WITHOUT SOLUTION GAS</b>	<b>11</b>
<b>FIGURE 2-4</b>	<b>MULTIPLE WELL PAIR SAGD</b>	<b>17</b>
<b>FIGURE 3-1</b>	<b>SCHEMATIC DRAWING OF EXPERIMENTAL CELL</b>	<b>27</b>
<b>FIGURE 3-2</b>	<b>TEST FACILITY: TEST CELL WITH TWO WELL PAIRS</b>	<b>27</b>
<b>FIGURE 3-3</b>	<b>INJECTOR/PRODUCTION WELL</b>	<b>28</b>
<b>FIGURE 3-4</b>	<b>TEST FACILITY: ONE PAIR OF WELL INCLUDING INJECTOR AND PRODUCTION WELLS IN THE TEST MODEL</b>	<b>29</b>
<b>FIGURE 3-5</b>	<b>SCHEMATIC DRAWING OF THERMOCOUPLES IN TEST CELL</b>	<b>30</b>
<b>FIGURE 3-6</b>	<b>TEST FACILITY: 15 THERMOCOUPLE RODS DISTRIBUTED IN THE TEST</b>	<b>30</b>
<b>FIGURE 3-7</b>	<b>NUMBER ORDER AND LOCATION OF THERMOCOUPLES IN TEST CELL</b>	<b>30</b>
<b>FIGURE 3-8</b>	<b>TEST FACILITY: A THERMOCOUPLE TO MEASURE OVERBURDEN TEMPERATURE</b>	<b>31</b>
<b>FIGURE 3-9</b>	<b>TEST FACILITY: PRESSURE TRANSDUCERS MOUNTED OUTSIDE OF THE PRESSURE VESSEL</b>	<b>32</b>
<b>FIGURE 3-10</b>	<b>TEST FACILITY: PRESSURE VESSEL AND SAFETY VALVE</b>	<b>33</b>
<b>FIGURE 3-11</b>	<b>TEST FACILITY: COMBINATION OF TWO PRESSURE VESSELS</b>	<b>33</b>
<b>FIGURE 3-12</b>	<b>TEST FACILITY: PRESSURE VESSEL AND 2D TEST CELL</b>	<b>34</b>
<b>FIGURE 3-13</b>	<b>TEST FACILITY: TWO PRODUCTION STATIONS</b>	<b>35</b>

<b>FIGURE 3-14</b>	<b>SCHEMATIC OF STEAM STATION: STEAM SUPPLYING AND CONTROLLING SYSTEM</b>	36
<b>FIGURE 3-15</b>	<b>SCHEMATIC OF FLOW PROCESS---DATA ACQUISITION AND CONTROL SYSTEM</b>	37
<b>FIGURE 3-16</b>	<b>SCHEMATIC OF DATA ACQUISITION AND CONTROL SYSTEM</b>	38
<b>FIGURE 3-17</b>	<b>OPERATOR INTERFACE OF DATA ACQUISITION USING PARAGON PROGRAM</b>	39
<b>FIGURE 3-18</b>	<b>TEST FACILITY: EMPTY TEST CELL BEFORE SAND PACKING</b>	40
<b>FIGURE 3-19</b>	<b>TEST CELL PACKED WITH US SILICA SAND: -20 TO +40 MESH FRACTIONS</b>	41
<b>FIGURE 3-20</b>	<b>LEAKAGE TEST ON THE TEST CELL PACKED WITH SANDS</b>	42
<b>FIGURE 3-21</b>	<b>TEST MODEL IN A WATER TANK FOR LEAKAGE</b>	42
<b>FIGURE 3-22</b>	<b>TEST MODEL IN THE PRESSURE VESSEL BEFORE THE VESSEL WAS BOLTED AND CLOSED</b>	43
<b>FIGURE 3-23</b>	<b>EXPERIMENTAL FACILITY: WATER SATURATION BY INJECTING WATER WITH A DBR CYLINDRICAL PISTON PUMP</b>	44
<b>FIGURE 3-24</b>	<b>WATER SATURATION BY INJECTING WATER FROM THE BOTTOM TO THE TOP OF THE MODEL</b>	44
<b>FIGURE 3-25</b>	<b>VISCOSITY OF DRY BURNT LAKE BITUMEN</b>	45
<b>FIGURE 3-26</b>	<b>60-L STEEL CYLINDRICAL CONTAINER USED TO SATURATE DRY BURNT LAKE BITUMEN WITH METHANE</b>	46
<b>FIGURE 3-27</b>	<b>ONE 5-L STEEL CYLINDRICAL CONTAINER WITH A PISTON ISOLATING LIVE OIL AND WATER</b>	46
<b>FIGURE 4-1</b>	<b>STEAM INJECTION RATES FOR DUAL SAGD WELL PAIRS</b>	50
<b>FIGURE 4-2</b>	<b>PRODUCTION PRESSURE AND OVERBURDEN PRESSURE</b>	50
<b>FIGURE 4-3</b>	<b>LIQUID PRODUCTION AT THE LEFT SIDE</b>	52
<b>FIGURE 4-4</b>	<b>GAS PRODUCTION AT THE LEFT SIDE</b>	52
<b>FIGURE 4-5</b>	<b>LIQUID PRODUCTION AT THE RIGHT SIDE</b>	53
<b>FIGURE 4-6</b>	<b>GAS PRODUCTION AT THE RIGHT SIDE</b>	53
<b>FIGURE 4-7</b>	<b>REAL TIME LOGGING TEMPERATURE READINGS AT THE 60<sup>TH</sup> MINUTE</b>	54
<b>FIGURE 4-8</b>	<b>REAL TIME LOGGING TEMPERATURE READINGS AT THE 120TH MINUTE</b>	54
<b>FIGURE 4-9</b>	<b>REAL TIME LOGGING TEMPERATURE READINGS AT THE 180TH MINUTE</b>	54

<b>FIGURE 4-10</b>	<b>REAL TIME LOGGING TEMPERATURE READINGS AT THE 240TH MINUTE</b>	55
<b>FIGURE 4-11</b>	<b>REAL TIME LOGGING TEMPERATURE READINGS AT THE 300TH MINUTE</b>	55
<b>FIGURE 4-12</b>	<b>REAL TIME LOGGING TEMPERATURE READINGS AT THE 360TH MINUTE</b>	55
<b>FIGURE 4-13</b>	<b>REAL TIME LOGGING TEMPERATURE READINGS AT THE 420TH MINUTE</b>	56
<b>FIGURE 4-14</b>	<b>REAL TIME LOGGING TEMPERATURE READINGS AT THE 480TH MINUTE</b>	56
<b>FIGURE 4-15</b>	<b>REAL TIME LOGGING TEMPERATURE READINGS AT THE 527TH MINUTE</b>	56
<b>FIGURE 5-1</b>	<b>PRODUCTION (OIL, WATER, AND GAS) RATE AT THE LEFT PRODUCER</b>	58
<b>FIGURE 5-2</b>	<b>PRODUCTION (OIL, WATER, AND GAS) RATE AT THE RIGHT PRODUCER</b>	58
<b>FIGURE 5-3</b>	<b>PRODUCTION PRESSURE AND DIFFERENTIAL PRESSURE BETWEEN TWO PRODUCERS</b>	59
<b>FIGURE 5-4</b>	<b>DIFFERENTIAL PRESSURE VERSUS LIQUID PRODUCTION RATE AT THE LEFT PRODUCER</b>	60
<b>FIGURE 5-5</b>	<b>DIFFERENTIAL PRESSURE VERSUS LIQUID PRODUCTION RATE AT THE RIGHT PRODUCER</b>	60
<b>FIGURE 5-6</b>	<b>OIL PRODUCTION RATES AT BOTH PRODUCERS</b>	61
<b>FIGURE 5-7</b>	<b>CUMULATIVE OIL PRODUCTION OF BOTH PRODUCERS</b>	62
<b>FIGURE 5-8</b>	<b>OIL RECOVERY OF BOTH PRODUCERS</b>	62
<b>FIGURE 5-9</b>	<b>CUMULATIVE WATER PRODUCTION OF BOTH PRODUCERS</b>	63
<b>FIGURE 5-10</b>	<b>CUMULATIVE GAS PRODUCTION OF BOTH PRODUCERS</b>	64
<b>FIGURE 5-11</b>	<b>COMPARISON OF CUMULATIVE STEAM INJECTION AND WATER PRODUCTION AT THE LEFT PRODUCER</b>	65
<b>FIGURE 5-12</b>	<b>COMPARISON OF STEAM INJECTION RATE AND WATER PRODUCTION RATE AT THE LEFT PRODUCER</b>	66
<b>FIGURE 5-13</b>	<b>COMPARISON OF CUMULATIVE STEAM INJECTION AND CUMULATIVE WATER PRODUCTION AT RIGHT SIDE</b>	66
<b>FIGURE 5-14</b>	<b>COMPARISON OF STEAM INJECTION RATE AND WATER PRODUCTION RATE AT THE RIGHT PRODUCER</b>	67
<b>FIGURE 5-15</b>	<b>COMPARISON OF CUMULATIVE STEAM INJECTION AND CUMULATIVE WATER PRODUCTION IN TOTAL</b>	67

<b>FIGURE 5-16</b>	<b>COMPARISON OF STEAM INJECTION RATE AND WATER PRODUCTION RATE IN TOTAL</b>	68
<b>FIGURE 5-17</b>	<b>COMPARISON OF CUMULATIVE STEAM INJECTION AND CUMULATIVE OIL PRODUCTION AT THE LEFT PRODUCER</b>	68
<b>FIGURE 5-18</b>	<b>COMPARISON OF STEAM INJECTION RATE AND OIL PRODUCTION RATE AT THE LEFT PRODUCER</b>	69
<b>FIGURE 5-19</b>	<b>COMPARISON OF CUMULATIVE STEAM INJECTION AND CUMULATIVE OIL PRODUCTION AT THE RIGHT PRODUCER</b>	69
<b>FIGURE 5-20</b>	<b>COMPARISON OF STEAM INJECTION RATE AND OIL PRODUCTION RATE AT THE RIGHT PRODUCER</b>	70
<b>FIGURE 5-21</b>	<b>COMPARISON OF CUMULATIVE STEAM INJECTION AND CUMULATIVE OIL PRODUCTION IN TOTAL</b>	70
<b>FIGURE 5-22</b>	<b>COMPARISON OF STEAM INJECTION RATE AND OIL PRODUCTION RATE IN TOTAL</b>	71
<b>FIGURE 5-23</b>	<b>SOR (STEAM TO OIL RATIO) PROFILE IN TOTAL</b>	71
<b>FIGURE 5-24</b>	<b>CSOR (CUMULATIVE STEAM TO OIL RATIO) PROFILE IN TOTAL</b>	72
<b>FIGURE 5-25</b>	<b>TEMPERATURE CONTOUR PROFILE AT THE 30<sup>TH</sup> MINUTE</b>	73
<b>FIGURE 5-26</b>	<b>TEMPERATURE CONTOUR PROFILE AT THE 60<sup>TH</sup> MINUTE</b>	73
<b>FIGURE 5-27</b>	<b>TEMPERATURE CONTOUR PROFILE AT THE 90<sup>TH</sup> MINUTE</b>	73
<b>FIGURE 5-28</b>	<b>TEMPERATURE CONTOUR PROFILE AT THE 120<sup>TH</sup> MINUTE</b>	73
<b>FIGURE 5-29</b>	<b>TEMPERATURE CONTOUR PROFILE AT THE 150<sup>TH</sup> MINUTE</b>	74
<b>FIGURE 5-30</b>	<b>TEMPERATURE CONTOUR PROFILE AT THE 180<sup>TH</sup> MINUTE</b>	74
<b>FIGURE 5-31</b>	<b>TEMPERATURE CONTOUR PROFILE AT THE 210<sup>TH</sup> MINUTE</b>	74
<b>FIGURE 5-32</b>	<b>TEMPERATURE CONTOUR PROFILE AT THE 240<sup>TH</sup> MINUTE</b>	74
<b>FIGURE 5-33</b>	<b>TEMPERATURE CONTOUR PROFILE AT THE 270<sup>TH</sup> MINUTE</b>	75
<b>FIGURE 5-34</b>	<b>TEMPERATURE CONTOUR PROFILE AT THE 300<sup>TH</sup> MINUTE</b>	75
<b>FIGURE 5-35</b>	<b>TEMPERATURE CONTOUR PROFILE AT THE 330<sup>TH</sup> MINUTE</b>	75
<b>FIGURE 5-36</b>	<b>TEMPERATURE CONTOUR PROFILE AT THE 360<sup>TH</sup> MINUTE</b>	75
<b>FIGURE 5-37</b>	<b>TEMPERATURE CONTOUR PROFILE AT THE 390<sup>TH</sup> MINUTE</b>	76
<b>FIGURE 5-38</b>	<b>TEMPERATURE CONTOUR PROFILE AT THE 420<sup>TH</sup> MINUTE</b>	76
<b>FIGURE 5-39</b>	<b>TEMPERATURE CONTOUR PROFILE AT THE 450<sup>TH</sup> MINUTE</b>	76
<b>FIGURE 5-40</b>	<b>TEMPERATURE CONTOUR PROFILE AT THE 480<sup>TH</sup> MINUTE</b>	76
<b>FIGURE 5-41</b>	<b>TEMPERATURE CONTOUR PROFILE AT THE 510<sup>TH</sup> MINUTE</b>	77
<b>FIGURE 5-42</b>	<b>TEMPERATURE CONTOUR PROFILE AT THE 527<sup>TH</sup> MINUTE</b>	77
<b>FIGURE 5-43</b>	<b>TEST MODEL AFTER THE TOP LID WAS CUT OPEN</b>	77
<b>FIGURE 5-44</b>	<b>LEFT HALF PORTION OF THE TOP LAYER OF TEST MODEL</b>	78

<b>FIGURE 5-45</b>	<b>THIRD LAYER OF THE TEST MODEL AFTER THE SECOND ONE WAS SAMPLED</b>	78
<b>FIGURE 5-46</b>	<b>THE OIL SAND REMAINED NEAR THE LEFT PAIR WELLS AT THE BOTTOM LAYER OF THE TEST MODEL</b>	78
<b>FIGURE 5-47</b>	<b>RESIDUAL OIL SATURATION (%) OF THE TEST CELL</b>	79
<b>FIGURE 5-48</b>	<b>RESIDUAL WATER SATURATION (%) OF THE TEST CELL</b>	79
<b>FIGURE 6-1</b>	<b>GRID BLOCK SETTING IN THE NUMERICAL SIMULATION</b>	89
<b>FIGURE 6-2</b>	<b>OIL VISCOSITIES VERUS TEMPERATURE</b>	91
<b>FIGURE 6-3</b>	<b>WATER AND OIL RELATIVE PERMEABILITY FOR NUMERICAL SIMULATION</b>	92
<b>FIGURE 6-4</b>	<b>GAS-OIL RELATIVE PERMEABILITY FOR NUMERICAL SIMULATION</b>	92
<b>FIGURE 6-5</b>	<b>CUMULATIVE STEAM INJECTION IN THE EXPERIMENT AND NUMERICAL SIMULATION</b>	95
<b>FIGURE 6-6</b>	<b>BOTTOM HOLE PRESSURES IN THE LEFT SIDE OF THE EXPERIMENT AND NUMERICAL SIMULATION</b>	96
<b>FIGURE 6-7</b>	<b>BOTTOM HOLE PRESSURES IN THE RIGHT SIDE OF THE EXPERIMENT AND NUMERICAL SIMULATION</b>	96
<b>FIGURE 6-8</b>	<b>ABIENT TEMPEARTURE IN THE EXPERIMENT AND NUMERICAL SIMULATION</b>	97
<b>FIGURE 6-9</b>	<b>SIMULATION RESULT: COMPARISON OF CUMULATIVE OIL PRODUCTION IN THE EXPERIMENT AND NUMERICAL SIMULATION</b>	98
<b>FIGURE 6-10</b>	<b>SIMULATION RESULT: COMPARISON OF CUMULATIVE WATER PRODUCTION IN THE EXPERIMENT AND NUMERICAL SIMULATION</b>	98
<b>FIGURE 6-11</b>	<b>SIMULATION RESULT: COMPARISON OF CUMULATIVE GAS PRODUCTION IN THE EXPERIMENT AND NUMERICAL SIMULATION</b>	99
<b>FIGURE 6-12</b>	<b>SIMULATION RESULT: COMPARISON OF STEAM CHAMBER IN THE EXPERIMENT (TOP) AND NUMERICAL SIMULATION (BOTTOM) AT THE 60<sup>TH</sup> MINUTE</b>	100
<b>FIGURE 6-13</b>	<b>SIMULATION RESULT: COMPARISON OF STEAM CHAMBER IN THE EXPERIMENT (TOP) AND NUMERICAL SIMULATION (BOTTOM) AT THE 120<sup>TH</sup> MINUTE</b>	100

<b>FIGURE 6-14</b>	<b>SIMULATION RESULT: COMPARISON OF STEAM CHAMBER IN THE EXPERIMENT (TOP) AND NUMERICAL SIMULATION (BOTTOM) AT THE 180<sup>TH</sup> MINUTE</b>	101
<b>FIGURE 6-15</b>	<b>SIMULATION RESULT: COMPARISON OF STEAM CHAMBER IN THE EXPERIMENT (TOP) AND NUMERICAL SIMULATION (BOTTOM) AT THE 240<sup>TH</sup> MINUTE</b>	101
<b>FIGURE 6-16</b>	<b>SIMULATION RESULT: COMPARISON OF STEAM CHAMBER IN THE EXPERIMENT (TOP) AND NUMERICAL SIMULATION (BOTTOM) AT THE 300<sup>TH</sup> MINUTE</b>	102
<b>FIGURE 6-17</b>	<b>SIMULATION RESULT: COMPARISON OF STEAM CHAMBER IN THE EXPERIMENT (TOP) AND NUMERICAL SIMULATION (BOTTOM) AT THE 360<sup>TH</sup> MINUTE</b>	102
<b>FIGURE 6-18</b>	<b>SIMULATION RESULT: COMPARISON OF STEAM CHAMBER IN THE EXPERIMENT (TOP) AND NUMERICAL SIMULATION (BOTTOM) AT THE 420<sup>TH</sup> MINUTE</b>	103
<b>FIGURE 6-19</b>	<b>SIMULATION RESULT: COMPARISON OF STEAM CHAMBER IN THE EXPERIMENT (TOP) AND NUMERICAL SIMULATION (BOTTOM) AT THE 480<sup>TH</sup> MINUTE</b>	103
<b>FIGURE 6-20</b>	<b>SIMULATION RESULT: COMPARISON OF STEAM CHAMBER IN THE EXPERIMENT (TOP) AND NUMERICAL SIMULATION (BOTTOM) AT THE 527<sup>TH</sup> MINUTE</b>	104
<b>FIGURE 6-21</b>	<b>SIMULATION RESULT: COMPARISON OF CUMULATIVE OIL PRODUCTION BASED ON NUMERICAL MODEL</b>	107
<b>FIGURE 6-22</b>	<b>SIMULATION RESULT: COMPARISON OF CUMULATIVE GAS PRODUCTION BASED ON NUMERICAL MODEL</b>	108
<b>FIGURE 6-23</b>	<b>SIMULATION RESULT: COMPARISON OF CUMULATIVE STEAM INJECTION</b>	109
<b>FIGURE 6-24</b>	<b>COMPARISON OF EMERGING STEAM CHAMBERS AT THE 270<sup>TH</sup> MINUTE OF RUNING TIME</b>	110
<b>FIGURE 6-25</b>	<b>TOP: STEAM CHAMBER AT THE 270TH MINUTE IN CASE C; BOTTOM: GAS SATURATION PROFILE AT THE 270TH MINUTE IN CASE C</b>	111

## LIST OF SYMBOLS AND ABBREVIATIONS

A=	Cross-Sectional Area, $m^2$ .
$\alpha$ =	Thermal Diffusivity, $m^2/day$ .
$B_3$ =	Dimensionless Numbers Used in Gravity Drainage Theory.
$g$ =	Acceleration due to Gravity, $9.80665 m/s^2$ .
$h$ =	Net Pay of Reservoir or Lab Model, $m$ .
$k_H$ =	Horizontal Permeability of the Medium, <i>Darcy</i> .
$k_V$ =	Vertical Permeability of the Medium, <i>Darcy</i> .
$\frac{k_H}{k_V}$ =	Ratio of Horizontal Permeability to Vertical Permeability.
L=	Length of Reservoir or Lab Model, $m$ .
$m$ =	Dimensionless Parameter Used in Gravity Drainage Theory, Which Depends on Oil Viscosity and Temperature Curve $T_R$ and
	$T_S; m = \left[ v_s \int_{T_R}^{T_S} \left( \frac{1}{v} - \frac{1}{v_R} \right) \frac{dT}{T - T_R} \right]^{-1} .$
$\rho$ =	Fluid's Density, $gram/cm^3$ .
$\Delta P$ =	Differential Pressure, $kPa$ .
q=	Fluid Flow Rate, $m^3/s$ .

$\phi$	=	Porosity of the Medium, %.
$S_{or}$	=	Residual Oil Saturation, %.
$S_o$	=	Oil Saturation, %.
$S_{oi}$	=	Initial Oil Saturation, %.
$\Delta S_o$	=	$S_o - S_{or}$ .
$S_w$	=	Water Saturation, %.
$S_{wi}$	=	Initial Water Saturation, %.
$t^*$	=	Dimensionless Times Used in Gravity Drainage Theory.
$T_R$	=	Reservoir Temperature, °C.
$T_S$	=	Steam Temperature, °C.
$V$	=	Bulk Volume, $cm^3$ .
$\nu_R$	=	Kinematic Viscosity of Oil at Reservoir Temperature, $m^2/s$ .
$\nu_S$	=	Kinematic Viscosity of Oil at Steam Temperature, $m^2/s$ .
$w$	=	Half Inter-well Distance, $m$ .
DP	=	Differential Pressure, $kPa$ .
OOIP	=	Initial Oil in Place, $grams$ .
GOR	=	Gas Oil Ratio, $std\ m^3/m^3$ .
RF	=	Recovery Factor, %.
SOR	=	Steam Oil Ratio.

# 1 INTRODUCTION

## *1.1 Overview*

With the growing global demand for energy, oil production from the declining conventional crude oil resources can not meet current and future energy requirements. The high price of crude oil makes deposits of heavy oil, especially bitumen resources, economically attractive to oil producers.

Canada owns the world's largest crude bitumen resource, and the quantity of bitumen reserves is comparable to the conventional oil resource in the Middle East. The heavy oil and bitumen deposits are all almost entirely located in the province of Alberta, where the Athabasca deposit possesses the majority of the initial crude bitumen in place. In a small part of the Athabasca deposit around Fort McMurray, the oil sands reservoirs have a shallow overburden depth of only 40 to 75 meters, which is suitable for mining and extraction. Open pit surface mining operations cause significant landscape disruption, including tailings treatment and clay and sands disposal issues with severe environmental damage concerns. The bitumen in deposits at great depths has to be recovered by underground or in-situ recovery methods.

In the last few decades, numerous in-situ technologies have been developed and applied in heavy oil and bitumen recovery. In-situ bitumen recovery methods could be categorized into four groups: cold production, thermal recovery, solvent based recovery, and hybrid processes. In the relatively thin net pay zone with low viscous heavy oil, cold

production is one feasible and economic way to recover heavy oil. However, the tremendously viscous bitumen can not flow at the drawdown pressure under reservoir condition unless extra energy is applied to enhance its mobility. The thermal recovery methods include Steam Flooding (SF), Cyclic Steam Stimulation (CSS), Steam Assisted Gravity Drainage (SAGD), combustion, and Toe-To-Heel Air Injection (THAI), of which CSS and SAGD dominate heavy oil and bitumen recovery in Alberta. Hybrid processes consist of Extended Solvent SAGD (ES-SAGD), or thermal solvent, or SAGD with Non-Condensable Gas (NCG) injection. Vapour Extraction (VAPEX) is one of the non-thermals and solvent-based recovery processes which is still being developed for potential commercial application.

The CSS process has considerable environmental and technical advantages over the cold production technology for recovering bitumen in terms of relatively high recovery factor and little or no cost for sand disposal. However, a 20% - 25% recovery factor from CSS is not considered satisfactory for oil producers. Also, the requirement of steam injection with high temperature and high pressure limits its application in the area of heavy oil and bitumen recovery.

The SAGD process is a more effective recovery process for heavy oil and bitumen. It involves one pair of parallel horizontal wells drilled in the formation, which are spaced vertically a short distance apart. The concept of SAGD with a single well pair of injector and producer has been studied extensively in the past. To cover a large reservoir area, multiple well pairs are drilled and operated in today's commercial projects.

## ***1.2 Statement of the Problem***

The performance enhancement of oil recovery is of utmost practical importance in petroleum engineering. Optimization of steam injection rate in the SAGD operation for maximizing wellbore productivity is of utmost importance to the economic health of the project. The operation of multiple well pairs can not only reduce the capital and operation cost, but also can achieve systematic drainage of the reservoir and thus obtain the best investment return. One single well pair SAGD process has been well examined in the last decade, in which produced some practical techniques

achieving promising SAGD process performance and behavior. However, these strategic concepts and numerical simulations were conducted on single well pair SAGD operation and limited the potential effectiveness of such operating strategies for a commercial SAGD project with multiple well pairs/pads.

There are several significant issues emerging from the application of multiple well pairs. One issue is the employing of appropriate operating strategies to maximize and accelerate the overall production from each individual well pair in multiple well pairs' projects. The second issue is the recovery of oil from the areas between adjacent well pairs. The third one is the role of the solution gas on oil recovery in the reservoir. These issues are associated with the impact of the interfering steam chambers on the process performance in the transition area among well pairs. However, the impact of the interference from adjacent chambers on the SAGD performance may be more complicated than expected. SAGD performance can not be simply analyzed based on single well pair performance only, and can not be considered to be a summation of the production from all the single well pairs. It is, therefore, necessary to understand the operating mechanisms of the multiple well pair SAGD process.

Experimental runs with live heavy oil to examine the effects of solution gas on the dual well pair SAGD process are essential for multiple well pair SAGD operation strategies. The process mechanisms and performance related to multiple well pairs need to be proven and validated from scaled physical model experiments and field practices.

### ***1.3 Research Objective***

The objective of this project is to understand the mechanisms involved in the multiple well pair SAGD process and thus develop operating strategies to improve SAGD performance. Better understanding of the mechanisms of heavy oil recovery using multiple well pairs in the SAGD operation is a step towards maximizing productivity with a minimum level of steam injection and a minimum number of infill wells drilled. This study intends to produce qualitative fundamentals, and hence make a contribution to the development of a numerical model by which the process performance can be examined to explore appropriate operating strategies for multiple well pairs SAGD.

## ***1.4 Methodology and Scope of the Research***

Three or more well pairs are ideal to examine the impact of the interfering steam chambers on SAGD performance. To simplify this complicated problem and reduce cost of the research, experimental study of dual well pair SAGD has been considered to investigate the conceptual strategy.

In this study, laboratory models were designed to be able to simulate the gravity drainage and lateral drive mechanisms during thermal recovery operations. This model and experimental results provided sufficient data on the oil, water and gas production rates resulting from the injection pattern. Other data obtained were the steam injection rates, chamber growth pattern, and the profiles of residual oil and water saturations. The study intended to produce qualitative fundamentals to verify a numerical model for demonstrating SAGD process performance under different operating schemes.

This study focuses on experimental investigations to evaluate conceptual strategies with dual well pair SAGD operation using live oil. Numerical simulation study including history match of the experiment was also conducted using CMG's STARS thermal simulator. SAGD process, which were operated in different performance can be examined and compared with the verified numerical model.

## ***1.5 Structure of the Thesis***

This thesis consists of eight sections beginning with the Introduction. Section 2 is followed by a comprehensive literature review covering the description of the SAGD process and its applications. After the role of solution gas on the recovery performance of the SAGD process is reviewed, major developments and efforts aimed at improving the performance of SAGD operation are integrated into the discussion. Section 3 focuses on the description of the experimental design and preparation. The experimental apparatus will be introduced in this section. Section 4 presents the experimental procedure and displays the experimental raw data including the profiles of steam injected,

production pressure, fluid production and temperature at different stages. The analysis and explanation on experiment will be provided in section 5. Section 6 then presents the numerical simulation and results. Comparison of several operating strategies, and discussion related to the simulation will be covered in this section as well. Section 7 summarizes the experimental and numerical simulation results. The thesis ends with Section 8 which presents all references cited in the study.

## 2 LITERATURE REVIEW

Heavy oil and bitumen resources are mainly distributed in the countries of Canada, Venezuela, USA and China. [Table 2-1](#) shows the heavy oil and bitumen resources distribution in detail. Canada possesses the world’s largest crude bitumen deposits, which are almost entirely located in three major oil sands areas: Athabasca, Cold Lake, and Peace River in the province of Alberta.

**TABLE 2-1 HEAVY OIL RESERVES AND PRODUCTION BY 2006**

Countries	Venezuela	China	USA	Canada
<b>Heavy oil &amp; Oil Sands Reserves, 10<sup>9</sup>m<sup>3</sup></b> <b>(10<sup>9</sup> bbl)</b>	47.7 (300)	1.3 (8)	3.2 (20)	270.3 (1700)
<b>Heavy Oil Production, 10<sup>3</sup>m<sup>3</sup>/day</b> <b>( 10<sup>3</sup>bbl/day)</b>	95.4 (600)	23.8 (150)		199 (1250)

(Source: [Bagci et al. 2008](#), [AEUB 2007](#))

Bitumen possesses an extremely high viscosity value at reservoir condition. [Figure 2-1](#) shows that the Athabasca-type bitumen has the greatest viscosity among these three types of heavy oil and bitumen. The average viscosity of the Athabasca-type bitumen ranges from 17,000 to 265,000 centipoises @24 °C, while the Cold Lake and Peace River bitumen have a lower average viscosity ([Sadler et al. 2005](#)). The extremely viscous nature of the bitumen prevents it from flowing under normal reservoir conditions and generally does not respond to primary production and water flooding. However, the

viscosities of all bitumen are very sensitive to temperature. Viscosities decrease dramatically as the temperature increases (Puttagunta et al. 1993).

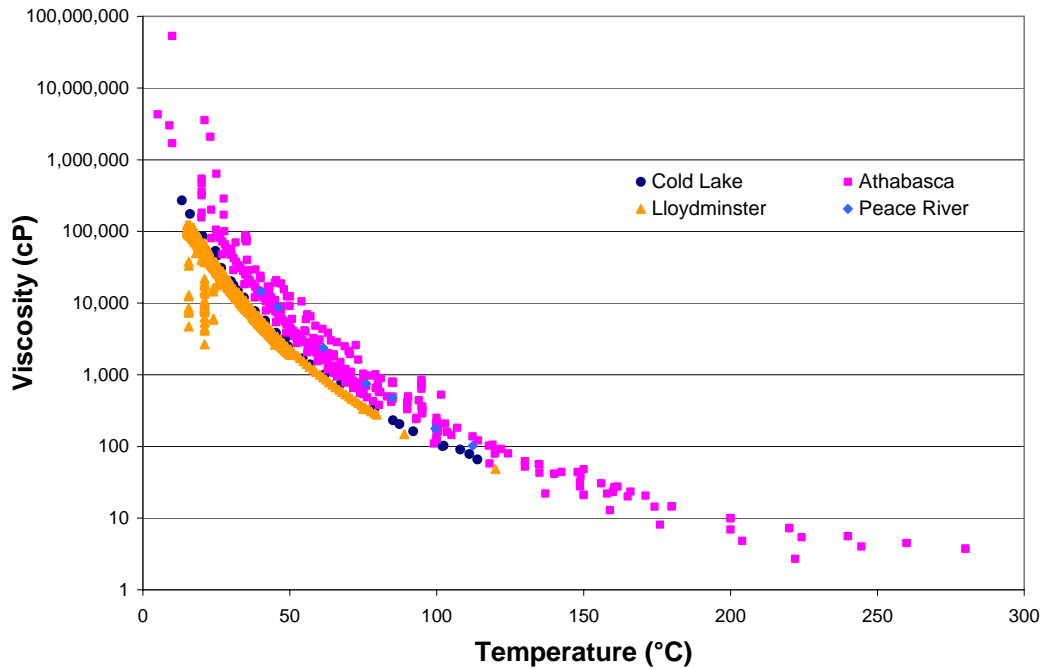


**FIGURE 2-1 VISCOSITIES AT DIFFERENT TEMPERATURE**  
(Reproduced after Puttagunta et al. 1993)

## 2.1 SAGD Process and Application

As the viscous bitumen can barely flow under reservoir conditions, the bitumen viscosity must be reduced and then a sufficient drive must be applied to the mobilized bitumen for continuous well production and in-situ recovery. Thermal recovery involving injecting hot fluids such as water and steam into the reservoir has been used for several decades to reduce viscosity and enhance the mobility of the bitumen in place.

The force of gravity, which exists universally, can be utilized to drive mobilized bitumen. Cardwell and Parson (1949) presented a strict gravity drainage theory early in 1949. Dykstra (1978) broadened the application of Cardwell and Parsons' previous prediction method and developed it under free-fall gravity drainage. However, Farouq-Ali (1997) considered Doscher as the first to recognize the role of gravity in the steam injection process for the California-type reservoir.

The gravity drainage mechanism had been initially used to produce conventional oil. However, because of low effective permeability, high oil viscosity, and small dip of the formation, most heavy oil and bitumen reservoirs can not apply gravity drainage alone to produce economically. [Butler et al. \(1981\), \(2001\)](#) initially proposed the concept of steam assisted gravity drainage (SAGD) in late 1978. Beginning in 1979, Butler applied this concept to in-situ thermal processes for heavy oil and bitumen recovery. He and his former colleagues carried out field tests in Imperial Oil's pioneering pilot at Cold Lake in 1980, which featured one of the first horizontal wells with vertical injectors in the industry. Imperial Oil developed and patented the SAGD recovery process in 1982 ([Butler 1982](#)). In the early concept of SAGD, the well configurations were all based on vertical wells and horizontal fracture ([Donnelly 1998](#)). Although there are still some SAGD implementations combining vertical injectors with horizontal producers today, configurations with dual horizontal well SAGD are more common ([Edmunds et al. 1995](#)). [Edmunds et al. \(1989\)](#) developed this original process as a more systematic technique for bitumen recovery and patented today's SAGD process in 1989. The Alberta Science and Research Authority currently owns this patent.

As [Figure 2-2](#) illustrates, the steam is injected through the upper well and the fluids, including the condensed steam and the crude oil or bitumen, are produced from the lower one. The injected steam heats the bitumen and sands in the reservoir, and reduces the viscosity of the bitumen. The condensed steam and bitumen flow towards the horizontal well and are recovered at the surface by artificial lift or gas lift.

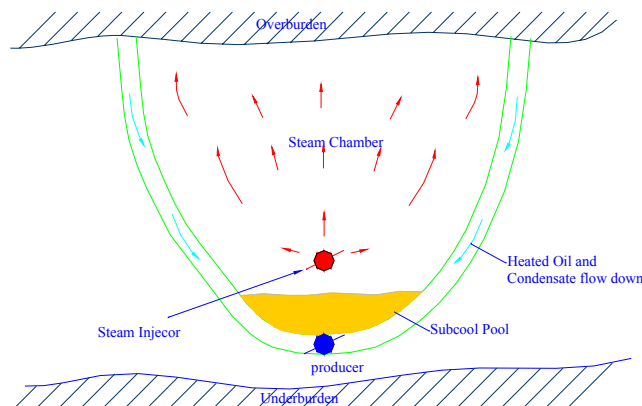


**FIGURE 2-2 SCHEMATIC OF SAGD PROCESS**

It is commonly agreed that a steam chamber is generated and rises upwards steadily during a SAGD operation. When it touches the top of the formation, it spreads towards both sides gradually. The steam chamber's growth is mainly measured and analyzed through the temperature changes at observation wells.

In order to validate the concept of SAGD, the project UTF Phase A was initiated by the Alberta Oil Sands Technology and Research Authority (AOSTRA) in 1984 at Fort McMurray (O'Rourke 1997). The AOSTRA and nine industry partners funded and participated in this UTF project. The test consisted of three pairs of 60 m long horizontal injectors and producers, which were drilled from a tunnel. The steam injection well was placed 5 m above the producing well which was located 1-2 m above the limestone under-burden. This was the first successful field demonstration of the SAGD process and it provided sufficient data to guide the commercial application.

The SAGD process at the AOSTRA UTF had proven that the process mechanisms worked in the field as expected. The horizontal wells in Phase A were placed on production in 1988 (Birrell et al. 2003). Following the success of the UTF Phase A, Phases B, D, and E were carried out in the 1990s (O'Rourke 1997, Nasr et al. 1998). The test of Phase B was close to commercial dimensions (Mukherjee et al. 1995), and the main objectives of Phase B were to demonstrate that the encouraging Phase A productivities could be scaled up in proportion to the length of the wells, and could be sustained for a producing life proportional to the pattern spacing.

The successful application of UTF A and B encouraged oil operators to apply this thermal recovery to Athabasca bitumen. Since then, SAGD technology for heavy oil and bitumen recovery has been applied in full-scale commercial operations in Alberta and Saskatchewan, such as Christina Lake by EnCana, Firebag by Suncor, MacKay River by Petro-Canada, Mic Mac and Burnt Lake by CNRL, and Long Lake by OPTI Canada (Butler 2001).

Attempts to apply the SAGD process in different types of reservoirs have been made in the last decade. This technology has been widely evaluated through numerical simulations and field tested in some other countries (Asquez et al. 1999, Sedae 2006, Albahlani et al. 2008, Hang et al. 2006).

## ***2.2 Effect of Solution Gas on SAGD Performance***

Many SAGD projects in Canada have produced promising results and performed according to expectations. SAGD operation performance is directly tied to a number of parametrical factors: natural conditions such as formation characteristics and reserve quality, and imposed conditions such as well configuration, initialization strategies, and operational strategies.

Solution gas, one of naturally parametrical factors in reservoir formations, plays an active role and generates significant impact on the performance of the SAGD process. When the production pressure declines below the saturation pressure, solution gas starts to appear in terms of gaseous status in the reservoir. Also, solution gas will exsolve from live oil when the temperature in the reservoir rises over the saturation temperature due to steam injection. The immigrating trend of the dissolved gas is one big issue to bitumen recovery. Scaled model experiments and numerical simulations (Yuan et al. 2006) indicated that the solution gas tended to accumulate in the steam front in the SAGD process. Yee et al. (2004) observed and measured for the first time a significant amount of gas that traveled ahead of the apparent top of the steam chamber.

Therefore, the presence of non-condensable gas would impede steam chamber expansion and reduce oil production in the SAGD operation. The impact of solution gas on the SAGD operation was that the oil sands with a lower GOR were likely to be recovered more easily than those with a higher GOR. Ito et al. (2005)'s simulation study showed that steam chambers had greater height for dead oil than those for live oil with solution gas (see Figure 2-3).

However, field evidence in North Tangleflags operated by Sceptre Resources (now CNRL), indicated a higher initial GOR of 11 std. m<sup>3</sup>/m<sup>3</sup> did not show a negative impact on the SAGD operation when compared with classic Athabasca reservoirs that had a GOR of 1-3 std. m<sup>3</sup>/m<sup>3</sup>. Yee et al. (2004) and Kisman et al. (1995) advised that the presence of a moderate amount of solution gas should be beneficial to the recovery process.

There were several other publications (Bharatha et al. 2005, Canbolat et al. 2004, Gates et al. 2005) discussing the effect of non-condensable gas on SAGD performance.

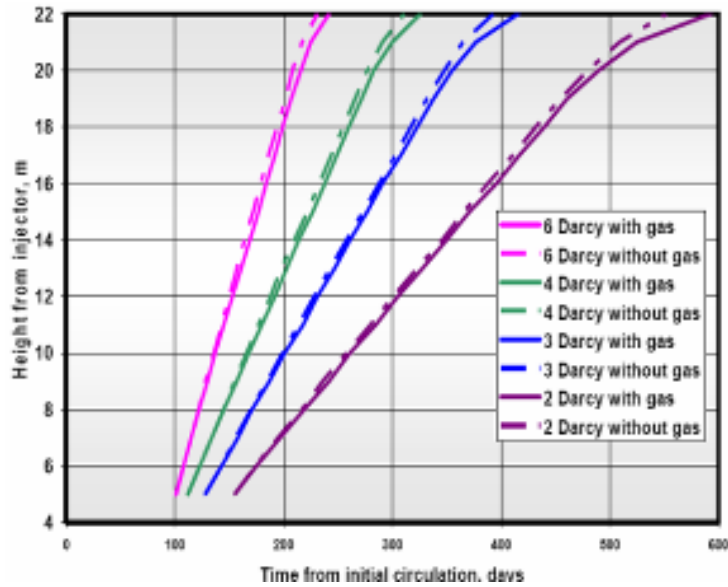


**FIGURE 2-3 STEAM CHAMBER GROWTH WITH OR WITHOUT SOLUTION GAS**

(After: Ito et al. 2005)

### ***2.3 Single Well Pair SAGD Performance Enhancement***

Butler (1991) developed the flow equations and analytical models to predict production by the SAGD process. The key variables were the steam chamber height, oil viscosity at steam condition, oil saturation, and oil rate. In practice, the initial production was usually estimated using Butler's analytical model and reservoir simulation. It was reported that the theoretical prediction agreed well with the homogenous reservoirs and model experiments (Yang et al. 1992) and real production (Birrell et al. 2005, Saltuklaroglu et al. 2003).

Some assumptions were made in Butler's (1981) analytical models. Heat was assumed to transfer beyond the interface by thermal conduction, and the interface was assumed to be at steam temperature. The total drainage flow was obtained using Darcy's equation and gravity driving force. One end of the interface curve remained attached to the production

well and the other end spread to a vertical no-flow boundary located half way to the next adjacent wells, which indicated no interfering relation among steam chambers from neighbour well pairs.

In order to enhance operation performance and reduce the high cost associated with drilling and completion of two horizontal wells, industry has sought alternatives since the first SAGD field trial. Based on literature, most efforts were focused on the adjustment of the SAGD well configurations. Some others were trying to utilize the heat remaining in the reservoir to improve SAGD performance.

There are two methods reported in public literature related to SAGD enhancement. One is to employ specific operation schemes with a classic dual well. Another is to apply differential pressure on the wells. Two types of differential pressure (DP) occurring in the SAGD operation include the DP between the injector and producer, and the DP between pairs of SAGD wells.

### **2.3.1 Numerical Simulation Study**

SAGD performance is associated with operational conditions, which can be optimized through running numerical simulation to enhance performance in terms of oil production rate, steam-oil ratio (SOR), and cumulative steam-oil ratio (cSOR). Numerical simulation indicated that the cSOR decreased with increasing injection rate ([Shin et al. 2007](#)).

Operational optimization can be obtained through adjusting the steam injection rate and the producer liquid withdrawal rate during different SAGD operation periods. [Yang et al. \(2007\)](#) presented an example to quantitatively assess the uncertainty of its economic forecast on a real field case from application of experimental design to response surface generation. The results showed that the economics of this project were improved considerably through optimization. The optimum operating conditions obtained use a high initial steam rate and high production rate to develop the steam chamber. After the instantaneous steam-oil ratio reaches a certain value, both steam rate and production rate are lowered to prevent steam breakthrough to the bottom water.

In the classic SAGD, the steam is injected continuously through the injection well. There is considerable energy existing in terms of higher temperature even when steam injection is shut in after operation for some time. The steam chamber will continue to spread for a while. To efficiently utilize the existing heat in the reservoir, the concept of seasonal or cyclic exploitation was proposed for energy saving and seasonal adjustment (Birrel et al 2005). This operational strategy indicated that the oil production could be controlled through the amount of injected steam. Based on the bitumen and gas prices, the operational strategy could be adapted to gain optimal return.

Based on a numerical simulation, Vanegas et al. (2005) suggested that higher differential pressure (DP) induced higher oil flow rate peaks especially in warm regions. A preferential flow path between the wells should have been avoided when DP was applied to the SAGD operation. This indicated that too large a DP would be detrimental to the operation.

### **2.3.2 Experimental Observation**

Sasaki et al. (1998) conducted scaled physical simulations to study an enhanced SAGD process by adding intermittent steam-stimulation on the lower horizontal production-well (SAGD-Isslw) for heavy oil recovery by video and infrared visualization techniques. The new process used a lower horizontal well with both functions of intermittent steam injection and continuous oil production instead of the usual SAGD production well. However, as in usual SAGD, the steam was also injected continuously through the upper well. The benefits of the new concept were quick build up of a warm steam chamber and a higher oil production rate. The process also had advantages in setting longer vertical well spacing and keeping consistent temperature of flowing heavy oil in the surface-drilled SAGD wells with the single well configuration.

### **2.3.3 Field Observation**

This field practice indicated that the steam chamber could be controlled somewhat, through altering operating conditions such as injection rate, injection frequency, and production rate and production pressure. In practice, injection pressure is usually kept slightly above reservoir pressure.

The oil production rate is highly sensitive to steam injection and production pressure. Any steam injection alteration might result in fluctuating operation performance. Higher steam temperature yields higher heat fluxes into the formation and brings in higher oil rates. JACOS experienced operating pressure alteration in the SAGD project at the Hangingstone reservoir (Ito et al. 2004). A significant effect of the pressure change on performance was observed during the SAGD process. The chamber growth rate showed a significant change at some of the observation wells due to the reduction of the injection pressure. After the injection pressure was increased to the normal level, the vertical growth of the steam chamber resumed.

The ESAGD field trial operated from November 1993 through to 2001 with generally disappointing results (Ding et al. 2006). The final steam to oil ratio (SOR) was 10, compared with the expected 3.2, and with a final estimated recovery efficiency of 10%. The simulated history match and the temperature observation wells indicated that most of the pilot bitumen production came from the highly permeable bottom zone of the reservoir where water saturations were also high. Furthermore, the steam zone did not rise much above this basal zone, due to be limited by the vertical permeability of the reservoir. The fact that the steam chambers did not fully develop implies that the ESAGD process in this pilot was not adequately tested.

### **2.3.4 Integrated Studies: Non-Condensable Gas (NCG) Injection**

The SAGD process consumes massive amounts of natural gas to generate steam. Efforts in seeking new techniques aimed at reducing gas consumption are being attempted. One promising technique proposed in the last decade was non-condensable gas injection. This

was one of the most active research areas related to SAGD operation performance enhancement (Bagci et al. 2008, Butter 1997, Zhao et al. 2005).

A large amount of injected heat remained in the reservoir after a prolonged period of steaming (Yee et al. 2004). Approximately one third of the total heat injected went to the reservoir, one third to production, and one third to the chamber. Effective recovery of this stored energy is important to the overall process economics. When the SOR reaches a value of three, a specific operational strategy can be considered. Butler (2002) presented the mechanisms of NCG injection which improved SAGD operation. NCG lowered the average temperature of the depleted reservoir, which resulted in a reduction of the SOR by a factor of 1/3. The main mechanism was that fingers of rising gas penetrated through the condensation and warmed the oil that drained downwards. The fingers raised the pressure above the chamber that allowed drainage and pushed the oil downwards.

Several processes were proposed to improve the oil recovery of SAGD in its final operation stage including the following: periodic or continuous blow-down of steam from the steam chamber to prevent the excessive accumulation of non-condensable gas in the steam chamber; gas push down (Zhao et al. 2005), Steam and Gas Push (SAGP) (Butler 1997), or wind down strategies for mature SAGD operations. Experimental and numerical simulation studies showed that NCG injection within an appropriate time offered the best oil recoveries (Bagci et al. 2008, Shin et al. 2007, Zhao et al. 2005, Butler 1997, Jiang et al. 1998, Belgrave et al. 2007, and Komery et al. 1998). Continuous steam expanding without more steam injection represented the most productive period in the NCG injection processes.

The initial intention of non-condensable gas injection was to reduce heat loss to the overburden, utilize existing energy in the heated zone, and hence, improve the SOR. The timing to enforce such strategic processes was critical as the solution gas might impede the steam development before the steam chamber touched the top of the pay zone. Based on the laboratory scale experimental results, Yuan et al. (2006) advised that heat loss to the overburden was not a concern in the early stage before steam reached the top of the pay zone, and gas was encouraged to be produced as much as possible. In the later stage, when the steam chamber touched the overburden, gas was injected and pushed over to prolong the SAGD production. A differential pressure was then introduced between

adjacent well pairs to push the excessive gas from one steam chamber to the other for aggressive gas production. Simulation results showed that such strategies could result in a dramatic increase of cumulative oil production without increasing the steam to oil ratio (SOR). When the SOR increased in the late period of the SAGD operation, such a strategy could be considered to continue oil production without steam injection.

Phase B of the Dover Project (formerly UTF) had the longest production history and largest array (28) of observation wells (Yee et al. 2004). A small amount of natural gas was added continuously to the steam injection from April of 1998 to April of 2001, and unexpected good performance results were achieved. Beginning in April 1998, a small amount of natural gas was added continuously to the steam injection (Yee et al. 2001). The concentration of the NCG increased steadily in the following three years and the chamber pressure was maintained at around 2,000 kPa. Actual performance was substantially higher than the simulation production. The bitumen rates were higher than those predicted for the continued steaming case without gas injection. Flue gas injection was followed from May to September of 2001. To reduce the cost incurred from NCG use, air, nitrogen, and flue gas were considered to replace methane. Simulations studies showed that the wind down operation was insensitive to the type of NCG. The big challenge was how to control potential corrosion of the existing equipment. The exhaust gas from the steam generator was used through the Exhaust Gas Processor for additives to the steam injection (Yee et al. 2004).

Encana Corporation had a plan to apply the operation strategy of air injection in post-SAGD to improve the SAGD performance (Belgrave et al. 2007). Air injection was initiated after thermal communication had been established between well pairs with steam. Laboratory combustion tube tests were presented, along with numerical simulations of post-SAGD air injection. Numerical simulation results showed that the recovery factor could be increased up to 8% of OOIP over conventional SAGD. The successful implementation of this technology would have a profound impact on the overall process economics.

## 2.4 Multiple Well Pair Operating Strategy

It is practical to drill and operate more than one pair of injectors and producers in order to cover more areas and achieve systemic oil recovery. One significant issue emerges from the application of multiple well pair, which is the recovery of oil from the areas between adjacent well pairs. In the following schematic (Figure 2-4), it can be seen that the oil around and above the injection well will be easily recovered by the hot steam chamber. However, the oil in the transition area would hardly be swept by the steam chamber especially in the lower regions of the reservoir (Cyr et al. 2002).

Some operation strategies aimed at improving bitumen recovery in SAGD are being developed: Fast SAGD (Polikar et al. 2000, Shin et al. 2005), X-SAGD (Stalder 2005), Combination of Vertical and Horizontal Wells (Jespersen et al. 1993), Offsetting Vertical Wells (Miller et al. 2008), and so on. The basic concept of these strategies is to use the lateral driving force along with gravity force to move the remaining oil in the regions between the producing wells without drilling infill wells.

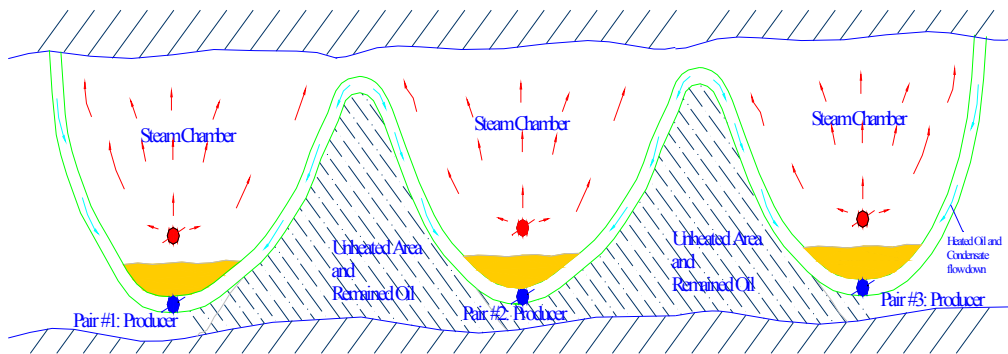


FIGURE 2-4 MULTIPLE WELL PAIR SAGD

The key scheme of these strategies is to design specific well configurations in the SAGD operation area, combined with cyclic steam stimulation to utilize the existing heat in the region between the adjacent steam chambers throughout the operation and hence accelerate merging of the chambers.

## 2.4.1 Numerical Simulation Study

**Cross SAGD (X-SAGD) or L-SAGD.** [Stalder \(2005\)](#) advised that production rate was limited to the spacing distance between the injector and producer in classic SAGD. Once the steam chamber was generated, the SAGD performance was enhanced with increasing spacing distance. The concept X-SAGD was proposed to employ specific operation strategies for steam injection through the injectors which were perpendicular to the producers. It attempted to utilize gravity and lateral drive to improve bitumen recovery. Consequently, more oil in the formation was expected to be reached and recovered than in the classic SAGD operation. His simulation study was conducted to test the X-SAGD concept and indicated that X-SAGD had advantage over classic SAGD at lower pressure (1500 kPa) than at higher pressure (3000 kPa). However, the process of X-SAGD was expected to face some serious practical challenges: extended initialization period, low initial production rate, and complicated operations.

**Fast SAGD.** In the theoretical concept of Fast-SAGD ([Polikar et al. 2000](#), [Shin et al. 2005](#)), the offset well was equipped and parallel to, but 50 meters away from, the SAGD producer. A pair of vertically spaced, parallel, co-extensive, horizontal injection and production wells and a laterally spaced, horizontal offset well were provided in a subterranean reservoir containing heavy oil. Fluid communication was established across the span of the formation extending between the pair of wells. This concept utilized the advantages of SAGD and CSS contemporaneously as laterally spaced horizontal wells lead to faster developing fluid communication between the two well locations ([Cyr et al. 1999](#)).

Based on results of numerical simulation, the process yielded improved oil recovery rates with improved steam consumption. The rates of bitumen production increased and the steam-oil ratio was reduced. [Shin et al. \(2007\)](#) claimed Fast-SAGD was a more efficient recovery process requiring less steam and had lower operating costs to produce the same amount of bitumen.

## 2.4.2 Experimental Study on Dual Well Pair SAGD

The concept of multiple well strategies was proposed and validated with the objective of improving SAGD performance in terms of efficiency and productivity. One experimental run was conducted at ARC aimed at evaluating such conceptual strategies (Deng et al. 2007). The experimental facility with dual well pair was built and the experimental procedure with dead oil was established. The results with dead Athabasca bitumen showed that the operation strategy of one injection well and two production wells worked properly by tuning the production pressures. The operation strategy of sweeping the oil between the two well pairs worked properly.

## 2.4.3 Field Observation

This field practice indicated that the existence of differential pressure between adjacent pair wells could enhance SAGD performance.

Goobie et al. (1994) developed the enhanced steam assisted gravity drainage (ESAGD) process by employing a pressure differential between adjacent well pairs. This drive process could be induced in the SAGD operation once sufficient bitumen mobility had been obtained between adjacent steam chambers. The process of steam flooding had a relatively high recovery factor for the conventional oil.

A field trial on a small pressure differential enforcement between adjacent pattern steam chambers was conducted in the Peace River area to enhance the SAGD process (Hamm et al. 1995, Ding et al. 2006). It utilized the same well configuration as the traditional SAGD process. The gentle drive due to the small pressure differential between adjacent pattern steam chambers helped to accelerate steam zone growth and bitumen production. The pressure differential tuning was done by lowering the steam injection pressure in one steam chamber, while maintaining pressure in the adjacent steam chamber. Chhina (1998) and Hamm et al. (1995) illustrated the process in detail, consisting of three operational components: start-up, SAGD operation, and SAGD stream drive. The lower well was located in the Basal Transition Zone, where it had sufficiently high water saturation to

allow fluid injection at initial conditions. The well pattern spacing was 50-78 m. A pressure differential of 500 kPa or less was established following start up.

[Edmunds \(1994\)](#) found that the Shaly zone between the injector and producer in the first pair of wells in phase A of the UTF produced a choking effect that restricted the downward path of bitumen and condensate. The producing pressure differential between the two wells was typically 1,000 kPa.

#### **2.4.4 Combination of Vertical and Horizontal Wells**

The process using a combination of vertical injector and horizontal wells can be viewed as an alteration of classic SAGD, although it is not a rigorous example of SAGD. However, the process still utilized horizontal producers to respond to steam injected from vertical wells which were located above the producers in the pay to drain oil between and beneath wells ([Miller et al. 2008](#)). In this proposed process, the steam was injected through an array of vertical wells, while the oil was produced through the horizontal wells.

Vertical steam drive, in combination with horizontal producing wellbores, was capable of causing very large increases in oil recovery efficiency. This technique was applied to a few projects of Sceptre (Now CNRL) in the North Tangleflags fields ([Jespersen et al. 1993](#)), and of Strike Bolney (now Husky) ([Miller et al. 2008](#)).

[Rose et al. \(1994\)](#) developed a numerical model regarding a combination of vertical injectors and horizontal producers. The simulation results showed the oil production from the vertical-horizontal combination approached 40% more production than that from the horizontal well pair. The oil-steam ratios of the vertical-horizontal combination and the horizontal well pair were comparable. Thus, [Rose et al. \(1994\)](#) advised that SAGD with a combination of vertical and horizontal wells had been demonstrated to be a viable scheme for the development of oil sand reservoirs.

The purpose of offsetting vertical wells was designed to access or mobilize the oil located beneath the production wells and between SAGD pairs. Vertical wells were strategically added halfway between two SAGD well pairs ([Miller et al. 2008](#)). The vertical infill

wells were perforated below the depth of the SAGD producers. Field observations and numerical simulation studies showed that properly placed vertical production wells could capture a significant amount of oil that was not produced by classic SAGD development and the unswept oil in the classic SAGD could be produced through the vertical infill wells (Miller et al. 2008). These vertical wells could also first be used for steam injection or temperature observation purposes, adding further enhancement to the performance of nearby classic SAGD pairs. Vertical wells had advantages over the horizontal wells due to the difficulty in drilling, completion, and some other practical aspects.

Chan et al. (1997) proposed a similar technique to deal with a 10 to 20 m thick Saskatchewan type heavy oil reservoir with an overlying gas cap and an underlying aquifer. Numerical simulation results suggested oil recovery could be increased up to 25% by offsetting the injector from the producer in their conventional SAGD well configuration, or by adopting a staggered well pattern.

During the SAGD operation in Phase A at the UTF, it was found that the second well pair produced the least bitumen of the three pairs. Edmunds (1994) thought that it was probably because of poorer quality pay and higher elevation of the second pair B. Slightly higher pressure on this pair might result in lower production rates on the second pair and higher production rates on the other two pairs. The pattern spacing was 25 meters, which was close enough to allow interference between adjacent steam chambers. Steam injection was continued for 10 months after the steam chamber reached the third injector and then the steam injected from the first well pair flowed to the third pair. It was found that steam consumption rate in the first injector rose in proportion to the third injector.

## ***2.5 Summary***

In Alberta, a number of the reservoirs with huge bitumen reserves will require low-pressure bitumen recovery technologies that exclude the CSS process. A SAGD process has been considered the only in-situ thermal recovery process economically suitable for these bitumen reserves.

The SAGD process is highly associated with steam injection and gravity drainage. SAGD performance is directly tied to natural conditions such as formation characteristics

including net pay, permeability (especially the vertical permeability), initial oil saturation, water bottom zone, and the imposed conditions such as well configuration, initialization strategies, chemical additive, and operational strategies. Efforts in operation strategies aimed at improving bitumen recovery in SAGD need to consider these conditional factors. Operational parameters can be optimized through running numerical simulation to enhance the performance in terms of oil production rate, SOR, and cumulative SOR. The operational optimization can be obtained through adjusting steam injection rate and producer liquid withdrawal rate during different SAGD operation periods.

It is practical to drill and operate more than one pair of injectors and producers in order to cover greater area and achieve systemic oil recovery. SAGD performance is often analyzed based on single well pair performance. However, the impact of the interference of adjacent chambers on SAGD performance may be more complicated than what is expected. Butler's analytical model to predict SAGD production did not reflect the interfering relation among steam chambers from neighbour well pairs. It is necessary to have a detailed analysis to understand the operating mechanisms of a multiple well pair SAGD process.

The presence of non-condensable gas would impede steam chamber expansion and hence reduce oil production in the SAGD operation. Gas production is encouraged in the early stage before the steam reaches the top of the pay zone. At the later stage, when the steam chamber touches the overburden, non-condensable gas could be injected and pushed to prolong SAGD production. A pressure difference is then introduced between adjacent well pairs to push the excessive gas from one steam chamber to the other for aggressive gas production. Simulation results showed that such strategies can result in a dramatic increase of cumulative oil production without increasing the steam to oil ratio.

The strategic concepts and numerical simulations which were conducted on single well pair SAGD operation limited the potential effectiveness of such operating strategies for a commercial SAGD project with multiple well pairs/pads. An experimental run with live heavy oil to examine the effects of solution gas on the dual well pair SAGD process is essential for multiple well pair SAGD operation strategies.

## **3 EXPERIMENTAL DESIGN AND APPARATUS**

### ***3.1 Experimental Objective***

The experimental model simulates and represents a slice with a 24 meter net pay, and a 160 meter long reservoir cell perpendicular to two pairs of horizontal injection and production wells. To investigate the impacts of multiple pair wells operation strategies on the performance of a SAGD process, some actual reservoir parameters in Cold Lake were employed in this project. The lab model would simulate a typical reservoir with sand porosity around 35%, with permeability to air around 1 Darcy, bitumen with viscosity of 33,000 cP, and gravity of 12° API.

### ***3.2 Experimental Design Criterion***

A scaled physical model, which simulates the field situation, must be set up and run in the laboratory. In order to simulate the SAGD process dominated by capillary, gravity, and viscous forces, the model design must match the ratios of these forces in the lab to the ratios in the field by employing dimensional analysis. In the laboratory model, scaling of capillary forces is frequently neglected to emphasize the gravity impact and thermal effects on the bitumen recovery operation.

The [Pujol and Boberg \(1972\)](#) scaling criterion was commonly used to scale such thermal process models. According to this criterion, the field and lab scaled models must encompass geometrically similar shapes, same parametrical properties of fluids and rock,

and be carried out with same initial and boundary conditions. Butler (2004) presented a similar scaling criterion: dimensional similarity between the model and the field. In other words, the dimensionless numbers  $B_3$  and  $t^*$  should be the same.

$$(B_3)_{model} = (B_3)_{field} \dots\dots\dots (3-1)$$

$$t^*_{model} = t^*_{field} \dots\dots\dots (3-2)$$

The dimensionless numbers are defined as the following expressions (3-3) and (3-4).

$$B_3 = \sqrt{\frac{kg h}{\phi \Delta S_o \alpha m v_s}} \dots\dots\dots (3-3)$$

$$t^* = \frac{t}{w} \sqrt{\frac{kg \alpha}{\phi \Delta S_o m v_s h}} \dots\dots\dots (3-4)$$

So,

$$\left( \sqrt{\frac{kg h}{\phi \Delta S_o \alpha m v_s}} \right)_{model} = \left( \sqrt{\frac{kg h}{\phi \Delta S_o \alpha m v_s}} \right)_{field} \dots\dots\dots (3-5)$$

The choice of model depends on the aspects of the process that are to be explored. Steam injection is one of the most critical parameters for SAGD performance and with injection of steam into the model the initial parameters and conditions would be altered during the experiment. Appropriate simulation of the properties of reservoir fluids and rocks with the variation of temperature is necessary in laboratory models. A model using reservoir fluids is advisable to obtain these data directly from a lab model. Since the reservoir fluids consist of water, bitumen, and gas, if water can not be scaled down and substituted by another low viscosity fluid, it is better to apply real bitumen with high viscosity to the laboratory simulation. Sand with high permeability is often employed in such thermal recovery experimental runs to use the same bitumen sample as in the actual reservoir. The main consideration is that the viscosity of heavy oil or bitumen is very sensitive to temperature variation.

Reservoir oil, pressures, and temperatures were used in this experiment. Therefore, the parameter  $m$  is the same or very close for the model and the field. In the meanwhile, the porosity, saturation, and thermal diffusivity are assumed the same as well.

Then,

$$(kh)_{model} = (kh)_{field} \dots\dots\dots (3-6)$$

Hence,

$$k_{model} = \frac{h_{field}}{h_{model}} k_{field} \dots\dots\dots (3-7)$$

It indicates that the permeability of the sand in the model is proportional to the ratio of reservoir net pay to the model height.

As

$$t^* = \left( \frac{t}{w \sqrt{\phi \Delta S_o}} \right)_{model} = \left( \frac{t}{w \sqrt{\phi \Delta S_o}} \right)_{field} \dots\dots\dots (3-8)$$

Hence,

$$\frac{t_{field}}{t_{model}} = \left( \frac{w_{field}}{w_{model}} \right) \sqrt{\frac{k_{model} h_{field}}{k_{field} h_{model}}} \dots\dots\dots (3-9)$$

Then,

$$t_{model} = \left( \frac{w_{model}}{w_{field}} \right) \left( \sqrt{\frac{k_{field} h_{model}}{k_{model} h_{field}}} \right) t_{field} \dots\dots\dots (3-10)$$

The experimental model is designed with 24 centimetre high and 160 centimetre long to represent a slice with a 24 meter net pay, and a 160 meter long reservoir cell perpendicular to two pairs of horizontal injection and production wells. The lab model used 100 Darcy sand to simulate a typical reservoir with permeability to air around 1 Darcy. Then the experimental running time is as following.

$$t_{model} = \left( \frac{0.4}{40} \right) \left( \sqrt{\frac{1 \times 0.24}{100 \times 24}} \right) t_{field} = \left( \frac{1}{100} \right)^2 t_{field} \dots\dots\dots (3-11)$$

It indicates that if the permeability for the model is scaled up by a factor of 100 and the geometry down by a factor of 100, the model scaling time would be yielded at 1/10,000. In other words, one year is scaled to 0.876 hours of lab time. To scale a field history of 10 years, an estimated run time of 8.8 hours is required for the lab model. Energy and steam flux rates will similarly scale down.

Based on the expression (3-6) and Darcy's law (3-12), which is an expression of conservation of momentum, injection flow rate is determined as following.

$$q = \frac{-kA}{\mu L} \Delta P \dots\dots\dots (3-12)$$

$$\left(-\frac{q\mu L}{kA \cdot \Delta P} \cdot h\right)_{model} = \left(-\frac{q\mu L}{kA \cdot \Delta P} \cdot h\right)_{field} \dots\dots\dots (3-13)$$

$$q_{model} = \frac{\left(\frac{\mu L}{\Delta P k A}\right)_{field} h_{field}}{\left(\frac{\mu L}{\Delta P k A}\right)_{model} h_{model}} q_{field} \dots\dots\dots (3-14)$$

The cross section area A in each case is proportional to L<sup>2</sup>. If the same fluids and same differential pressures are used in the model as in the field, then μ will be the same in each, The model geometry is scaled down by a factor as indicated above.

So,

$$q_{model} = \frac{k_{model}}{k_{field}} \frac{L_{model}}{L_{field}} \frac{h_{field}}{h_{model}} q_{field} = \frac{1}{100} q_{field} \dots\dots\dots (3-15)$$

Field flow rates will scale down by a factor of 100 as well. A steam injection rate in the field of 250 m<sup>3</sup>/d/500 m per well will scale down to 50 kg/d/m, or 2 kg/h (33 gram/min) for a 24 cm high and 10 cm wide pack. A steam injection rate will scale down to 2000 gram/h/24cm.

The criteria will correctly scale gravity drainage; however, these criteria do not correctly scale capillary forces. This test model will under-represent the contribution of capillarity to oil front advance and oil recovery.

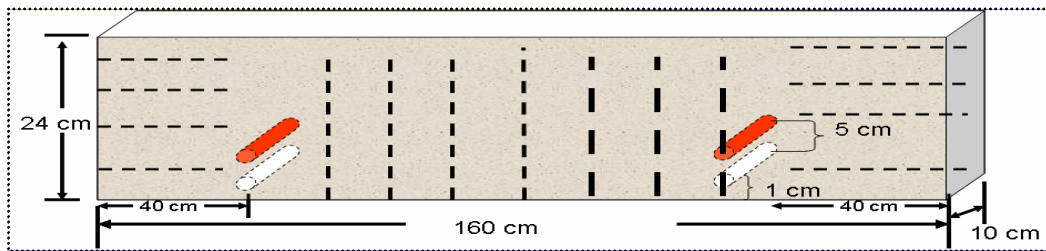
### ***3.3 Experimental Apparatus***

#### **3.3.1 Dual Well Pair SAGD Test Model**

A stainless steel model was fabricated from an 18 gauge SS-316 sheet. The whole model was made of welded construction using Tungsten Inert Gas (TIG) welding procedures. The lid was also welded as the same procedure.

The test cell, shown schematically in [Figure 3-1](#), had dimensions of 160 cm in length x 24 cm in height x 10 cm in width. The model contained two horizontal well pairs, eight saturation ports at the top of the pack lid, and six saturation ports at the bottom of the

pack, as shown in Figure 3-2. One pair of wells (left side pair) was located horizontally at 40 cm from the left edge of the test cell. Another pair (right side pair) was located horizontally at 40 cm from the right edge of the test cell. Thus, the spacing between the two well pairs was 80 cm. Injection wells were located 5 cm directly above their respective producing wells. Both producing wells were approximately 1 cm above the bottom of the test cell. All eight saturation ports at the top of the pack lid were connected through a ¼" tubing, which could easily go through the pressure vessel and connect to saturation containers. The six saturation ports at the bottom of the pack were connected through a ¼" tubing as well.



Thermocouples Location:      - - - - -

SAGD Well Pair:                      

**FIGURE 3-1 SCHEMATIC DRAWING OF EXPERIMENTAL CELL**

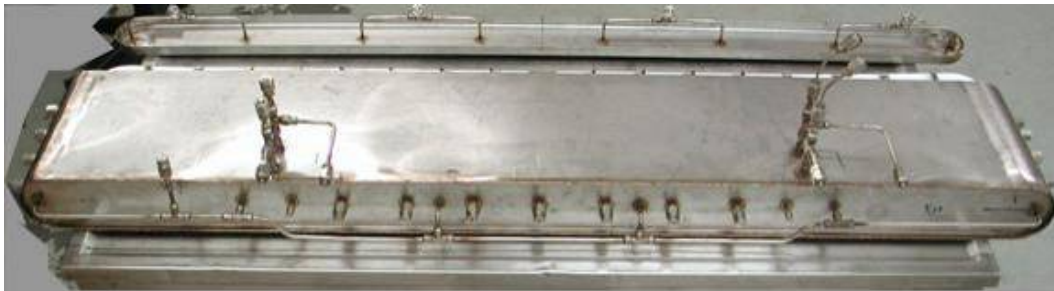


**FIGURE 3-2 TEST FACILITY: TEST CELL WITH TWO WELL PAIRS**

VCR fittings, which are very reliable under high pressure and temperature, were applied to most of the tubing and thermocouple connections. All the fittings attached to the models were SS-316 Swagelok type rated at 34,475 kPa (5000 psig).



**FIGURE 3-3 INJECTOR/PRODUCTION WELL**

The perforated wells were made of stainless steel tubing, shown in [Figure 3-3](#). It can be seen that there were totally eight well in this test cell, which are all listed in [Table 3-1](#) including their location and function in the experiment. [Figure 3-4](#) displays the image of the left pair of well including injector and production wells in the test model. All the wells were plugged with VCR plugs during experimental preparation.

**TABLE 3-1 WELLS IN THE TEST CELL**

Location		Left Well Pair	Right Well Pair	Function
Top	Upper	Well 1 'Inj_Left'	Well 5 'Inj_Right'	Regular Steam Injector
	Lower	Well 2 'Inj_Left_o'	Well 6 'Inj_Right_o'	Producer During Initialization
Bottom	Upper	Well 3 'Prod_Left_i'	Well 7 'Prod_Right_i'	Steam Injector During Initialization
	Lower	Well 4 'Prod_Left'	Well 8 'Prod_Right'	Regular Producer

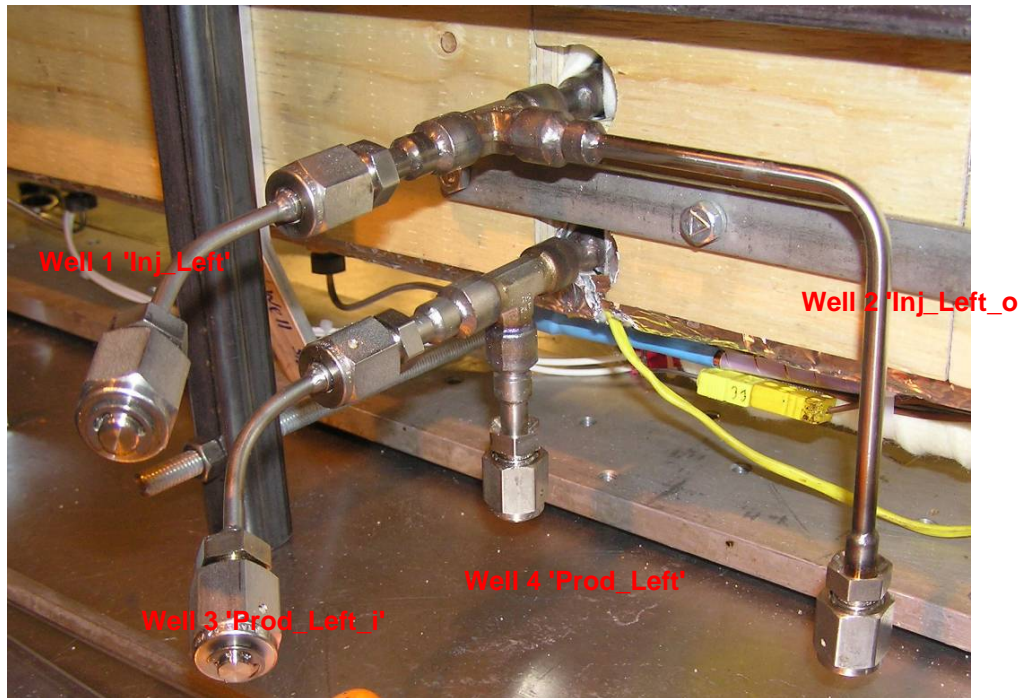


**FIGURE 3-4 TEST FACILITY: ONE PAIR OF WELL INCLUDING INJECTOR AND PRODUCTION WELLS IN THE TEST MODEL**

### **3.3.2 Thermocouple Distribution**

To better monitor a broader area in the experiment, there were totally fifteen thermocouple rods employed in this test cell. The 2D dual well pair model was equipped with eight horizontal thermocouple rods distributed along the height of the cell. Also, the model had seven vertical thermocouple rods distributed between the two well pairs. The locations of these thermocouple rods are shown schematically in [Figure 3-5](#) [Figure 3-6](#) and [Figure 3-7](#). Each horizontal thermocouple rod had a net length of 14" (35.6 cm) and could measure four temperature points with an interval of 4" (10.2 cm). Each vertical thermocouple rod had a net length of  $8\frac{3}{4}$ " (22.2 cm), with the exception of the thermocouple rod located in the center of the model, which had a length of  $8\frac{15}{16}$ " (22.7 cm). Each vertical thermocouple rod could measure four temperature points with an interval of  $2\frac{1}{2}$ " (6.4 cm). In addition, there were two single-point thermocouples placed between the injector and producer of each well pair (approximately 3.5 cm from the bottom of the cell). This thermocouple configuration allowed measurement of 62 temperature points in the test cell. [Figure 3-7](#) shows the identification code for each





**FIGURE 3-8 TEST FACILITY: A THERMOCOUPLE TO MEASURE OVERBURDEN TEMPERATURE**

### **3.3.3 Pressure Transducer**

Nine pressure transducers were installed to monitor pressure change during the experiment. One was located at the top of the pressure vessel to measure the core pressure in the test model as shown in [Figure 3-9](#). Overburden pressure was read through a transducer connected to the nitrogen supply line. Two transducers were connected to the left producer and the right producer separately underneath the pressure vessel. There were also two independent pressure transducers that were mounted in the steam supply system to record variation of the differential pressure between the entrance and the exit of the orifice.

Orifices were installed in the steam supplying pipes for the left side and right side well pairs separately. The pressure differences between the two producers and between the injector and producer of each well pair were monitored through the other three pressure transducers.

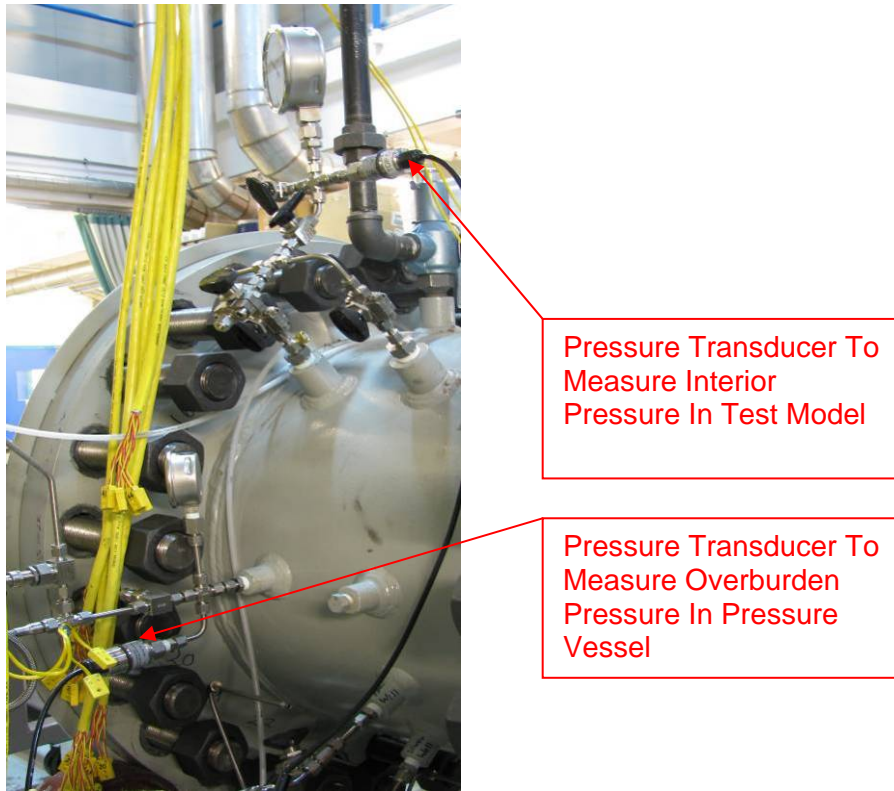


**FIGURE 3-9 TEST FACILITY: PRESSURE TRANSDUCERS MOUNTED OUTSIDE OF THE PRESSURE VESSEL**

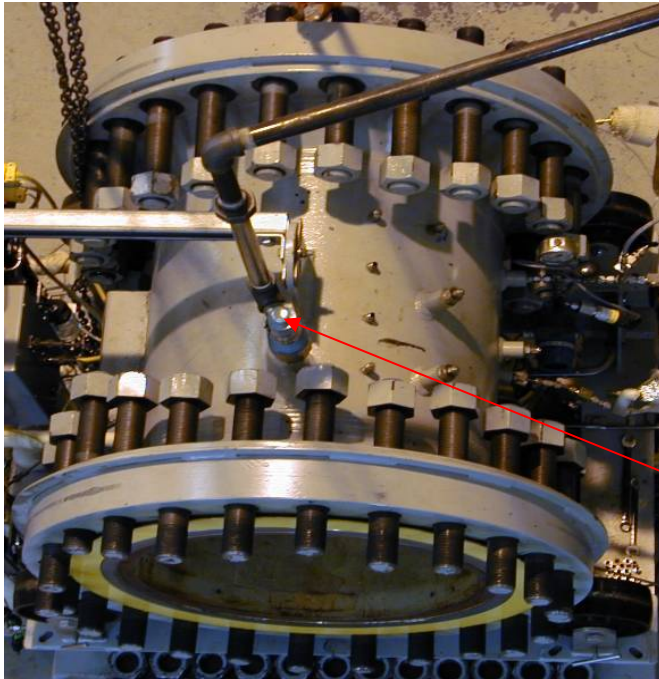
### **3.3.4 Pressure Vessel**

The regular confinement vessel for the 2D experiments with one SAGD well pair is an ALCO designed pressure vessel. The vessel has a cylindrical shape, with an end cap on each side as shown in [Figure 3-10](#).

The pressure vessel was designed as an extension of the existing pressure vessel to house the dual well pair model. It was a combination of two regular size confinement vessels united with bolts, nuts, and metal gasket, as shown in [Figure 3-11](#). This design brought dramatic reduction in cost and more efficient use of the physical space in the lab.

The pressure vessel setup for the dual well pair SAGD test was 57.2 cm of diameter and 182.9 cm of length (22.5 inch x 72 inch), with a total footprint of 1.52 m x 3.7 m (5 ft x 12 ft). Both vessels were designed with maximum working pressure of 7,580 kPa (1,100 psi) and working temperature of 250 °C (482 °F). The maximum running temperature inside the model for the test was 230 °C. The safety relief valve with a setting of 7,580

kPa (1,100 psi) was located on the top of the vessel. It consisted of two vent pipes which went through and out of the building.



Safety Relief Valve  
and Vent Pipes

**FIGURE 3-10 TEST FACILITY: PRESSURE VESSEL AND SAFETY VALVE**



**FIGURE 3-11 TEST FACILITY: COMBINATION OF TWO PRESSURE VESSELS**



**FIGURE 3-12 TEST FACILITY: PRESSURE VESSEL AND 2D TEST CELL**

Figure 3-12 shows the sand-packed model with its stand that was housed in the pressure vessel. The stand was mounted firmly to the interior base of the pressure vessel firmly to avoid moving and vibrating during the entire experiment.

### **3.3.5 Production Station and Injection Station**

As the 2D test cell had two SAGD well pairs, two similar production racks were combined in the operation. Figure 3-13 shows the production stations for the two SAGD well pairs. The production station collected all the samples and separated gas from the liquid sample. Its function was to control the pressure of the production wells, which was done through a backpressure regulation valve and pressure manometers. Also, in this station the liquids produced during the test were stored in two stainless steel accumulators that were alternately discharged to the storage plastic jars through the production exit pipe during the test. After the test, the amount of water and oil produced during each interval of the test could then be determined. The produced gas passed through a gas meter before being properly vented out of the lab.



**FIGURE 3-13 TEST FACILITY: TWO PRODUCTION STATIONS**

The steam was supplied by a high pressure steam boiler located at the Alberta Research Council. The maximum steam pressure was 2,965kPa (430 psi). [Figure 3-14](#) displays a bird-view of the injection station snapped from the second floor of the laboratory building. In this experiment, two branches of steam were originally split from one main steam pipe which was supplied by the same boiler. During the whole experiment, these two branches of steam supplied the upper left and upper right injection well separately before they flowed through two independent orifices installed in the steam tubing. One syringe pump was used to inject fresh water into a superheater that generated steam to supply both the lower left and lower right production well during the first 10 minutes of the experiment for interwell initialization.



**FIGURE 3-14 SCHEMATIC OF STEAM STATION: STEAM SUPPLYING AND CONTROLLING SYSTEM**

### **3.3.6 Data Acquisition System**

The experimental operation was monitored, controlled, and logged by a PC based data acquisition and control software - Paragon. [Figures 3-15](#) and [3-16](#) display the schematic of the data acquisition and process control system. The main computer monitored and remotely controlled three site computers through the internet. One of the three computers connected to the hardware OPTO 22 of the data acquisition system through a panel Ethernet I/O.

The process measurements mainly included:

- Running time
- All pressure measurements
  - Barometric pressure (4-20 mA output, 800-1100 mbar *Range*)
  - Production pressure (4-20 mA output, 0-6,895 kPa *Range*)
  - Overburden pressure (4-20 mA output, 0-6,895 kPa *Range*)
  - Model internal pressures (4-20 mA output, 0-6,895 kPa *Range*)

- Steam injection pressures (4-20 mA output, 0-6,895 kPa Range)
- Differential pressures (4-20 mA output, -50-200 kPa Range)
- Steam injection rates (0-4000 g/hour Range)
- All thermocouple measurements
  - Model internal temperatures (-50 to +50 mV output, - 200 to 1250°C)
  - Overburden temperature (-50 to +50 mV output, - 200 to 1250°C)
  - Steam temperatures (-50 to +50 mV output, - 200 to 1250°C)
  - Room temperatures (-50 to +50 mV output, - 200 to 1250°C)

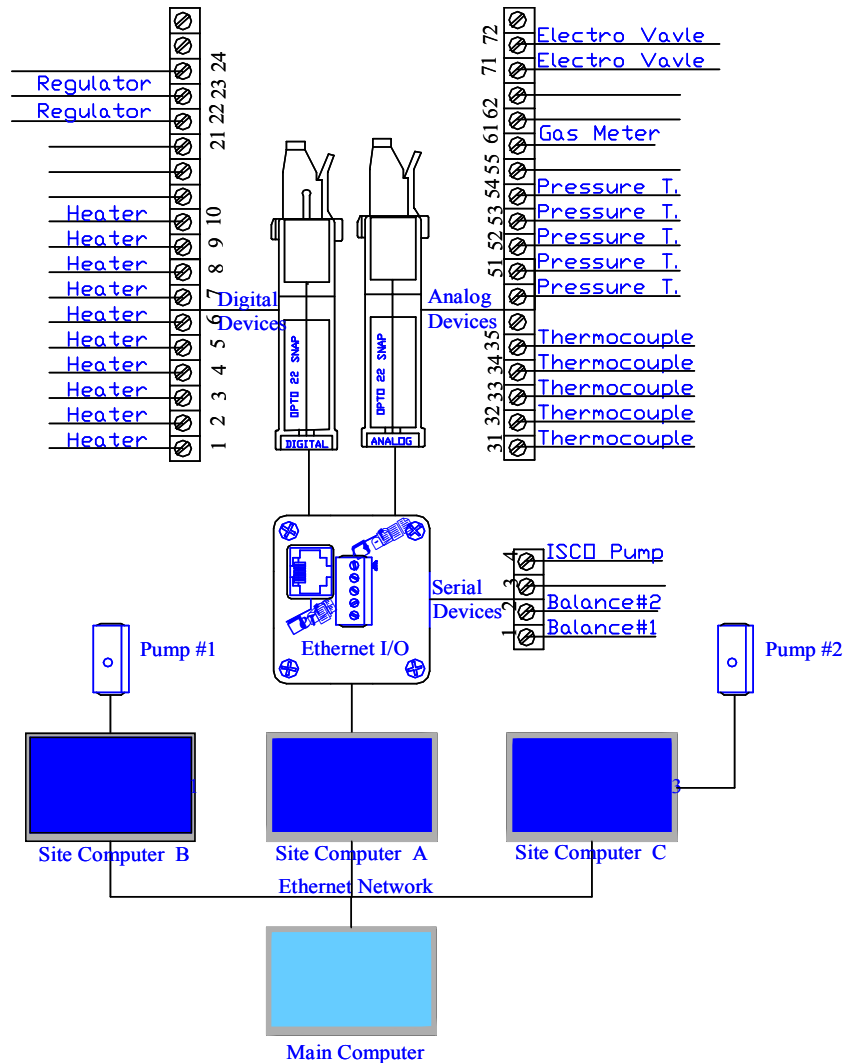


**FIGURE 3-15 SCHEMATIC OF FLOW PROCESS---DATA ACQUISITION AND CONTROL SYSTEM**

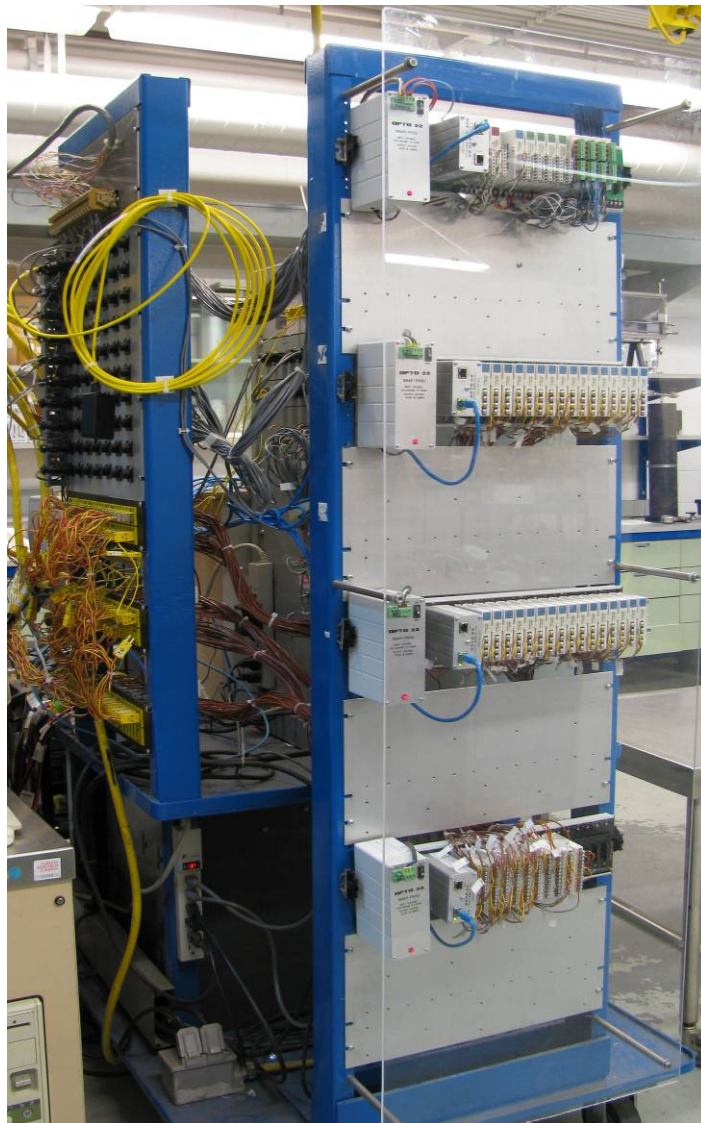


**FIGURE 3-16 SCHEMATIC OF DATA ACQUISITION AND CONTROL SYSTEM**

Figure 3-17 shows the data acquisition interface of the Paragon program during experimental preparation. The data logging button on this interface could be conveniently clicked by a mouse to start experimental data writing on a file with a certain time interval in spread sheet format.

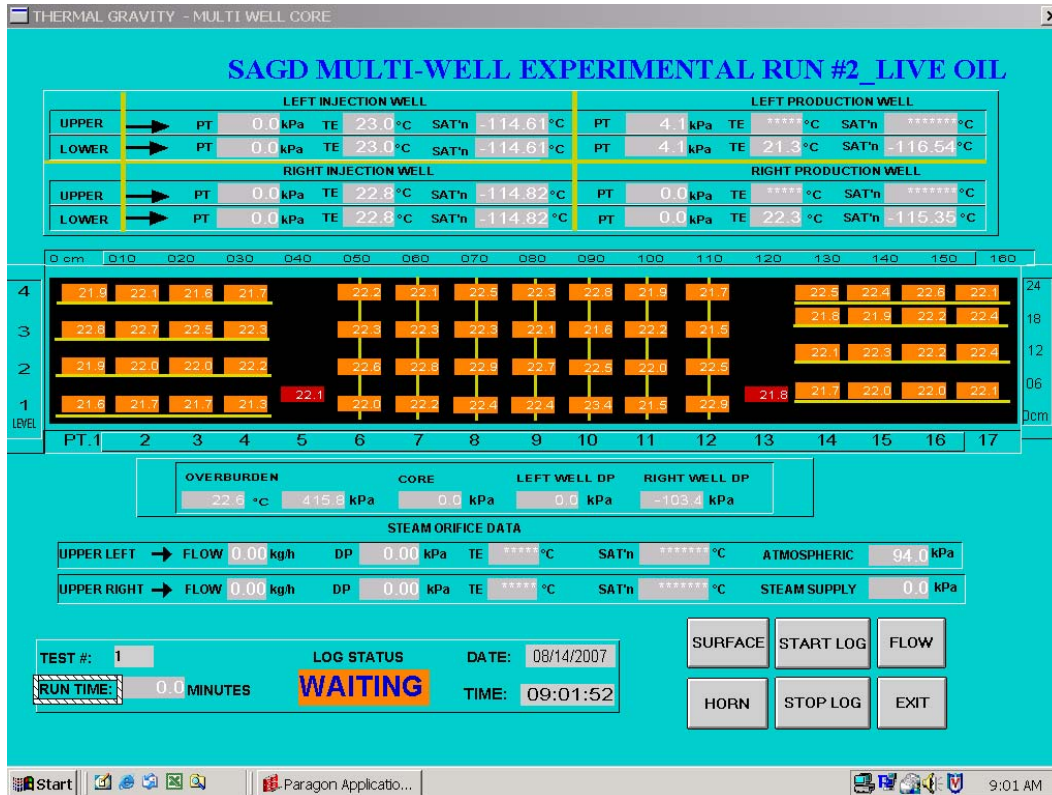


**FIGURE 3-17 OPERATOR INTERFACE OF DATA ACQUISITION USING PARAGON PROGRAM**

### 3.4 Sand Pack Preparation

To avoid/minimize fluids channelling or fingering along the internal walls of the model, a thin layer of oil coating was applied to the internal surface of the test model before it was packed with sand.

After the thermocouples were placed through the VCR fittings welded on the walls of the test model, the model was then enveloped by three layers of a Nomex insulation blanket on the exterior walls. Two plywood frames bolted to the steel bars were used to clamp the insulation blanket. The whole model was laid on a steel stand to hold it firmly in place. Figure 3-18 shows the empty test model inserted and mounted with fifteen thermocouple rods, was ready to be packed with sands.

The sand packed for the test was US Silica sand with -20 to +40 mesh fraction. The permeability with this sand was measured separately prior to the sand packing

preparation, which had a value of 73 Darcies. The test model was packed from the bottom to top by slowly pouring in the sand and tapping with a hammer. The tapping was mainly applied to the surface of the plywood and the steel bar. After the sand pack was completely filled, all the sand used and remaining was weighed to determine the weight of sand within the test model. The porosity of the pack was then calculated, using a specific gravity of 2.65 gram/cm<sup>3</sup> for the sand particle. Once the model was packed with sand which is shown in [Figure 3-19](#), a Teflon sheet was placed on the top sand surface, followed by the stainless steel lid which was welded into place.

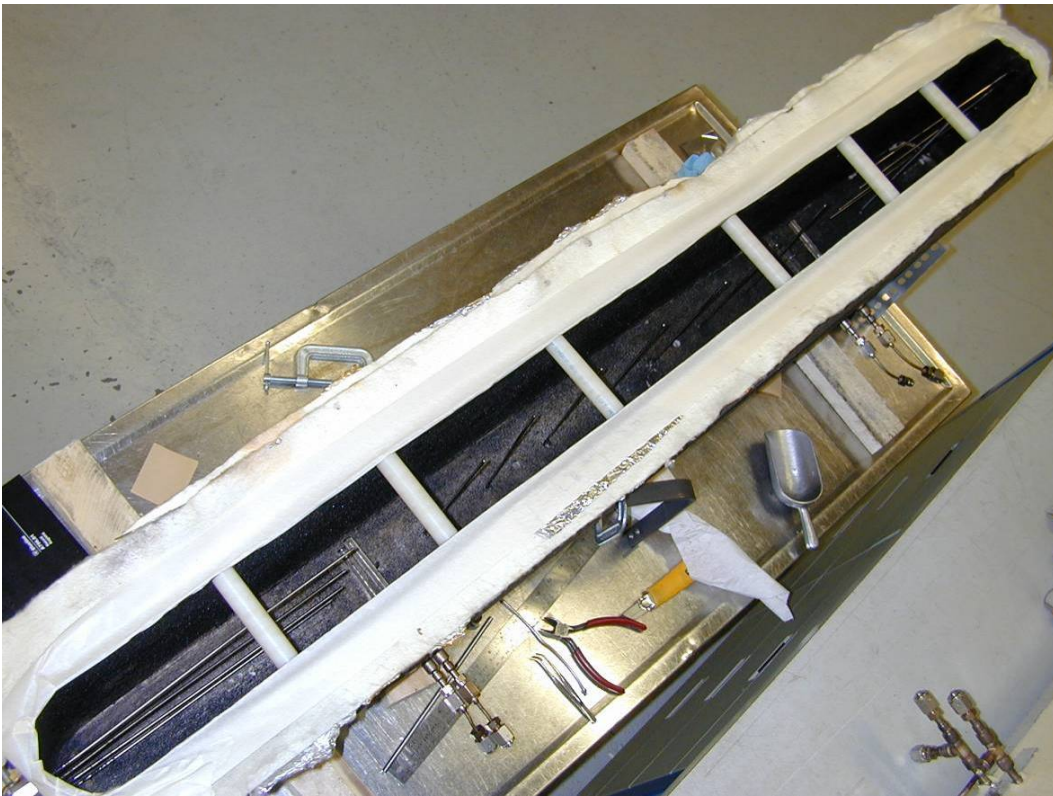


**FIGURE 3-18 TEST FACILITY: EMPTY TEST CELL BEFORE SAND PACKING**



**FIGURE 3-19 TEST CELL PACKED WITH US SILICA SAND: – 20 TO +40 MESH FRACTIONS**

### ***3.5 Leakage Test***

A leakage test was conducted to ensure a leak-free, sand packed test model. The first step was to evacuate the model and monitor the possible pressure variations through a vacuum gauge. When a pressure increase was found during the next several hours, leaking spots had to be determined. In order to discover them, the model was filled with helium at very low pressure to check high probability leak spots using a helium detector.

[Figure 3-20](#) displays the sand packed test model sitting on a table, which was being carried out a leakage test. Four square section steel bars were holding the test model with four long bolts to protect the model from deforming when a small pressure was applying to the model.

To ensure that there were no further leaks, the model was immersed in a big water tank and then filled with low pressure (around 15 kPa) helium. To operate conveniently and safely, the test model was placed side down and immersed in the water tank, which is shown in [Figure 3-21](#). This was very efficient and economical way to detect any possible leaks in the test model. If there still had been one small leak in the model, some bubbles would have emerged in the water tank. The late on successful experimental execution verified that the test model was a leak-free one.



**FIGURE 3-20 LEAKAGE TEST ON THE TEST CELL PACKED WITH SANDS**



**FIGURE 3-21 TEST MODEL IN A WATER TANK FOR LEAKAGE**

After the test model was completed with leakage test, it was taken from the water tank with a crane. The wet outside surfaces of the model should be blown with compressed air and dried out to avoid potential risk such as electrical circuit short-cut.

The leak-free, sand packed model was then loaded into the pressure vessel and all the exposed tubing was wrapped with two or three layers of a Nomex insulation blanket on

the exterior tubing walls. Then, all the connections of thermocouples, heat trace, and power were completed. Once all the connections were verified externally through the Paragon system and instrumental tools, the vessel was bolted and sealed with steel gaskets. [Figure 3-22](#) shows the test model was housing in the pressure vessel before the vessel was closed and bolted. Nitrogen was first charged into the pressure vessel to apply a small overburden pressure on the model. Then the vessel was gradually pressurized with nitrogen after both the model and the vessel were determined leak free.



**FIGURE 3-22 TEST MODEL IN THE PRESSURE VESSEL BEFORE THE VESSEL WAS BOLTED AND CLOSED**

### ***3.6 Water Saturation***

The leak-free, sand packed model was evacuated and flooded with carbon dioxide three times before water flooding. The sand pack was flooded with deionized water under vacuum condition at a constant flow rate. Water saturation was executed by injecting water with a DBR cylindrical piston pump ([Figure 3-23](#)) from the bottom to the top of the model to maintain a uniform and smooth interface. Once the core pressure was above zero, the valves controlling the outlet port of water saturation which is shown in [Figure 3-24](#), were opened. Water was then allowed to flow out of the model to a pail sitting on a scale balance. The water produced from the system was weighed by the scale. After

producing two pore volumes of water, the sand pack was isolated and the pressure vessel was pressurized with nitrogen to approximately 3,000 kPa for live oil saturation.



**FIGURE 3-23 EXPERIMENTAL FACILITY: WATER SATURATION BY INJECTING WATER WITH A DBR CYLINDRICAL PISTON PUMP**

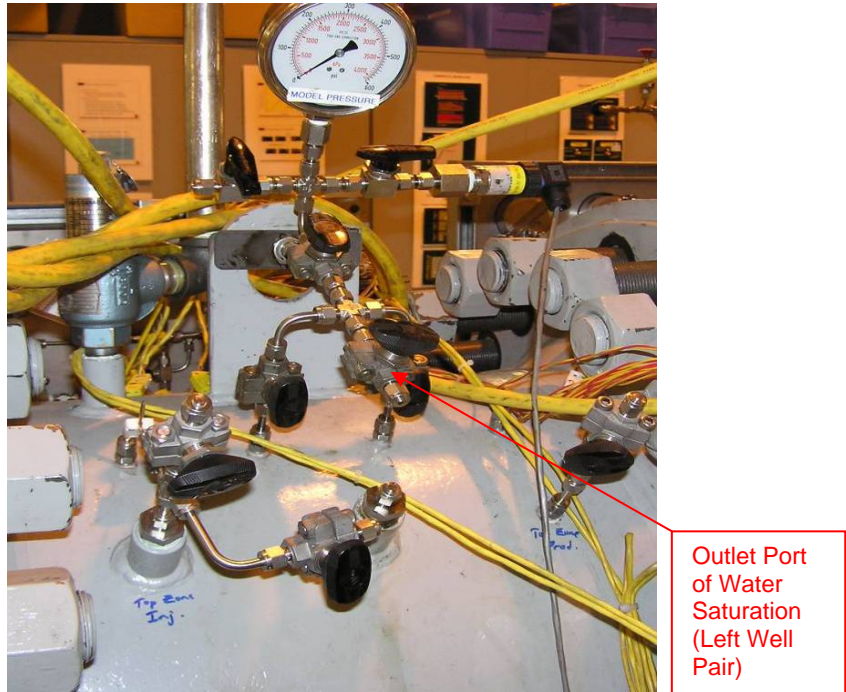


**FIGURE 3-24 WATER SATURATION BY INJECTING WATER FROM THE BOTTOM TO THE TOP OF THE MODEL**

### 3.7 Live Oil Preparation

Burnt Lake Bitumen was selected for the live oil dual well pair SAGD test. The temperature dependent viscosities of this dead heavy oil are plotted in [Figure 3-25](#).

Dry Burnt Lake Bitumen was saturated with methane in a 60-L steel cylindrical container ([Figure 3-26](#)) at room temperature. The container charged with dead oil was first evacuated and flushed with methane for several cycles. Then the container was pressurized to 2,200 kPa with methane, placed on a roller, and rolled at low speed. The pressure inside the container was monitored and read through the pressure gauge mounted in the container. The container was re-pressurized to 2,200 kPa with methane when the pressure declined. This procedure was repeated until the pressure within the sample container remained constant at 2,200 kPa, which was assumed that no more methane could be dissolved into bitumen sample and an equilibrium status was reached.

The mixed live oil was then transferred to three 5-L steel cylindrical containers ([Figure 3-27](#)). Each cylinder had one piston inside to isolate live oil and water. The ratio of gas to oil in the live oil was measured before the test model was saturated with live oil.

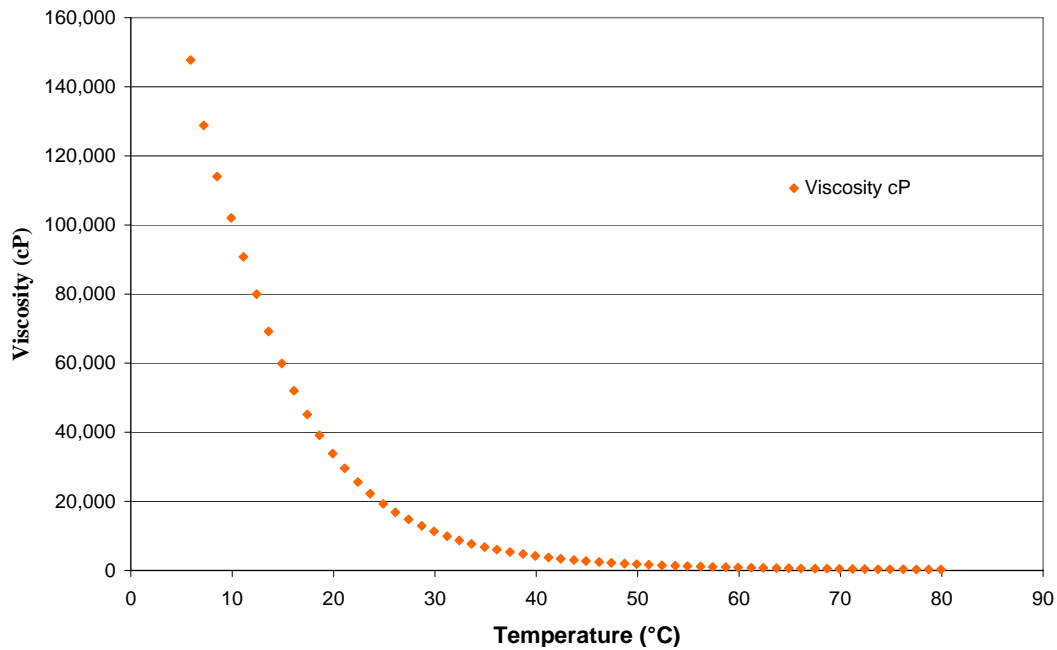


**FIGURE 3-25 VISCOSITY OF DRY BURNT LAKE BITUMEN**



**FIGURE 3-26 60-L STEEL CYLINDRICAL CONTAINER USED TO SATURATE DRY BURNT LAKE BITUMEN WITH METHANE**



**FIGURE 3-27 ONE 5-L STEEL CYLINDRICAL CONTAINER WITH A PISTON ISOLATING LIVE OIL AND WATER**

### 3.8 Live Oil Flooding

The water-flooded test model was saturated with live Burnt Lake bitumen by injecting the live oil from the top to the bottom of the model which considered the density difference between water and live oil. The injection rate of oil was set at a constant rate to maintain a uniform and smooth displacement interface. The oil saturation process was run at room temperature condition. Flow was controlled with a backpressure regulator to ensure pressure in the system was maintained above the live oil saturation pressure (2,200 kPa) during the course of oil saturation. The produced fluid was measured on a balance, and the flood was terminated when 1.5 pore volumes of live oil had been injected. The sand pack was then shut in.

The amount of oil (OOIP) in the test cell was 12,397 grams, and the total initial water in the test cell was 1,426 grams. [Table 3-2](#) summarizes the initial conditions and fluid properties of the experiment.

**TABLE 3-2 INITIAL CONDITION AND FLUID PROPERTIES**

Oil: Burnt Lake Bitumen	
Sand Mass in Pack, M (g)	72,939
Bulk Volume, V (cm <sup>3</sup> )	41,275
Pore Volume, V <sub>p</sub> (cm <sup>3</sup> )	13,751
Porosity, $\Phi$ (%)	33.3
Horizontal Permeability, k <sub>H</sub> (Darcy)	73
Vertical Permeability, k <sub>V</sub> (Darcy)	73
Ambient Temperature (°C)	21.0
Viscosity at 20 °C, $\mu$ (mPa·s)	33,800
Oil Density at 20 °C, $\rho$ (gram/cm <sup>3</sup> )	0.9962
Initial Water Saturation, S <sub>wi</sub> (%)	10.4
Original Water in Place, OWIP (g)	1,426
Initial Oil Saturation, S <sub>oi</sub> (%)	89.6
Original Oil in Place, OOIP (g)	12,397
GOR (std m <sup>3</sup> /m <sup>3</sup> )	6.45
Live Oil Saturation Pressure, (kPa)	2,196
Live Oil Saturation Temperature, (°C)	21.1

## 4 EXPERIMENT

### *4.1 Experimental Procedure*

The experiment began with an initialization period of ten minutes for both well pairs simultaneously. After the region between the injector and the producer in each well pair was heated by steam circulation, steam injection to the production wells was stopped and the wells were converted to pressure-controlled production mode. The production from the injectors was also stopped and steam injection into the injection wells continued at average temperature of 220 °C. At the 285<sup>th</sup> minute running time, the right side injector was shut-in. Two branches of steam lines were united and continued to inject to the left injection well. The steam rate for the left side injector was then doubled and was kept steady until the end of the experiment.

Back pressures for the two producers were initially set to be equal. In order to maintain continuous production from both producers, frequent tuning of the back pressures was done during the experiment. The production pressure on left side of the model was set slightly different from that on the right side. The inlet port of the DP cell for high pressure was connected to the left side producer, while the low inlet port was connected to the right side producer. Thus, the differential pressure between left side and right side was positive when the pressure on the left side was greater than one on the opposite side.

The whole test was planned to run for about nine hours. At the end of the test, the left injection well and two production wells of the test model were all shut-in immediately. At the same time, all the heaters and the data acquisition system were also shut in. The

pressure vessel with the test model was then turned 90° to reduce further vertical movement of the remaining fluid in the test model. Table 4-1 summaries the experimental operating scheme.

After the model cooled down, the pressure vessel was unassembled and the model unpacked. The sand pack was divided into eight layers from top to bottom. Each layer was cut into sixteen sections. There were a total of 128 sections of oil sand samples to be extracted. All the oil sand samples were analyzed by Dean Stark extraction for the contents of residual bitumen and water.

**TABLE 4-1 EXPERIMENTAL SCHEME: OPERATING STRATEGIES**

Mark	Time (min)	Injection Flow Rate (cc/min)	
		Left Well Pair	Right Well Pair
1	0~10	33	33
2	10	Shut in Well #2,3,6,7	
3	10~285	33	33
Turning time depends on the connection between chambers, or the temperatures on the central T/C.			
4	285		Shut in Well #5
5	285 ~ 525	66	0
Finishing time depends on the oil production and the steam chamber in the transition region			

## 4.2 Steam Injection Rate

Figure 4-1 plots the history of steam injection rates for the two injectors. During the first 10 minutes' initialization period, steam was circulated into the injection and production wells at an average rate of 33 cm<sup>3</sup>/min. After the initialization period, the steam injection rates were fluctuating at around 33 cm<sup>3</sup>/min for both injection well pairs. After the 285<sup>th</sup> minute running time, the right side injector was shut-in and the steam rate for the left side injector was then doubled to approximately 66 cm<sup>3</sup>/min until the end of the experiment. The actual steam injection rates were fluctuating during the test. The left side injected 22,305 grams of steam, nearly triple the amount of 8,791 grams from the right side at the end of test.

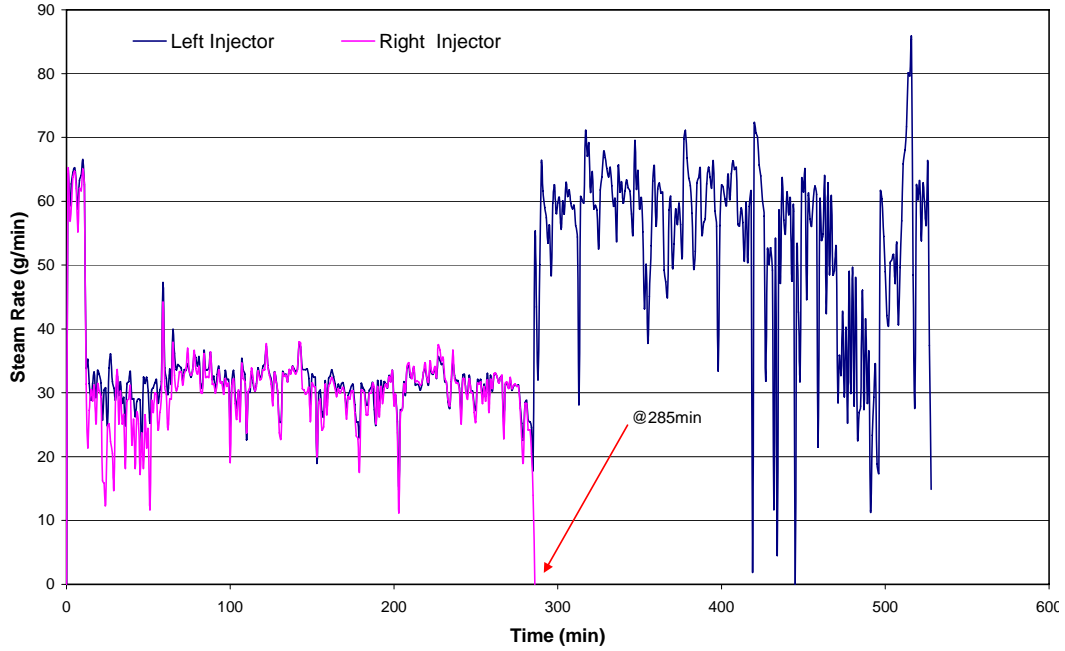


**FIGURE 4-1 STEAM INJECTION RATES FOR DUAL SAGD WELL PAIRS**

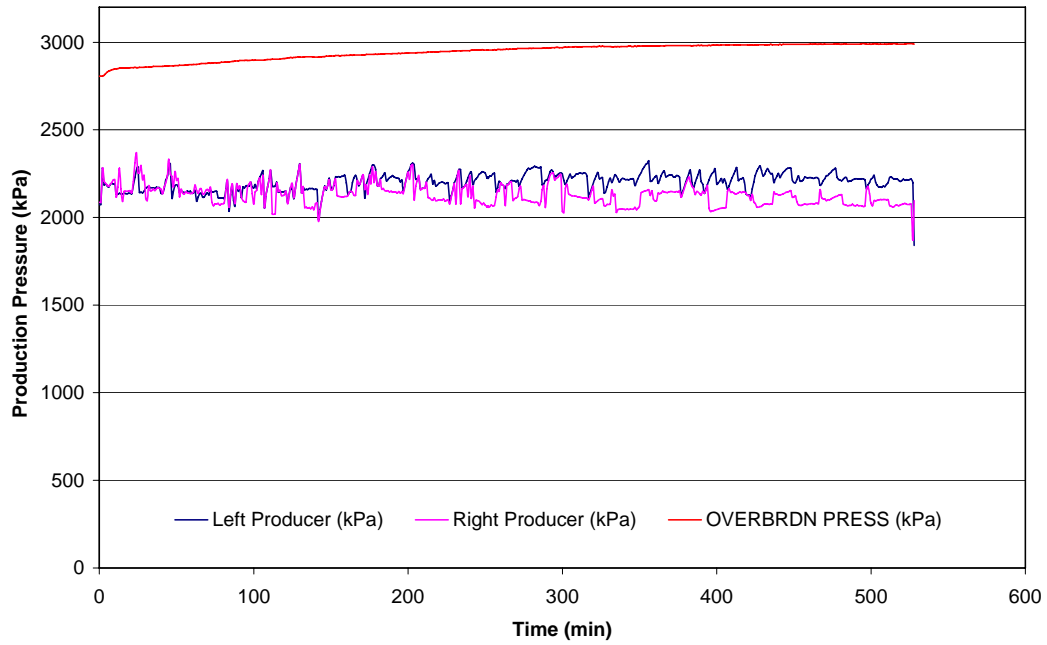


**FIGURE 4-2 PRODUCTION PRESSURE AND OVERBURDEN PRESSURE**

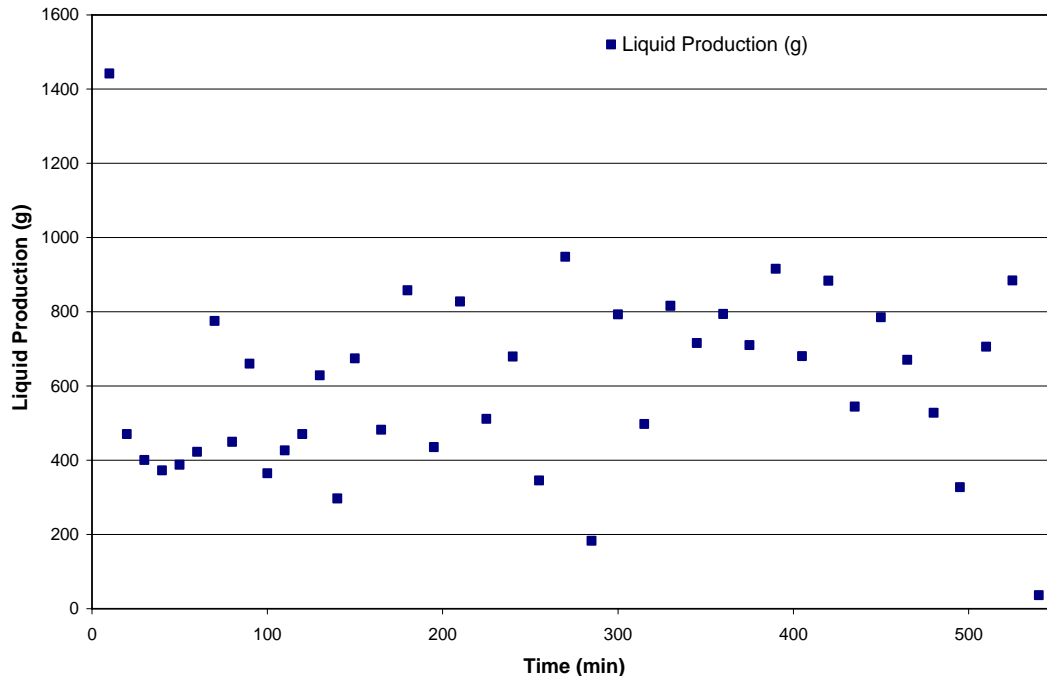
### ***4.3 Production and Overburden Pressure***

Figure 4-2 shows the profiles of production pressures for the two producers and the overburden pressure in the confinement vessel. It is noted that the overburden pressure was maintained above the production pressures during the whole experiment to ensure that the test model was firmly pressed. During the test, the pressures in both producers were maintained between 2,000-2,300 kPa. The overburden pressure increased from 2,806 kPa at the very beginning to 2,991 kPa at the end of test because the temperature increased from 23 °C to 47 °C inside the pressure vessel.

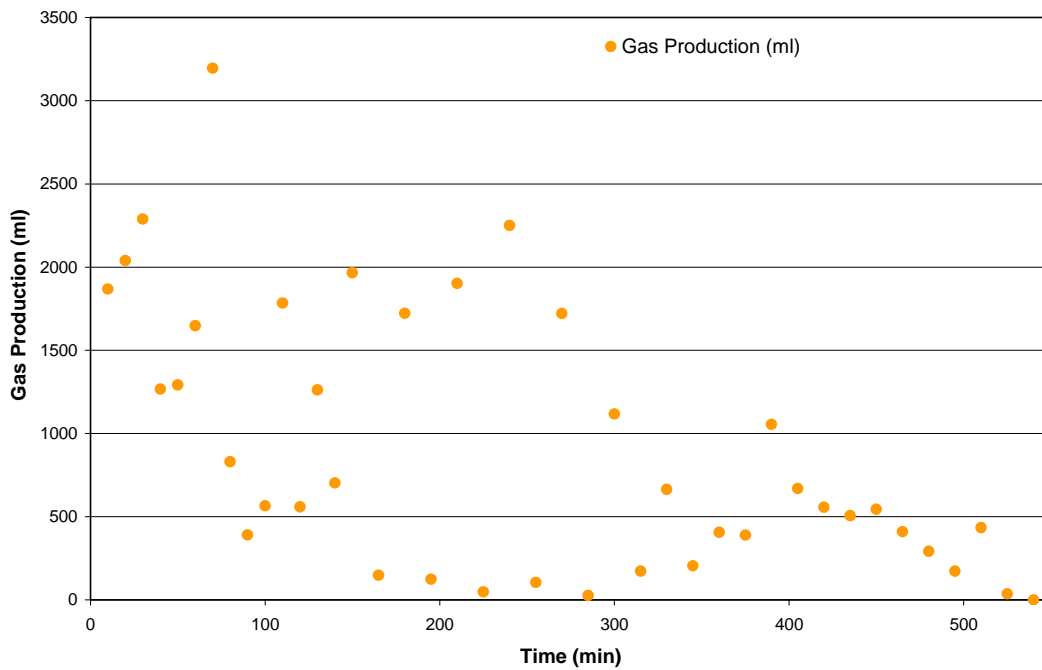
### ***4.4 Liquid and Gas Production***

Figure 4-3, 4-4, 4-5, and 4-6 plot the liquid and gas production behaviors of the both side well pairs. After the right steam injector was shut in at the 285<sup>th</sup> minute and the steam injection rate of the left injector doubled, both producers were able to produce fluids. It was observed that the liquid rates of both pairs fluctuated significantly during the experiment.

Totally, 39,450 grams of liquid were produced from the test cell, 24,801 grams of which was from the left well pair and 14, 649 grams from the right side. The gas rate of the right producer had a jump point at the 300th minute then returned to normal. The left side produced 37.3 litres of CH<sub>4</sub>; and the right side produced 32.1 litres of CH<sub>4</sub>. A total of 69.4 litres of CH<sub>4</sub> was produced at the end of test. The gas meter readings included the volume of gas methane produced from the test model and the volume increase due to displaced by liquid production. Therefore, the real gas volume had to exclude the liquid volume.



**FIGURE 4-3 LIQUID PRODUCTION AT THE LEFT SIDE**



**FIGURE 4-4 GAS PRODUCTION AT THE LEFT SIDE**

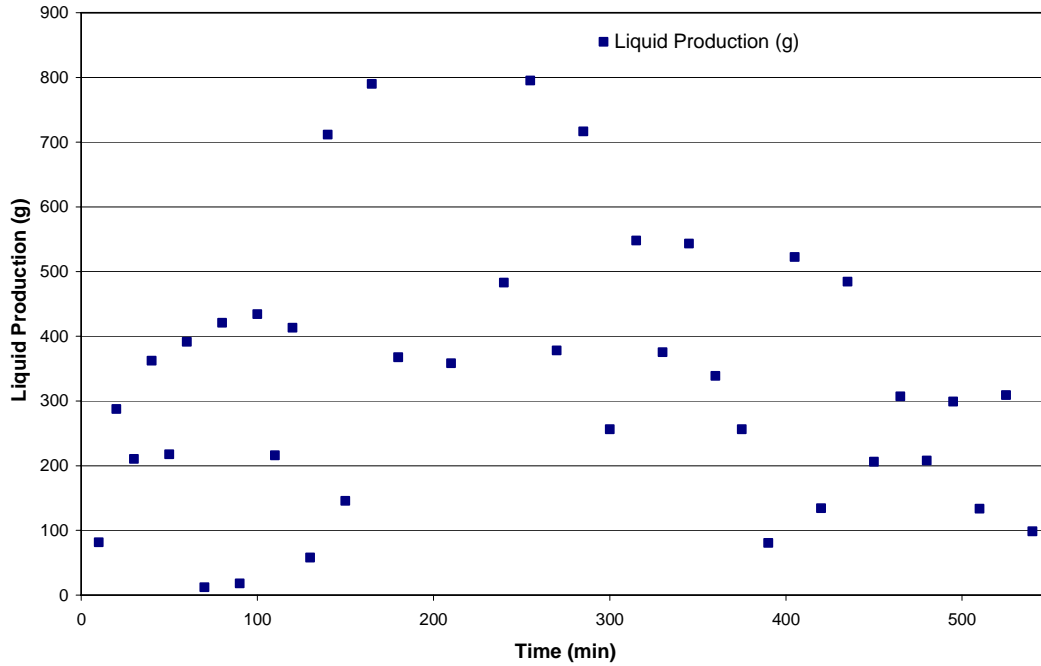


**FIGURE 4-5 LIQUID PRODUCTION AT THE RIGHT SIDE**

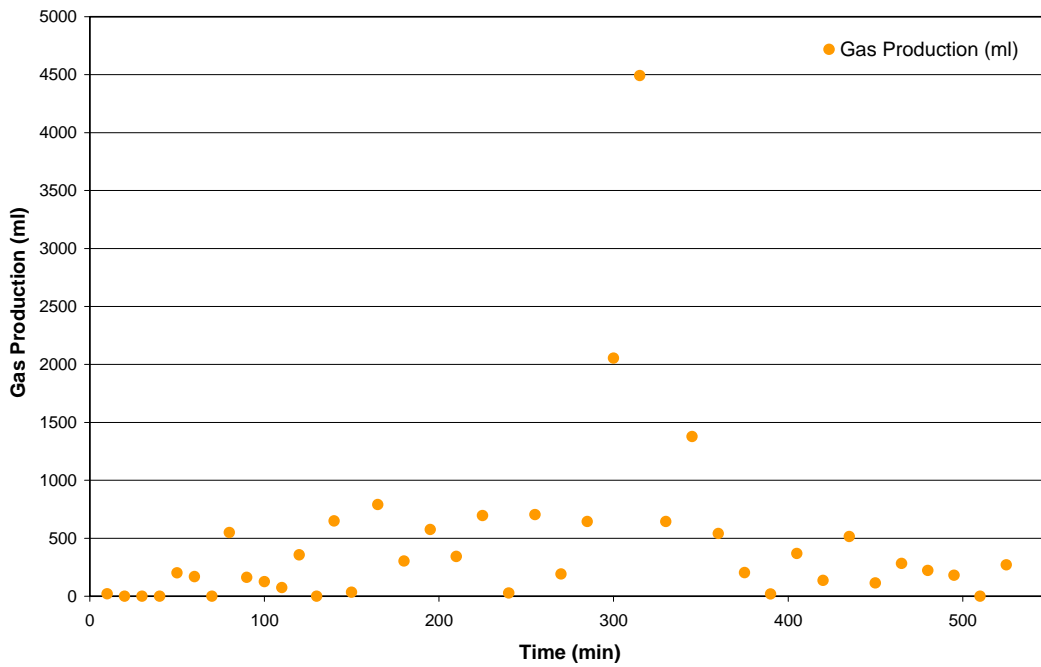


**FIGURE 4-6 GAS PRODUCTION AT THE RIGHT SIDE**

### 4.5 Chamber Temperature Reading

Figures 4-7 through 4-15 present the temperature readings of the test model in 60-minute intervals during the whole experiment. All the red numbers in the following Figures 4-7 through 4-15 are real time logging temperature readings in Celsius.

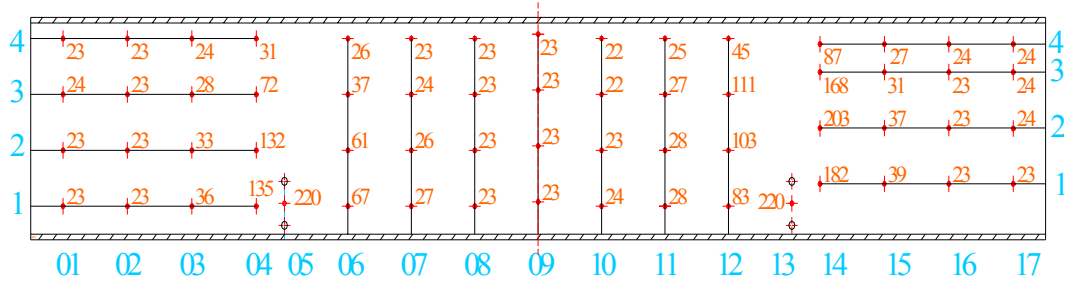


**FIGURE 4-7 REAL TIME LOGGING TEMPERATURE READINGS AT THE 60<sup>TH</sup> MINUTE**

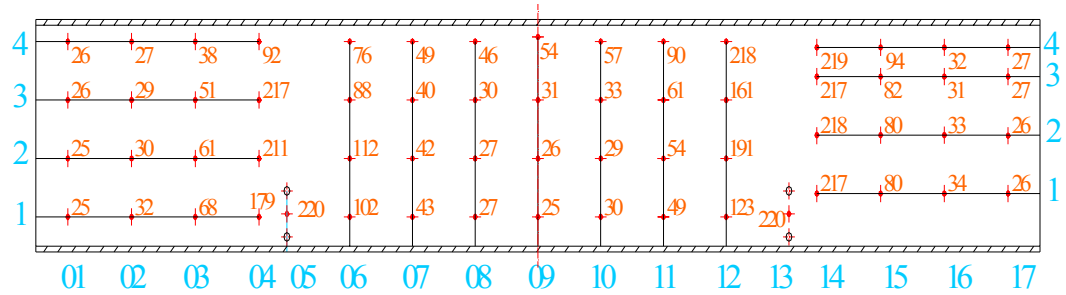


**FIGURE 4-8 REAL TIME LOGGING TEMPERATURE READINGS AT THE 120<sup>TH</sup> MINUTE**

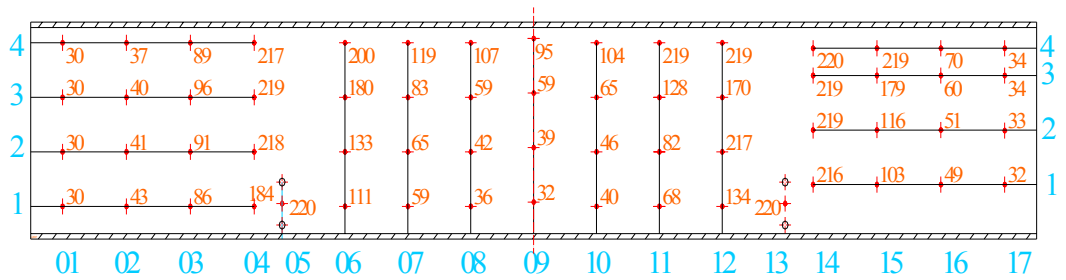


**FIGURE 4-9 REAL TIME LOGGING TEMPERATURE READINGS AT THE 180<sup>TH</sup> MINUTE**

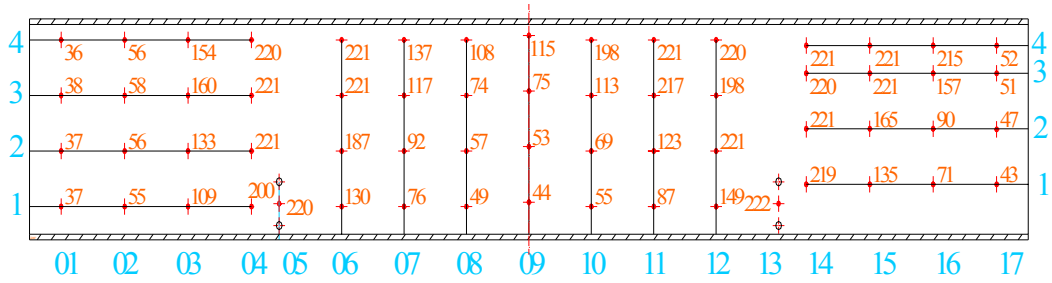


**FIGURE 4-10 REAL TIME LOGGING TEMPERATURE READINGS AT THE 240TH MINUTE**

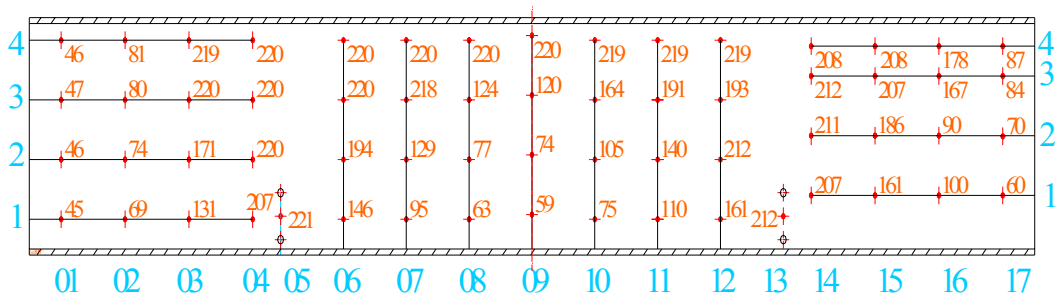


**FIGURE 4-11 REAL TIME LOGGING TEMPERATURE READINGS AT THE 300TH MINUTE**

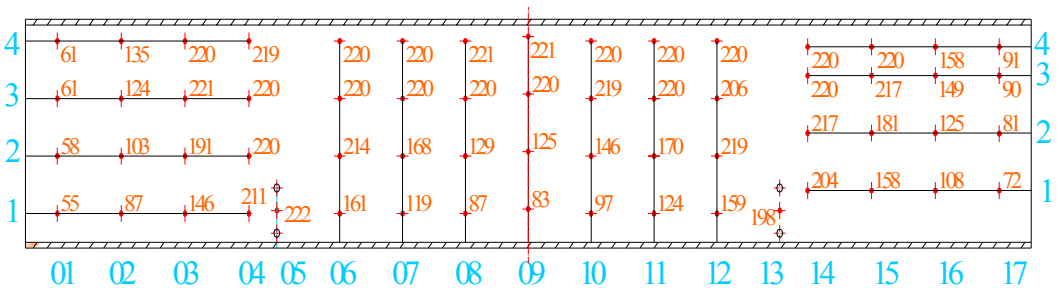


**FIGURE 4-12 REAL TIME LOGGING TEMPERATURE READINGS AT THE 360TH MINUTE**

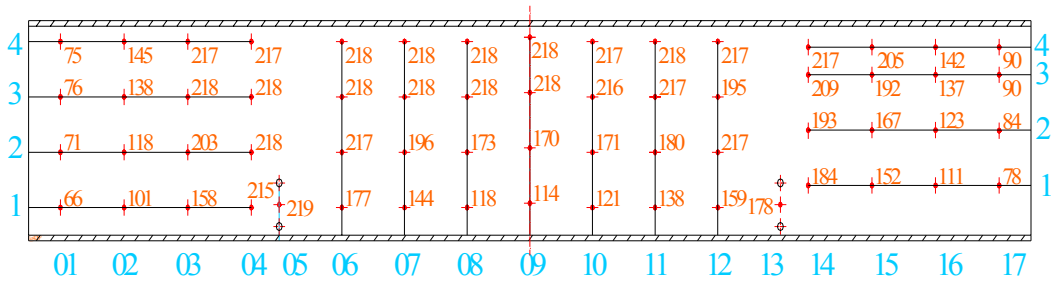


**FIGURE 4-13 REAL TIME LOGGING TEMPERATURE READINGS AT THE 420TH MINUTE**

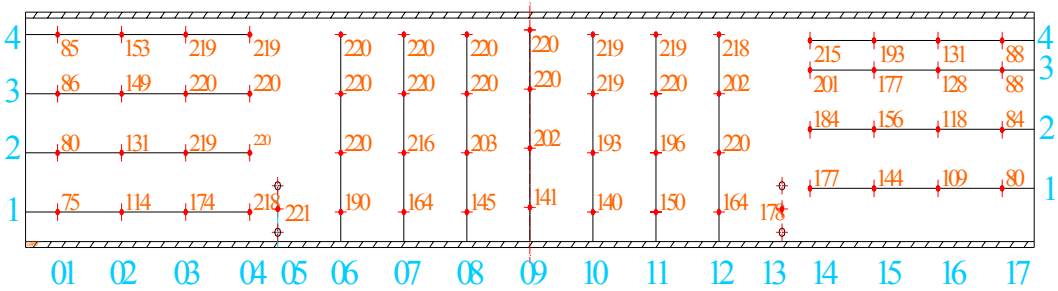


**FIGURE 4-14 REAL TIME LOGGING TEMPERATURE READINGS AT THE 480TH MINUTE**

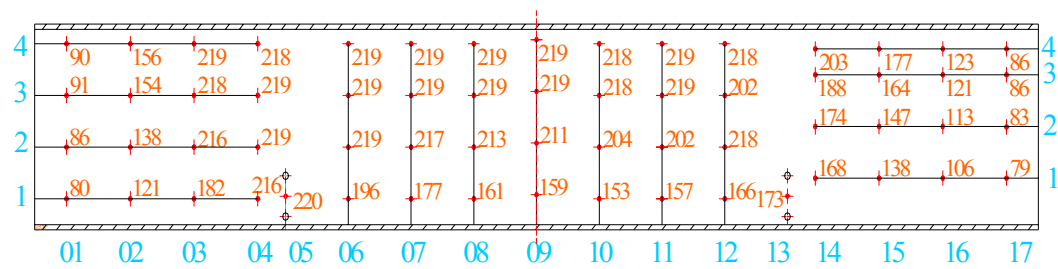


**FIGURE 4-15 REAL TIME LOGGING TEMPERATURE READINGS AT THE 527TH MINUTE**

## 5 RESULTS ANALYSIS AND DISCUSSION

### *5.1 Production Pressure and Rate*

After the experiment was completed, the liquid production samples were carried out for water and oil content analysis by Dean Stark analysis. [Figure 5-1](#) shows the history of production rates of oil, water, and gas from the left side well pair, respectively. [Figure 5-2](#) shows the production behaviors of the right side well pair. After the right steam injector was shut in at the 285<sup>th</sup> minute and the steam injection rate of the left injector doubled, both producers were still able to produce. On the right side, both the oil rate and gas rate started to decrease at around the 360<sup>th</sup> minute, while the water rate was fluctuating. The gas rate of the right producer had a jump point at the 300<sup>th</sup> minute then returned to normal. After the right injector was shut in at the 285<sup>th</sup> minute, oil production from the right producer continued until the end of the experiment.

It was observed that the production rates of both pairs fluctuated significantly during the experiment. The production pressure and differential pressure were investigated to study this trend.

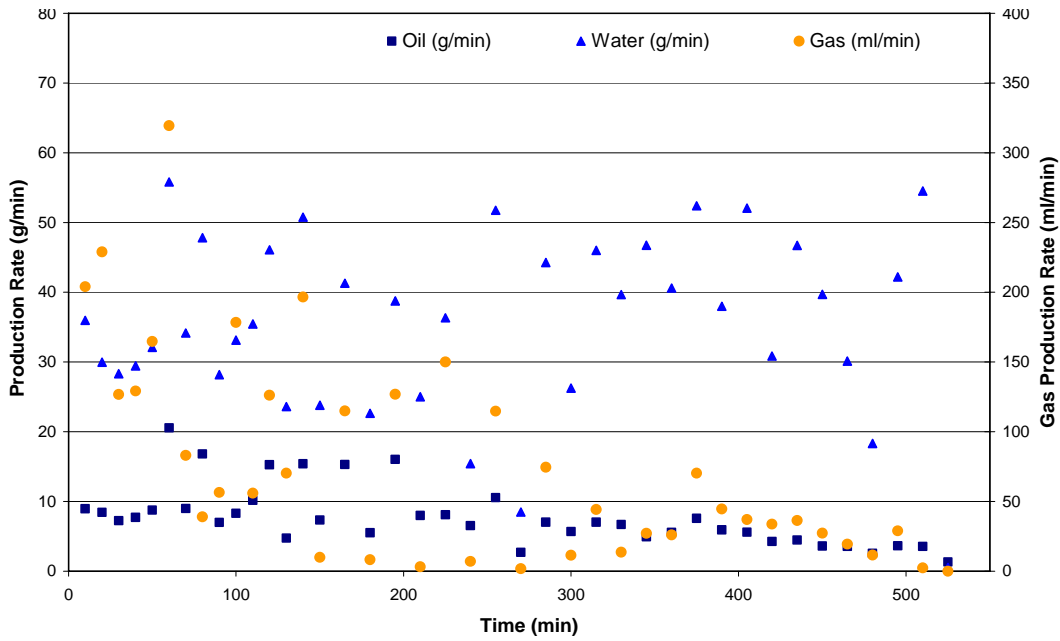


**FIGURE 5-1 PRODUCTION (OIL, WATER, AND GAS) RATE AT THE LEFT PRODUCER**

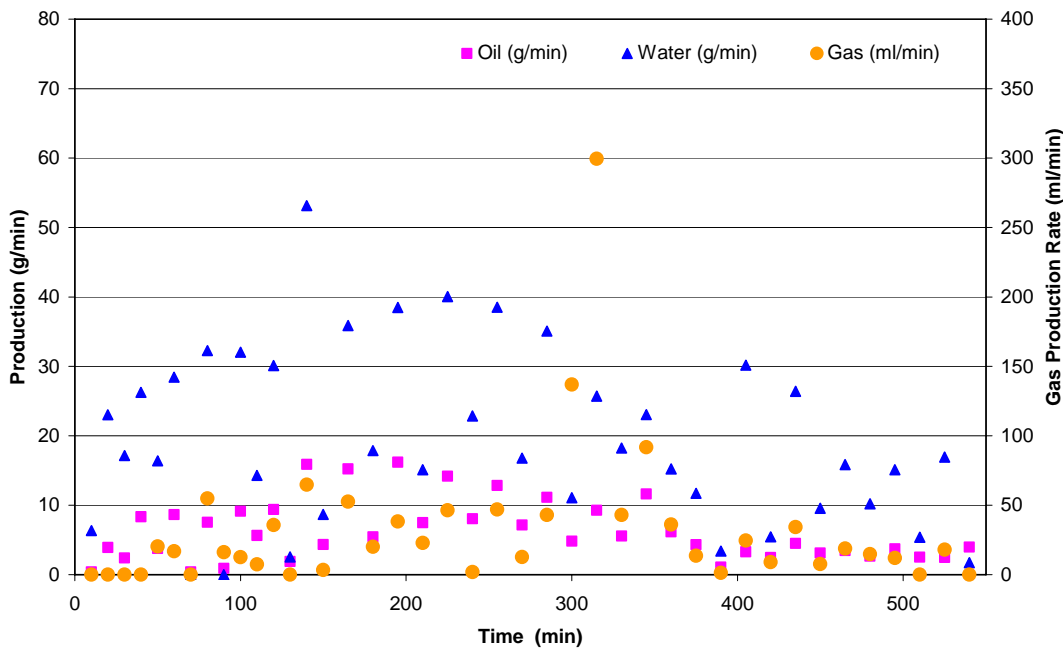


**FIGURE 5-2 PRODUCTION (OIL, WATER, AND GAS) RATE AT THE RIGHT PRODUCER**

Figure 5-3 shows the profiles of production pressures for the two producers and the pressure difference between the two producers. It is noted that the differential pressure (DP) was positive during the first 50 minutes because the initial setting in the Paragon

program for the DP between the two producers ranged from 0 to 200 kPa. At the 50<sup>th</sup> minute, the range was altered to -50~200 kPa. As shown in Figure 5-3, the differential pressure between left side and right side was maintained at a positive value for most of the experimental span after the 230<sup>th</sup> minute, which means that the left producer had a higher pressure than that of the right producer most of the late experimental time.

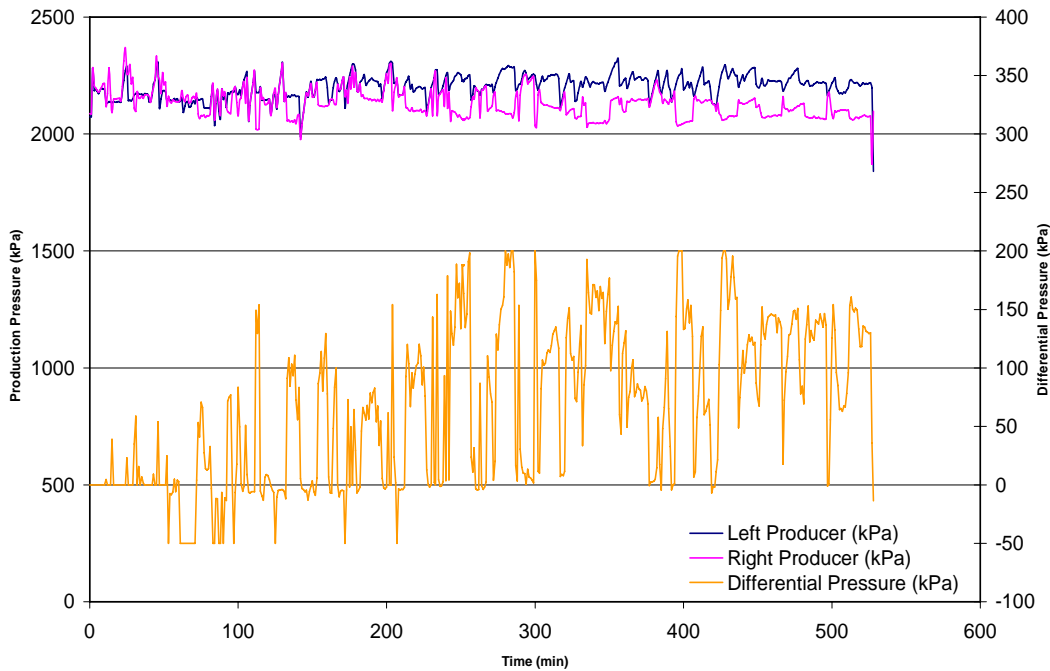


**FIGURE 5-3 PRODUCTION PRESSURE AND DIFFERENTIAL PRESSURE BETWEEN TWO PRODUCERS**

Figure 5-4 and Figure 5-5 show the profiles of liquid production rates (including water and oil) and the DP between the two producing wells. In the first 60 minutes, the variation in liquid rates did not follow the trend of the differential pressure between the two producers. However, after the 70<sup>th</sup> minute, the liquid rates on both well pairs appeared to be closely associated with the trend of the differential pressure between the two producing wells. It is noted that liquid rate on the left well pair increased and the liquid rate on the right side decreased when the differential pressure increased. It seemed that some kind of communication channel existed between the two producing wells. The experimental results indicated that the liquid production was sensitive to the differential pressure between the two producing wells.

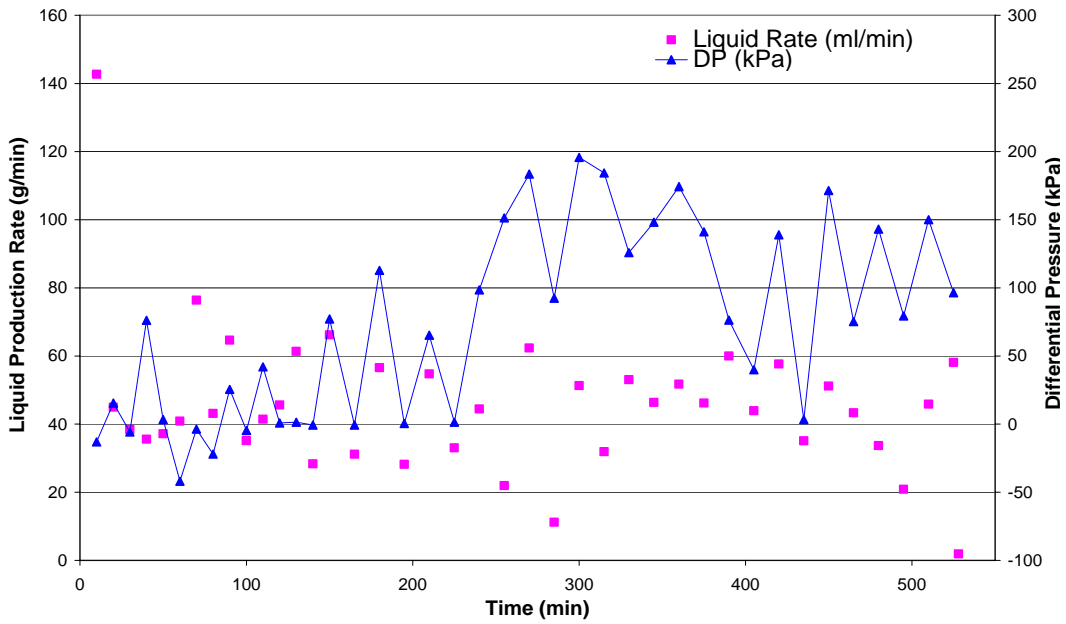


**FIGURE 5-4 DIFFERENTIAL PRESSURE VERSUS LIQUID PRODUCTION RATE AT THE LEFT PRODUCER**

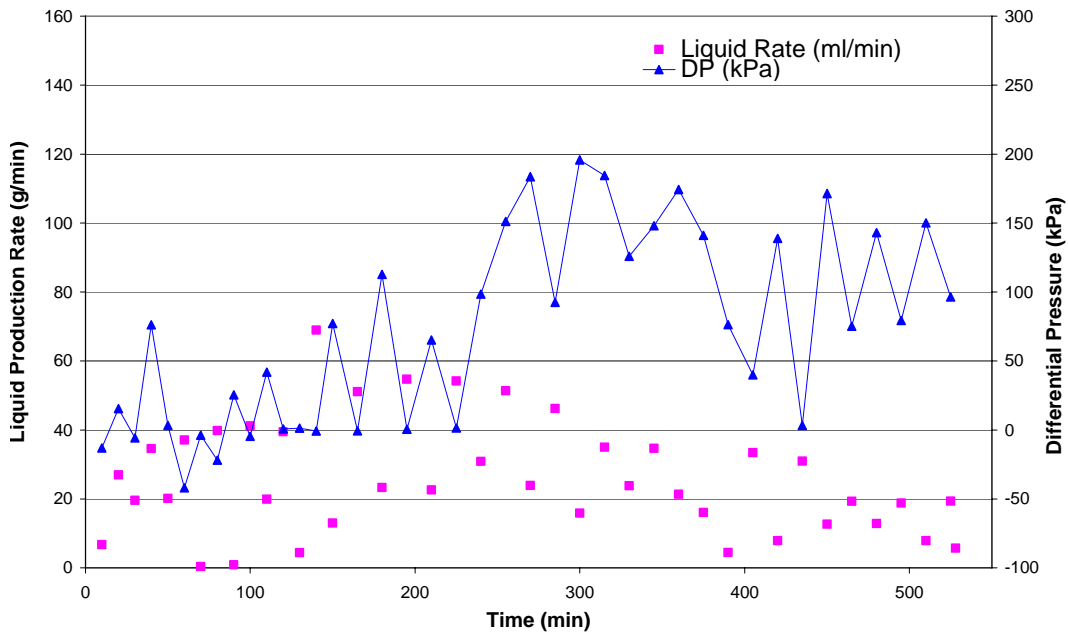


**FIGURE 5-5 DIFFERENTIAL PRESSURE VERSUS LIQUID PRODUCTION RATE AT THE RIGHT PRODUCER**

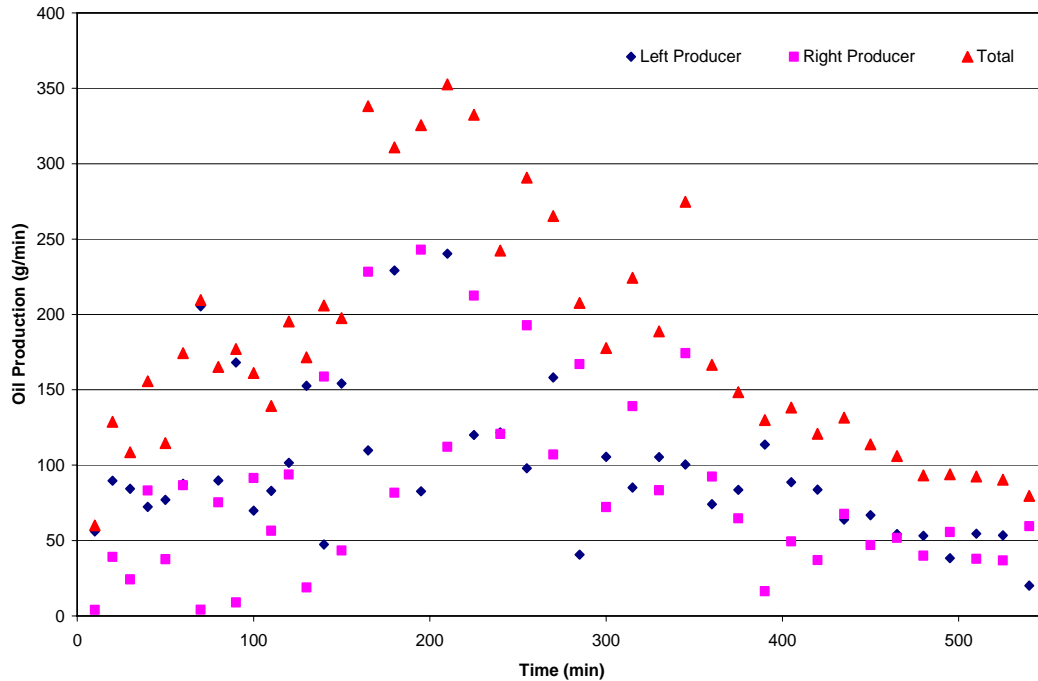


**FIGURE 5-6 OIL PRODUCTION RATES AT BOTH PRODUCERS**

Comparing oil production rates of both well pairs during the whole experiment (plotted in [Figure 5-6](#)) illustrated that the left producer had a higher average oil rate than that of the right side. The peak oil rate appeared at around the 220<sup>th</sup> minute.

## 5.2 Cumulative Production

[Figure 5-7](#) displays the cumulative oil production. The left side produced 3,984 grams of oil, compared with 3,417 grams from the right side. As a result, the left producer had an average oil production rate of 7.7 gram/min while the right one was 6.2 gram/min during the test.

[Figures 5-8](#) shows oil recovery – cumulative oil production (% OOIP) for the individual well pairs. The oil recovery for each well pair was calculated by dividing its cumulative oil production with half of the total initial oil in the whole test cell. The oil recovery from the left side well pair remained higher than that of the right side well pair throughout the test. At the end of the experiment, the oil recovery from the left side well pair was 70% OOIP, while it was 60% OOIP from the right side well pair. The total oil

recovery was 65% OOIP. In order to calculate the recovery factors, it was assumed that the sand pack had uniform porosity, initial oil, and water saturation.

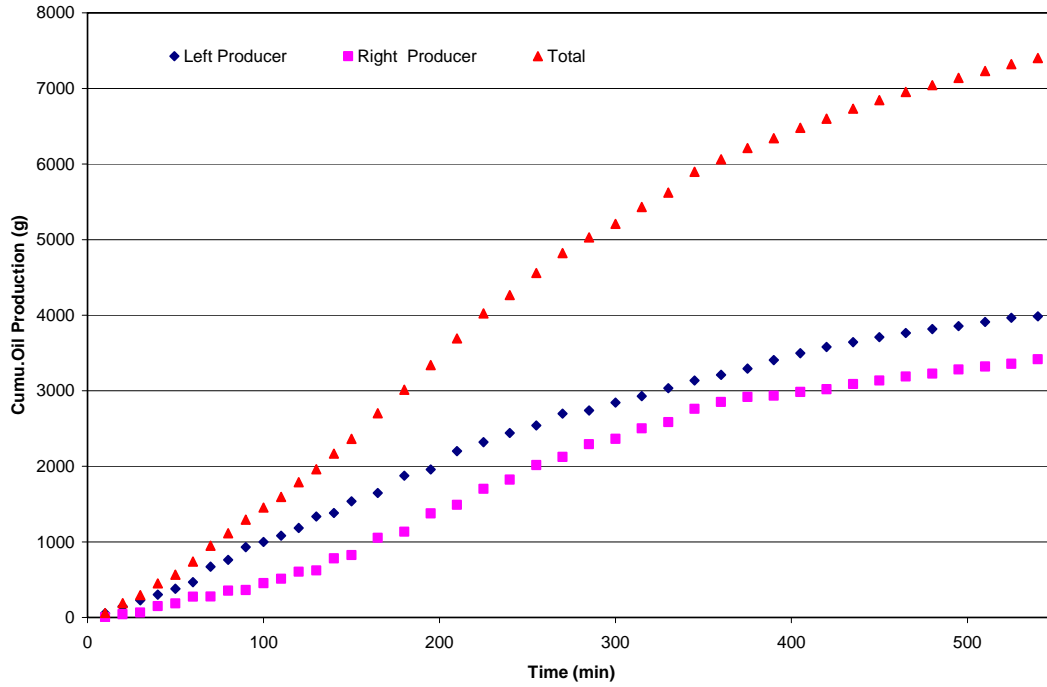


**FIGURE 5-7 CUMULATIVE OIL PRODUCTION OF BOTH PRODUCERS**

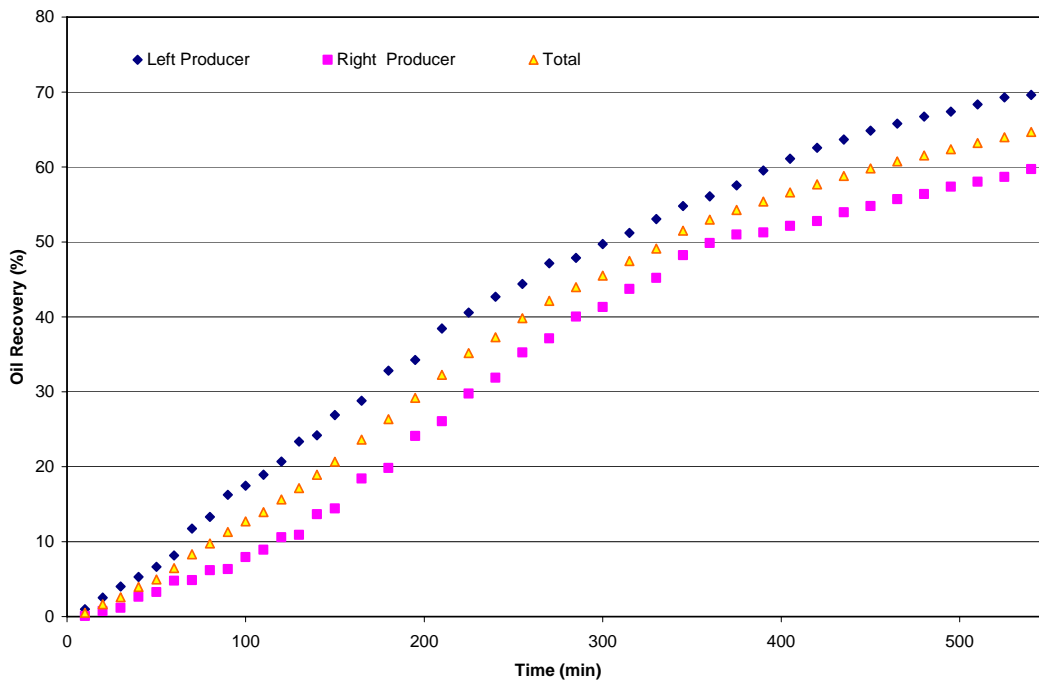


**FIGURE 5-8 OIL RECOVERY OF BOTH PRODUCERS**

The cumulative water and gas production were plotted in the [Figures 5-9](#) and [5-10](#) separately. The left side produced 20,167 grams of water, nearly twice the amount of 10,495 grams from the right side at the end of test. The left side produced 37.3 litres of CH<sub>4</sub>; the right side produced 32.1 litres of CH<sub>4</sub>. A total of 69.4 litres of CH<sub>4</sub> was produced at the end of test. At the 300<sup>th</sup> minute after the right injector was shut in, cumulative gas in the right producer had a dramatic increase. More gas produced from the right producer might be good for chamber growth and hence for creating more oil production.

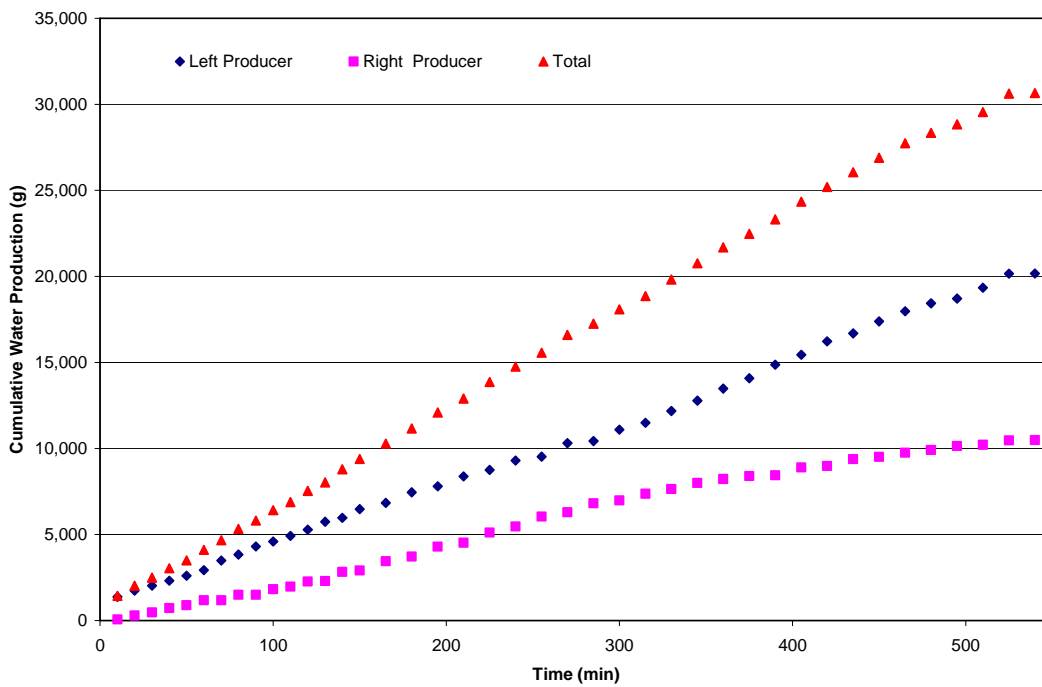


**FIGURE 5-9 CUMULATIVE WATER PRODUCTION OF BOTH PRODUCERS**

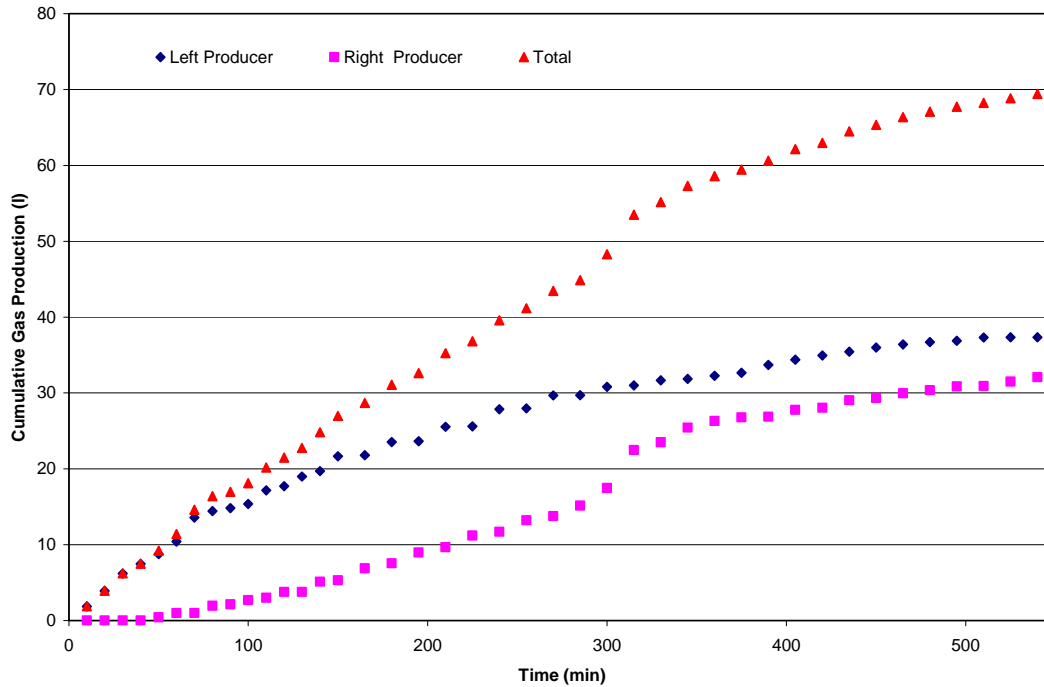


**FIGURE 5-10 CUMULATIVE GAS PRODUCTION OF BOTH PRODUCERS**

### ***5.3 Relationship between Steam Injection and Fluid Production***

Figures 5-11 through 5-14 present the experimental results of steam injection and water production (in terms of cumulative steam injection and water production, and rates of steam injection and water production) for the two producers, respectively. It is noted that before the 300<sup>th</sup> minute, the amount of water produced from the left producer was greater than the amount of steam injected at the left injector, while the right well pair produced less water than the amount of steam injected into the right injector. Figures 5-15 and 5-16 show the experimental results of the total cumulative steam injection and water production, and the rates of total steam injection and water production from both well pairs. It can be seen that the overall water balance in the test was good although the total water production was slightly less than the cumulative steam injection from the entire experimental period. During the period after the right injector was shut-in (at the 285<sup>th</sup> minute), the total water production rate from the two producers was equal to the steam injection rate of the left injector, indicating that a portion of steam injected from the left injector was distributed to the right side steam chamber and produced through the right producer.

Figures 5-17 through 5-20 illustrate the experimental results of steam injection and oil production from individual well pair, respectively. Figures 5-21 and 5-22 display the experimental results of total cumulative steam injection and oil production, rates of total steam injection and water production from the two well pairs. There were 31,093 grams of steam injected from both injectors and 7,402 grams of oil produced from both producers.

Figure 5-23 shows the variation of steam to oil ratio (SOR). During the first 10 minutes of initialization period, the SOR had a very high value since little oil was produced while much steam was injected. Figure 5-24 shows the trend of cumulative steam to oil ratio (cSOR), one of the most important parameters that determine the economics of SAGD. The cSOR had a high value of 21 at the very beginning, and then decreased to 10 at the 20<sup>th</sup> minute, 3.6 at the 285<sup>th</sup> minute, and 4.2 at the end of the test, resulting in an average SOR of 4.2.

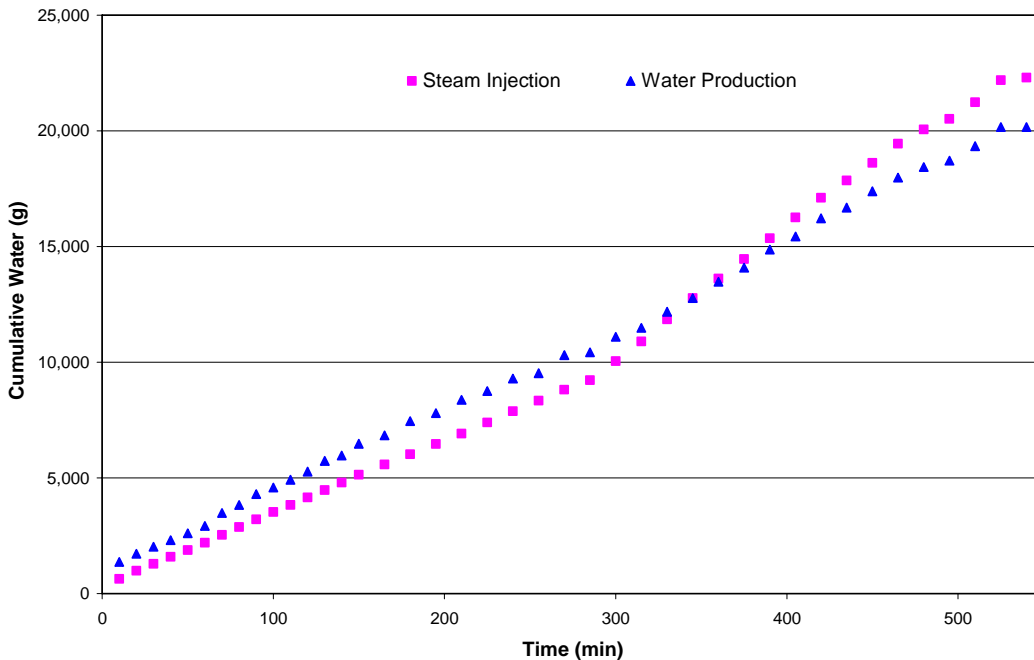


**FIGURE 5-11 COMPARISON OF CUMULATIVE STEAM INJECTION AND WATER PRODUCTION AT THE LEFT PRODUCER**

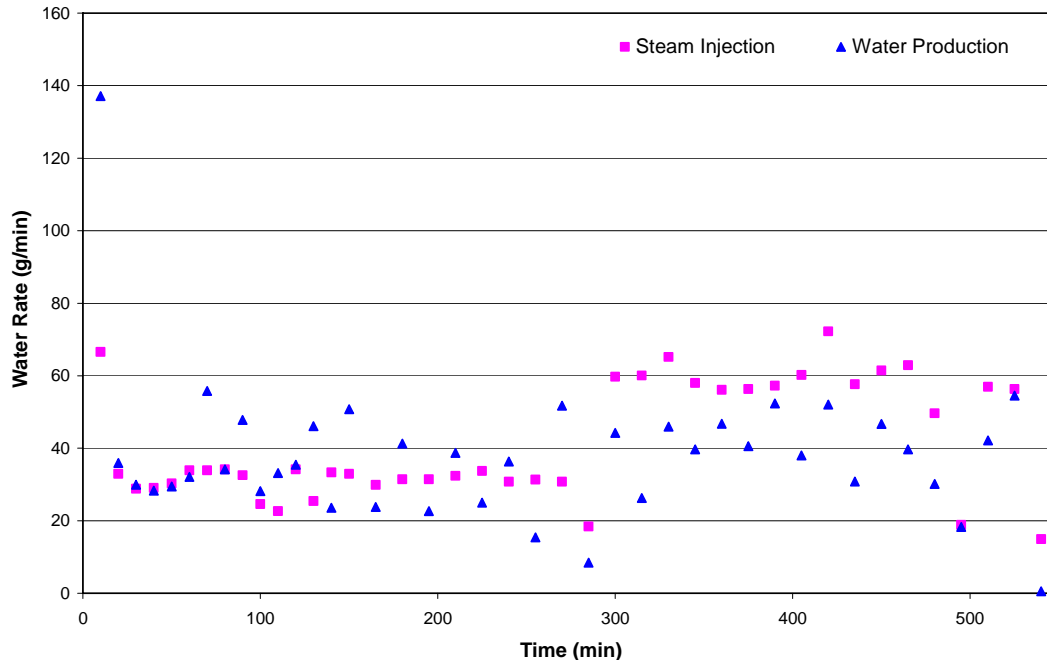


**FIGURE 5-12 COMPARISON OF STEAM INJECTION RATE AND WATER PRODUCTION RATE AT THE LEFT PRODUCER**

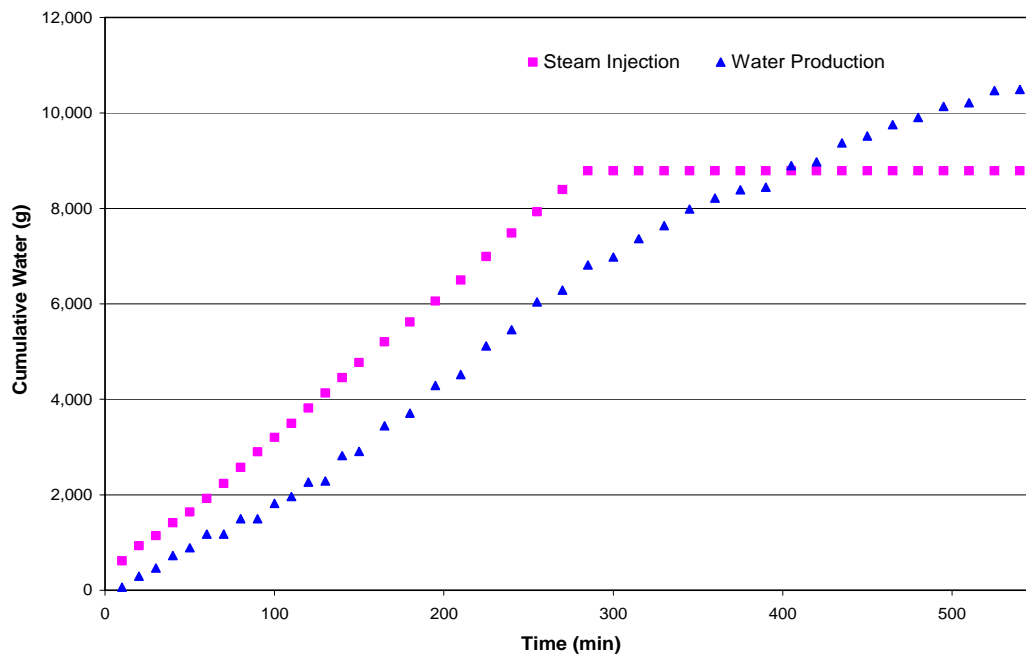


**FIGURE 5-13 COMPARISON OF CUMULATIVE STEAM INJECTION AND CUMULATIVE WATER PRODUCTION AT RIGHT SIDE**

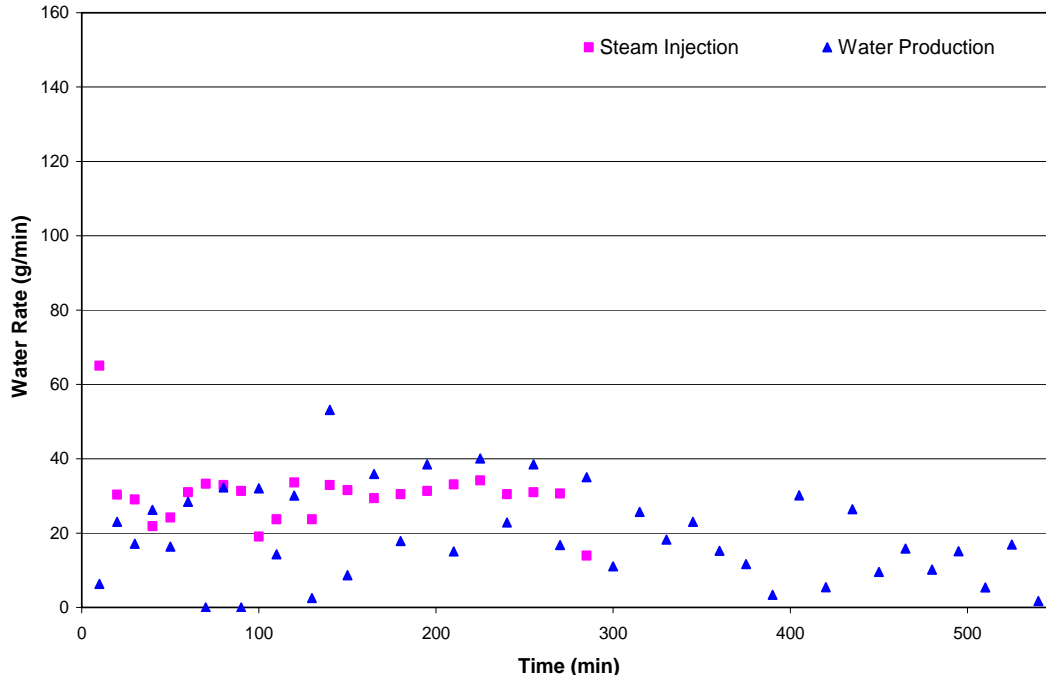


**FIGURE 5-14 COMPARISON OF STEAM INJECTION RATE AND WATER PRODUCTION RATE AT THE RIGHT PRODUCER**

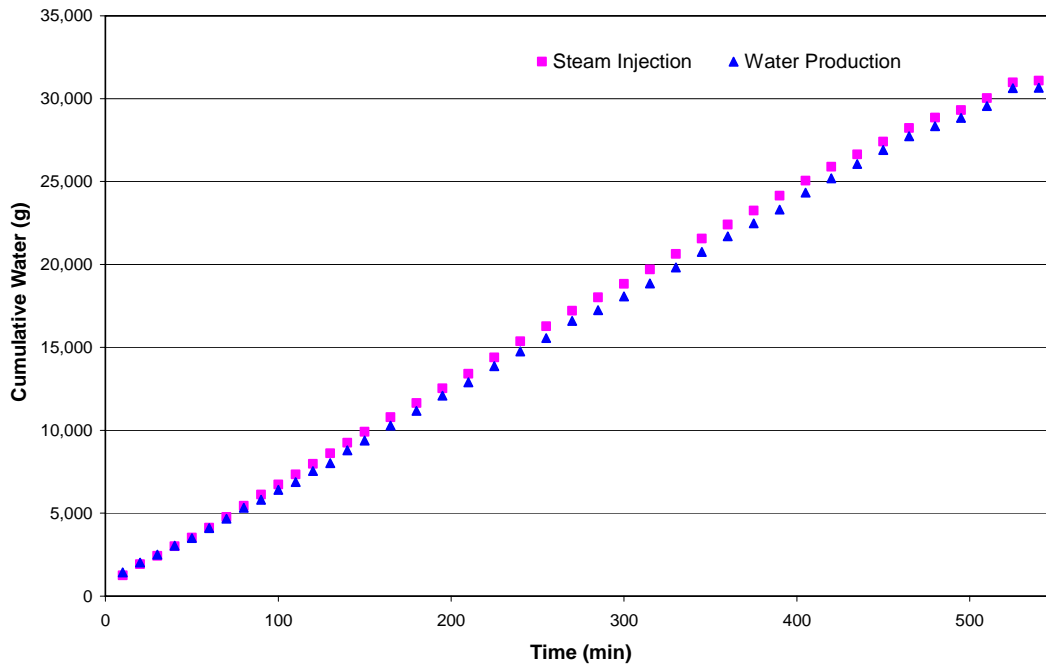


**FIGURE 5-15 COMPARISON OF CUMULATIVE STEAM INJECTION AND CUMULATIVE WATER PRODUCTION IN TOTAL**

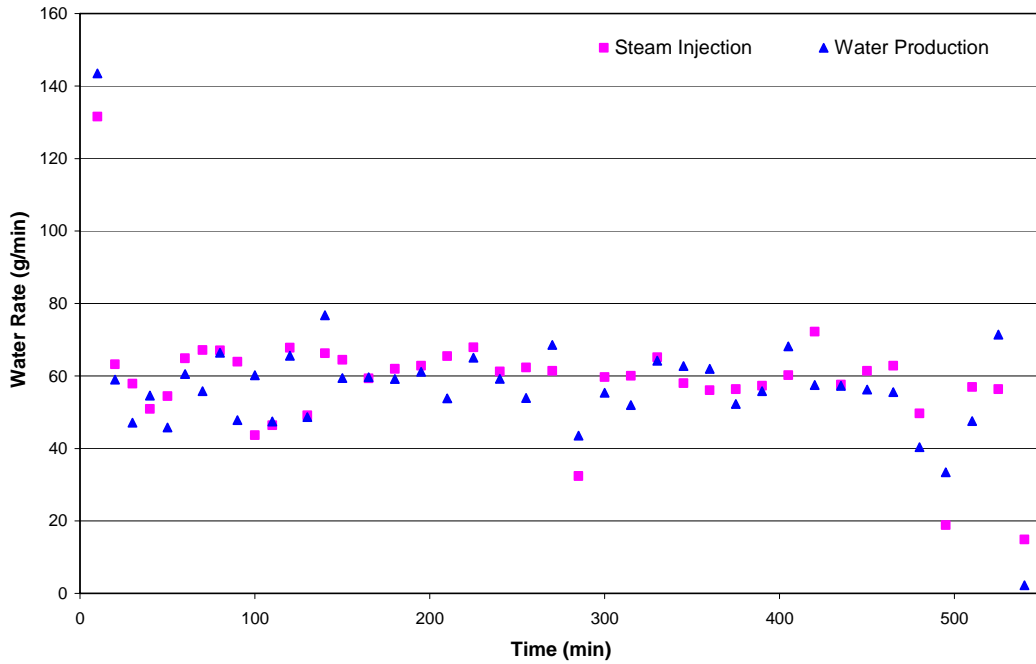


**FIGURE 5-16 COMPARISON OF STEAM INJECTION RATE AND WATER PRODUCTION RATE IN TOTAL**

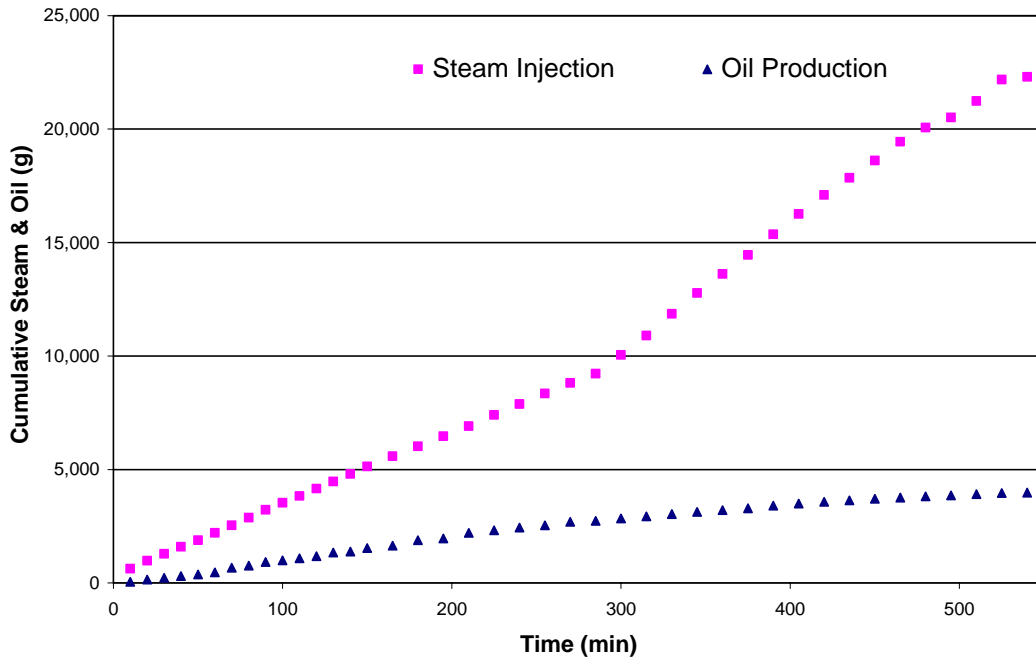


**FIGURE 5-17 COMPARISON OF CUMULATIVE STEAM INJECTION AND CUMULATIVE OIL PRODUCTION AT THE LEFT PRODUCER**

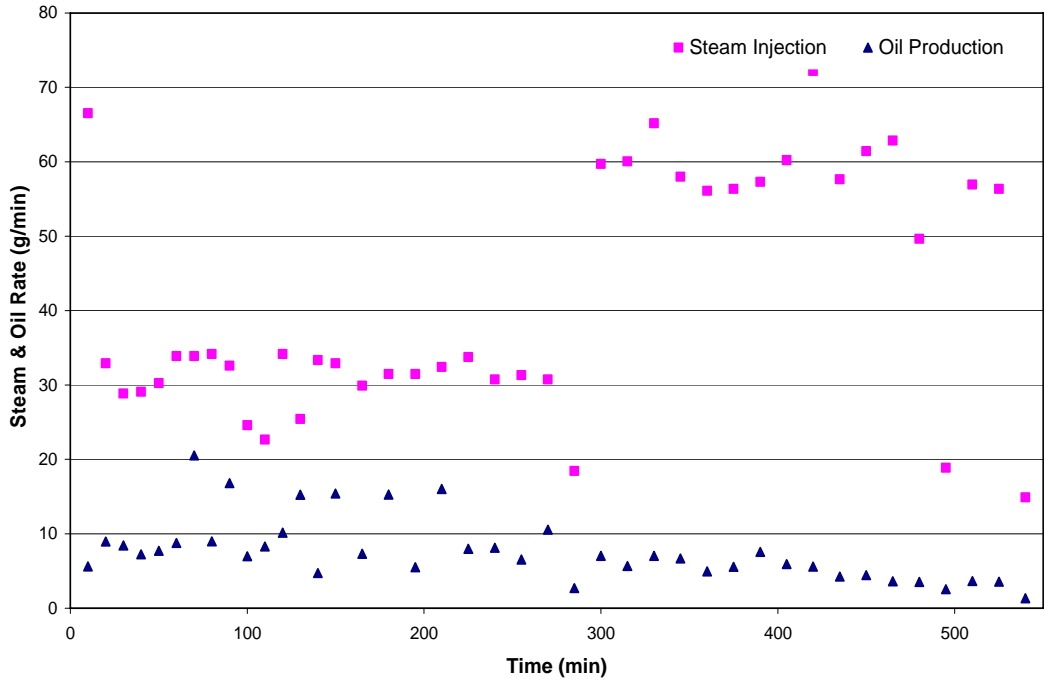


**FIGURE 5-18 COMPARISON OF STEAM INJECTION RATE AND OIL PRODUCTION RATE AT THE LEFT PRODUCER**

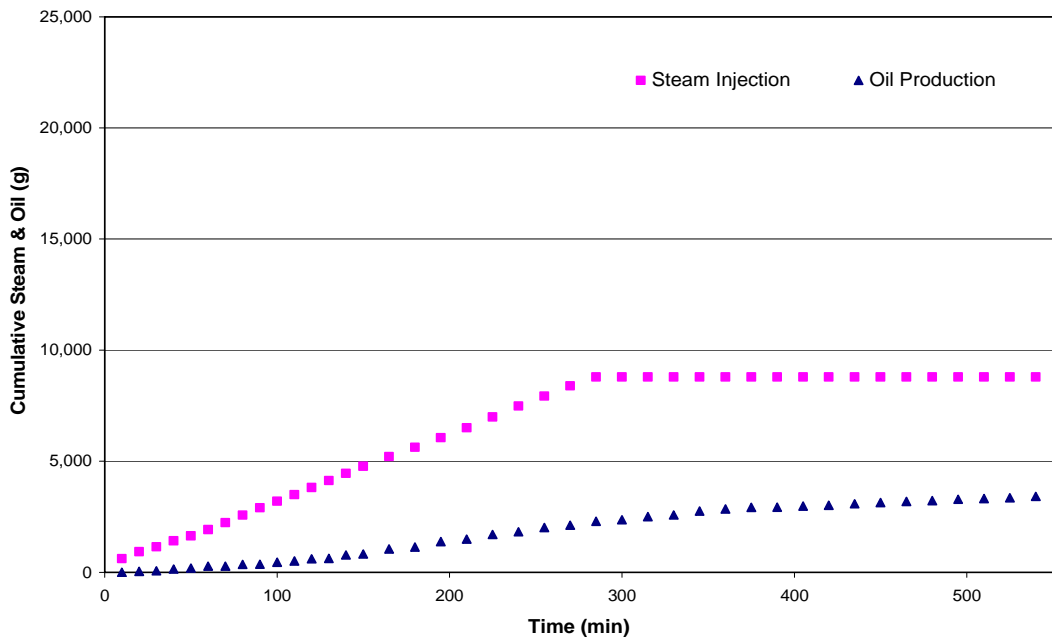


**FIGURE 5-19 COMPARISON OF CUMULATIVE STEAM INJECTION AND CUMULATIVE OIL PRODUCTION AT THE RIGHT PRODUCER**

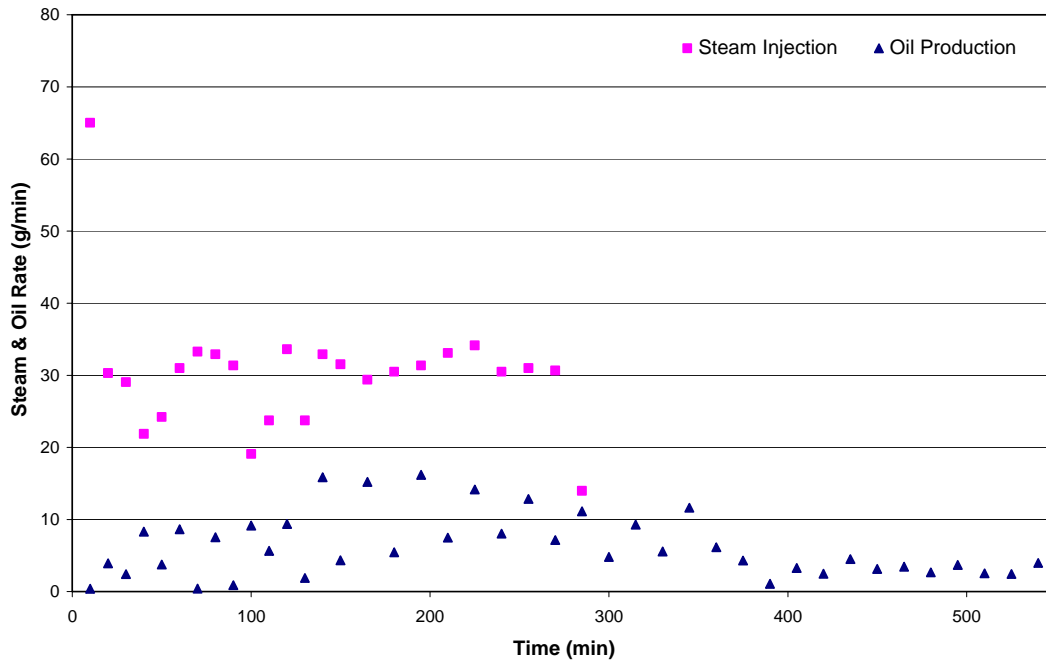


**FIGURE 5-20 COMPARISON OF STEAM INJECTION RATE AND OIL PRODUCTION RATE AT THE RIGHT PRODUCER**

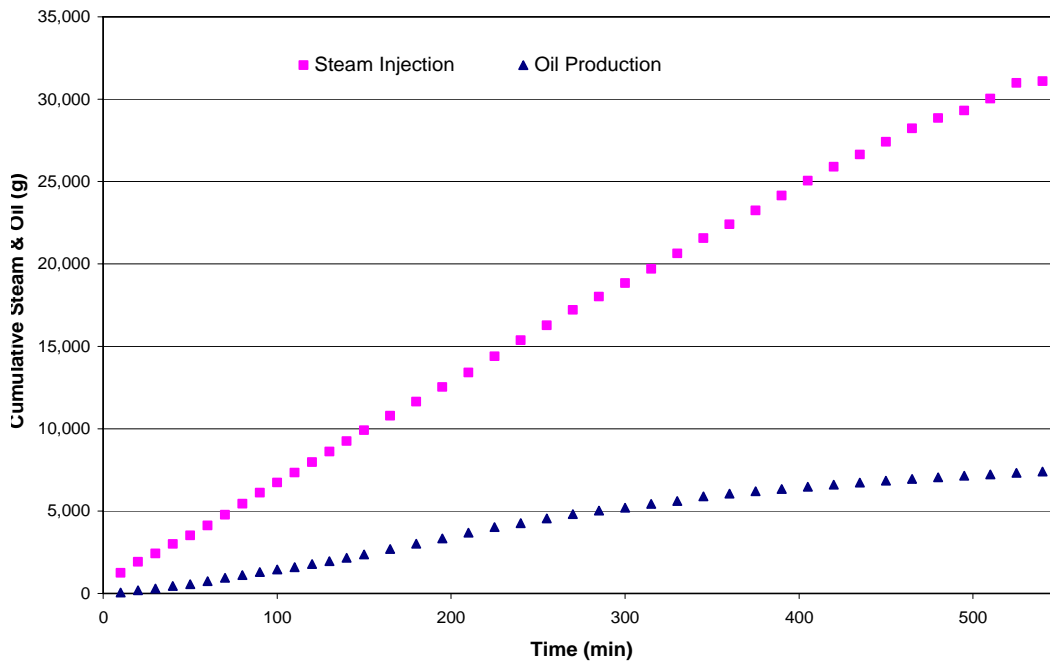


**FIGURE 5-21 COMPARISON OF CUMULATIVE STEAM INJECTION AND CUMULATIVE OIL PRODUCTION IN TOTAL**

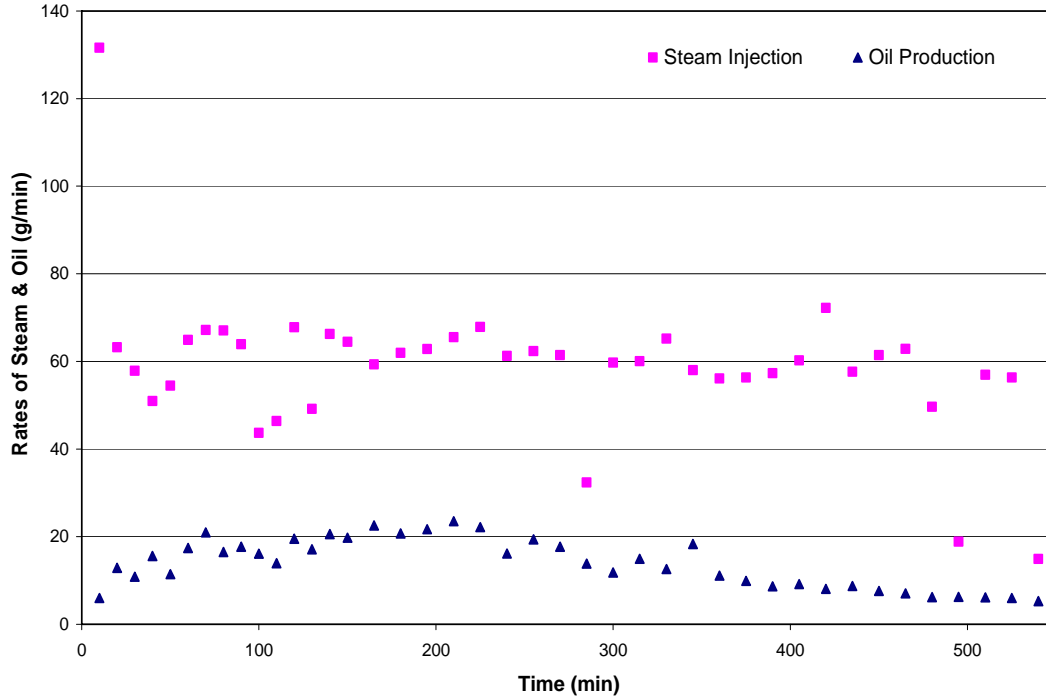


**FIGURE 5-22 COMPARISON OF STEAM INJECTION RATE AND OIL PRODUCTION RATE IN TOTAL**

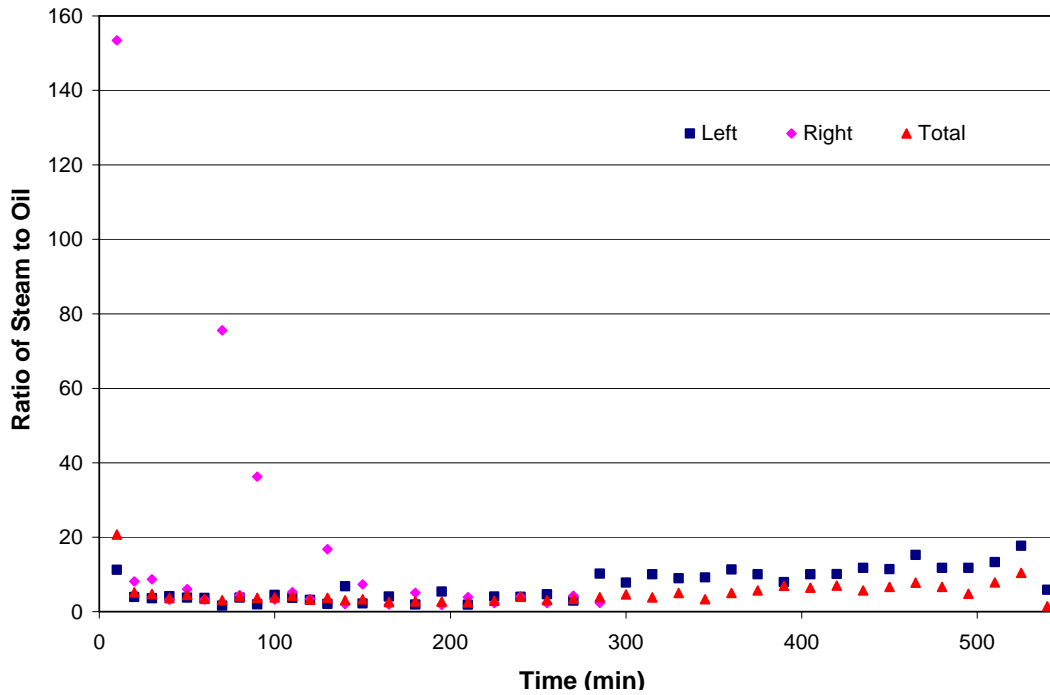


**FIGURE 5-23 SOR (STEAM TO OIL RATIO) PROFILE IN TOTAL**

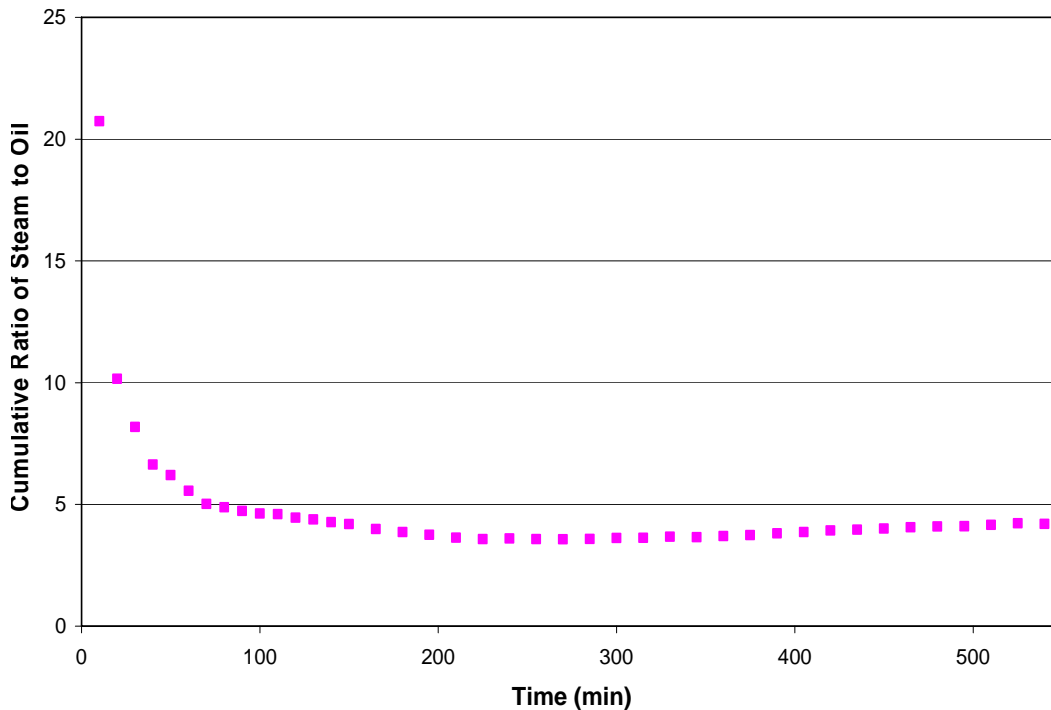


**FIGURE 5-24 CSOR (CUMULATIVE STEAM TO OIL RATIO) PROFILE IN TOTAL**

#### ***5.4 Steam Chamber Development***

Figures 5-25 through 5-42 present the temperature profiles of the test model in 30-minute intervals during the whole experiment. It is noted that both the left side and right side chambers grew mainly upward (predominately in the vertical direction) in the first 90 minutes. The temperature in the top middle part of the test model was only 23°C at the 60<sup>th</sup> minute and started to increase rapidly after the 90<sup>th</sup> minute of running time. It reached 54 °C at the 120<sup>th</sup> minute, 95 °C at the 180<sup>th</sup> minute, and 115 °C at the 240<sup>th</sup> minute; the communication between the chambers established rather quickly. The left chamber grew much more slowly than the right one did. The two steam chambers grew close to merging at about the 180<sup>th</sup> minute running time and became well communicated at the 300<sup>th</sup> minute. However, the temperature increase on the sides of both chambers, opposite to the transition area, indicated the growth was slow.

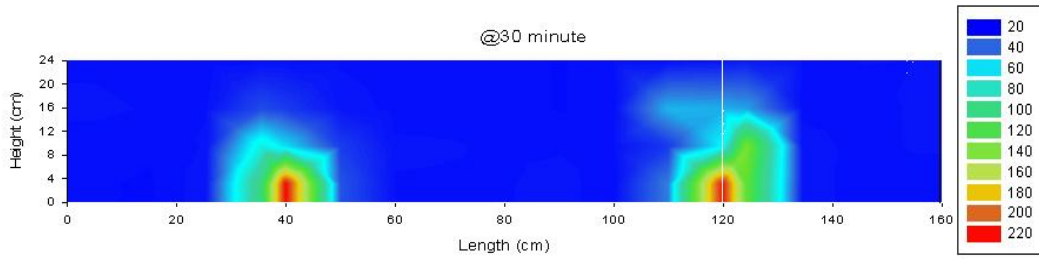


**FIGURE 5-25 TEMPERATURE CONTOUR PROFILE AT THE 30<sup>TH</sup> MINUTE**

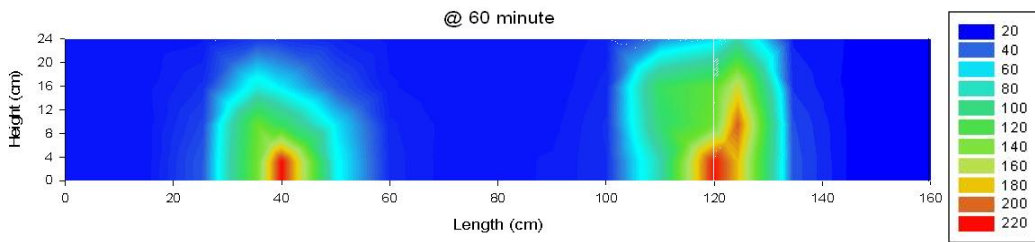


**FIGURE 5-26 TEMPERATURE CONTOUR PROFILE AT THE 60<sup>TH</sup> MINUTE**

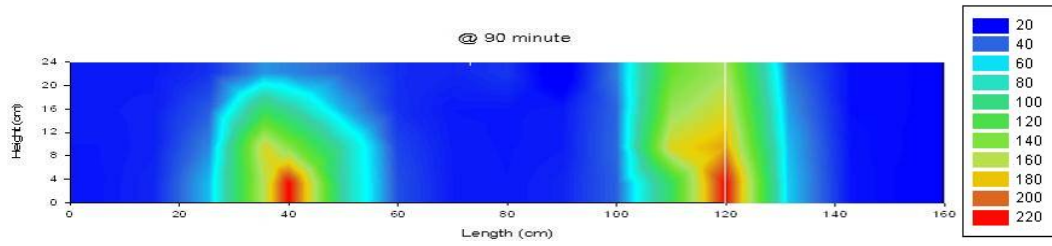


**FIGURE 5-27 TEMPERATURE CONTOUR PROFILE AT THE 90<sup>TH</sup> MINUTE**

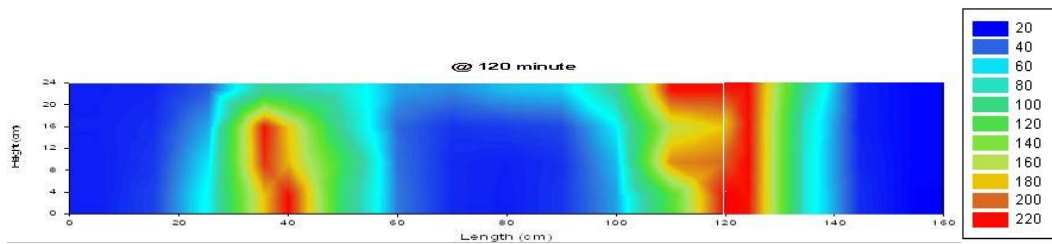


**FIGURE 5-28 TEMPERATURE CONTOUR PROFILE AT THE 120<sup>TH</sup> MINUTE**

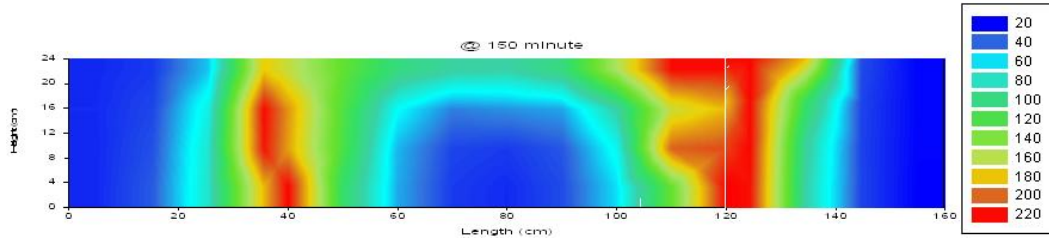


**FIGURE 5-29 TEMPERATURE CONTOUR PROFILE AT THE 150<sup>TH</sup> MINUTE**

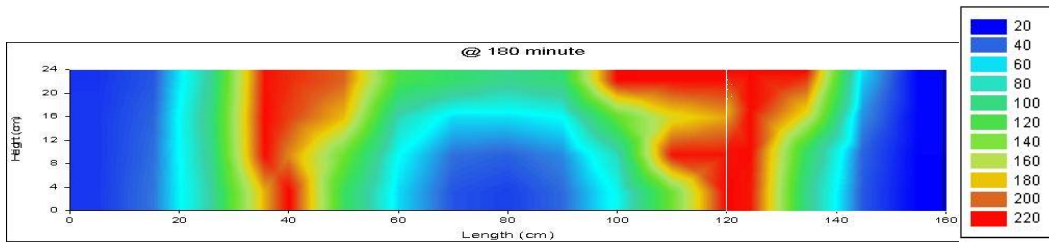


**FIGURE 5-30 TEMPERATURE CONTOUR PROFILE AT THE 180<sup>TH</sup> MINUTE**

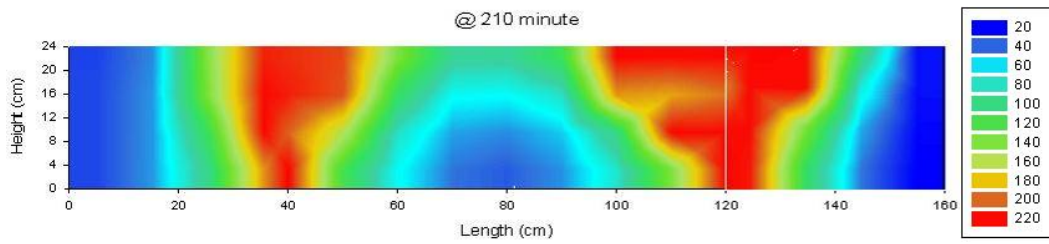


**FIGURE 5-31 TEMPERATURE CONTOUR PROFILE AT THE 210<sup>TH</sup> MINUTE**

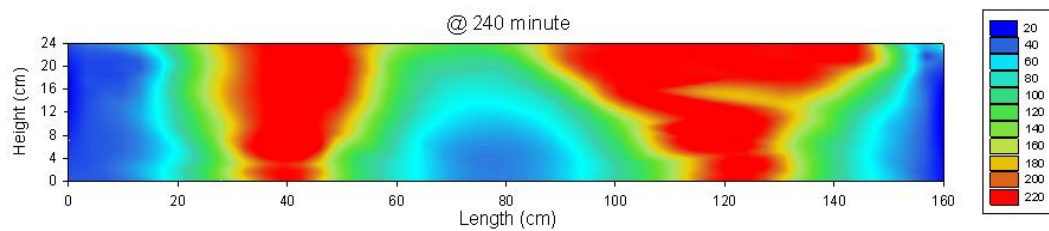


**FIGURE 5-32 TEMPERATURE CONTOUR PROFILE AT THE 240<sup>TH</sup> MINUTE**

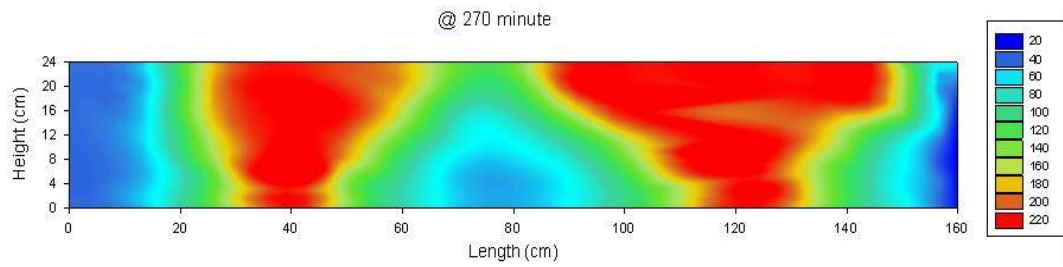


**FIGURE 5-33 TEMPERATURE CONTOUR PROFILE AT THE 270<sup>TH</sup> MINUTE**

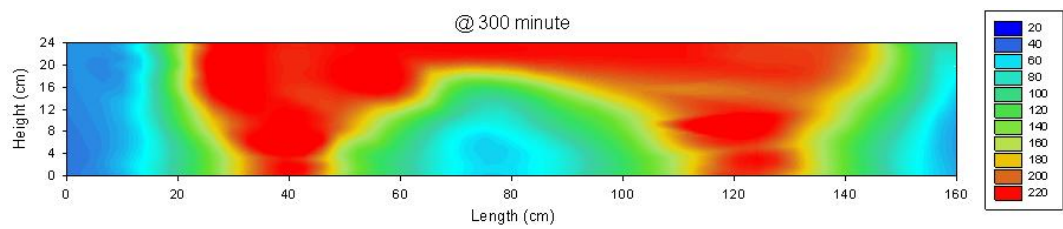


**FIGURE 5-34 TEMPERATURE CONTOUR PROFILE AT THE 300<sup>TH</sup> MINUTE**

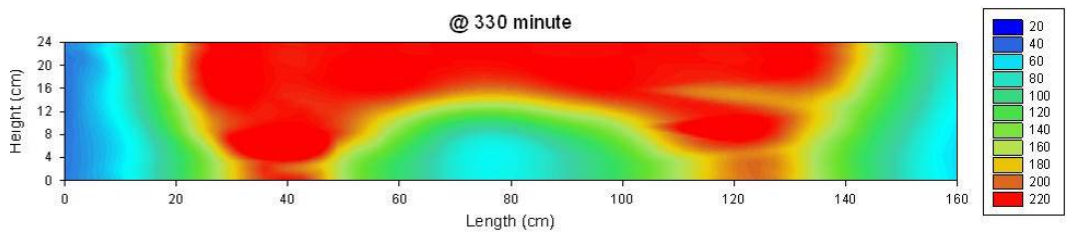


**FIGURE 5-35 TEMPERATURE CONTOUR PROFILE AT THE 330<sup>TH</sup> MINUTE**

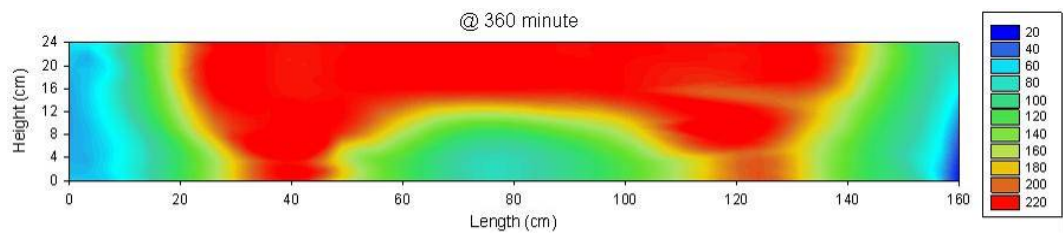


**FIGURE 5-36 TEMPERATURE CONTOUR PROFILE AT THE 360<sup>TH</sup> MINUTE**

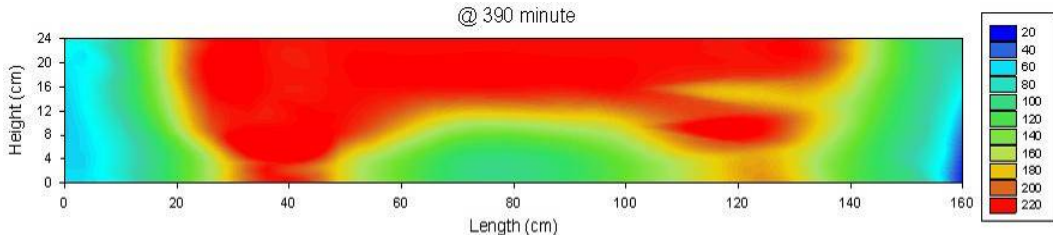


**FIGURE 5-37 TEMPERATURE CONTOUR PROFILE AT THE 390<sup>TH</sup> MINUTE**

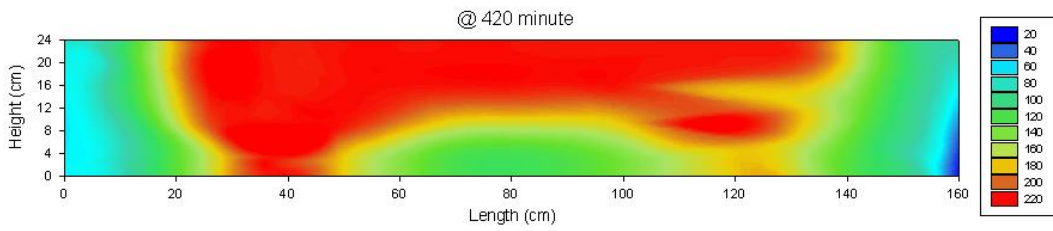


**FIGURE 5-38 TEMPERATURE CONTOUR PROFILE AT THE 420<sup>TH</sup> MINUTE**

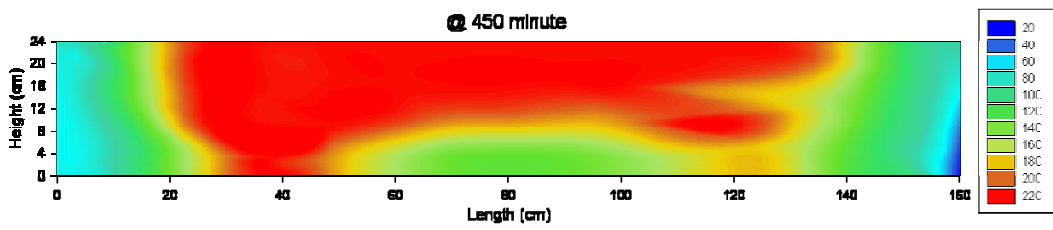


**FIGURE 5-39 TEMPERATURE CONTOUR PROFILE AT THE 450<sup>TH</sup> MINUTE**

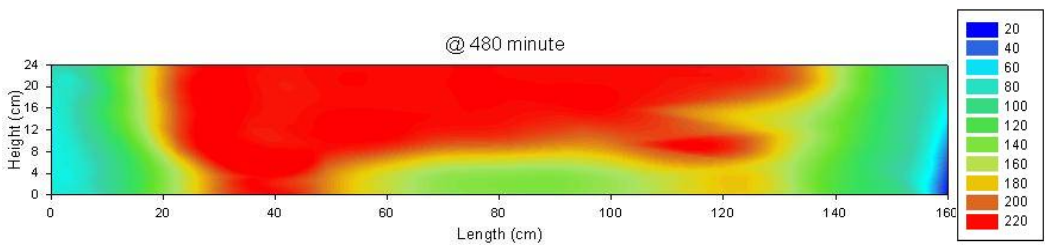


**FIGURE 5-40 TEMPERATURE CONTOUR PROFILE AT THE 480<sup>TH</sup> MINUTE**

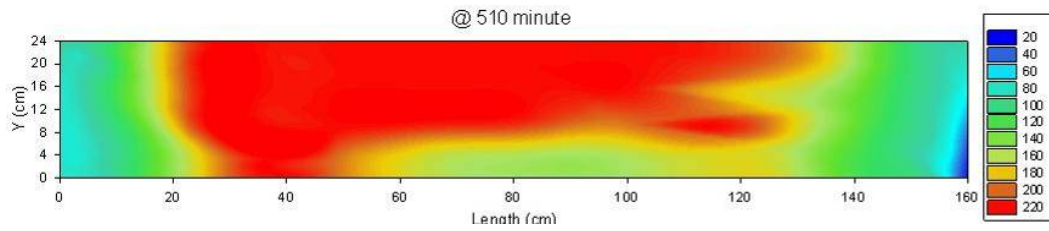


**FIGURE 5-41 TEMPERATURE CONTOUR PROFILE AT THE 510<sup>TH</sup> MINUTE**

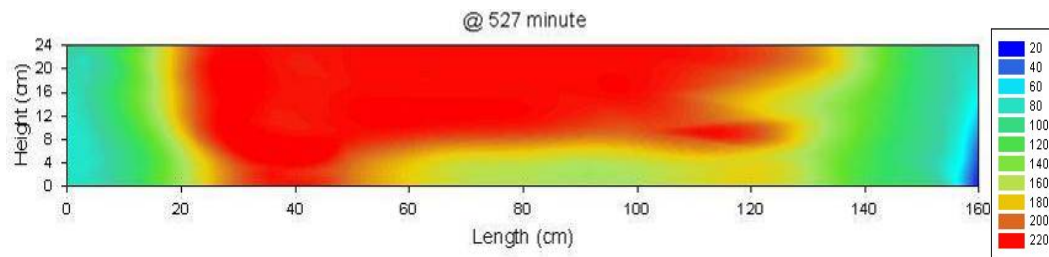


**FIGURE 5-42 TEMPERATURE CONTOUR PROFILE AT THE 527<sup>TH</sup> MINUTE**

### ***5.5 Residual Oil and Water Distribution***

The test model was removed from within the confinement vessel and unpacked after the test. The test model is shown in [Figure 5-43](#) after the top lid was cut open and removed by grinding the welded edges.



**FIGURE 5-43 TEST MODEL AFTER THE TOP LID WAS CUT OPEN**

The post run sand pack was sampled into collection jars in 3 cm height and 10 cm length intervals from left side to right one, which created 8 layers and 16 sections per each layer. This produced total 128 sections for determining the contents of residual bitumen and

water. Figure 5-44 shows the left half part of the top layer of the test model after the Teflon plate was removed from the test cell.



**FIGURE 5-44 LEFT HALF PORTION OF THE TOP LAYER OF TEST MODEL**

Figure 5-45 shows the third layer of the test model after the top two layers were removed and sampled. Figure 5-46 snapped the oil sand remaining near the left pair wells at the bottom layer of the test model. It is noted that the colour of oil sands sample in the test cell got darker and darker with the depth increasing



**FIGURE 5-45 THIRD LAYER OF THE TEST MODEL AFTER THE SECOND ONE WAS SAMPLED**

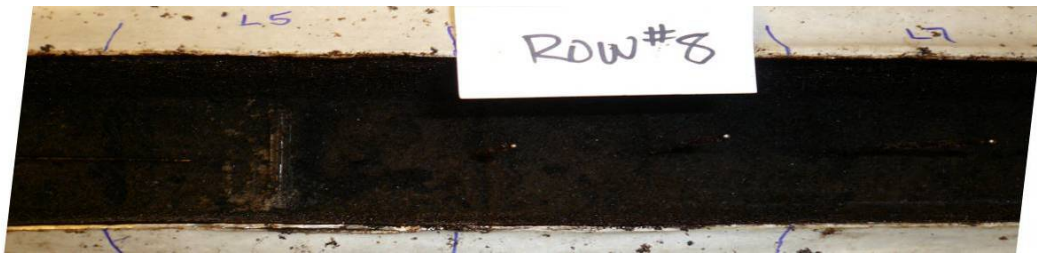


**FIGURE 5-46 THE OIL SAND REMAINED NEAR THE LEFT PAIR WELLS AT THE BOTTOM LAYER OF THE TEST MODEL**

After the model was excavated empty, it was then thoroughly washed out with toluene and the washings were likewise analyzed for total oil, water and solids. The oil sand pack samples as well as the fluid samples were analysed for the contents of bitumen and water. Considering the high temperature in the test cell at the end of the test, the

movement of fluids including oil and steam was hard to be stopped and stilled. Therefore, it is impractical to attain the real profile of residual oil/water saturation in the cell at the end of the test. [Figure 5-47](#) is believed to best represent the profile of residual oil saturation in the cell at the end of the test. The profile of residual water saturation shown in [Figure 5-48](#), is the best to schematically demonstrate the status at the end of the test.

It is noted that residual oil saturation in the region between the well pairs was lower than in the offset regions, suggesting that the operation strategy of sweeping the oil between the two well pairs worked properly. Relatively high residual water saturation at the bottom between the two well pairs reflected the fact that water drained from the top to the bottom and accumulated before it was produced from the producers during the experimental run.

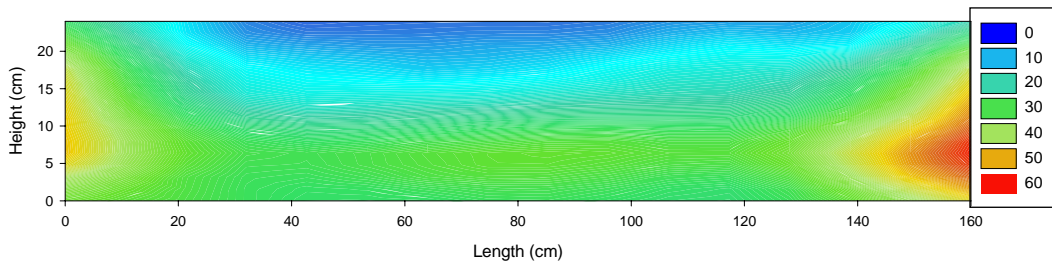


**FIGURE 5-47 RESIDUAL OIL SATURATION (%) OF THE TEST CELL**

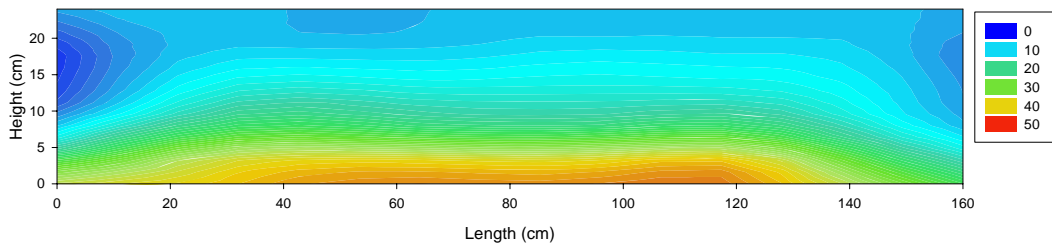


**FIGURE 5-48 RESIDUAL WATER SATURATION (%) OF THE TEST CELL**

## ***5.6 Well Production Behaviour***

After the right injector was shut-in at the 285th minute, oil production from the right producer continued until the end of the experiment. It was indicative that a portion of the steam injected from the left injector drove oil at the top transition region moving to the right side and produced it through the right producer. This observation demonstrated that the operation strategy of one injection well and two production wells works properly.

The fluid production from both producers occasionally experienced choking during the whole experiment. The flow rates varied simultaneously with the change made to the back pressure. It was necessary to adjust the back pressures through the back pressure regulators to maintain production. It was also observed that the back pressure change in one production well could influence the production in the other well pair. In fact the bitumen viscosity dropped dramatically with the rising temperature in the sand pack, which brought down the bitumen mobility ratio in the middle region of the sand pack. Some communication between the two steam chambers could happen because of fluctuating pressure. Apparently, control of differential pressure is a challenge in operating this type of experiment. More sophisticated pressure control systems/devices and modifications to the test facility are needed to allow better tuning of back pressures.

## ***5.7 Steam Chamber Behaviour***

It is noted that some of the temperature contours do not display smooth shapes, as shown in [Figures 5-28, 5-29, 5-30, 5-31, and 5-32](#). The main reason is that all the temperature contours were generated using data acquired from the measurement points. Increasing temperature measurement points in the test model would help generate a smoother contour representation of temperature profile. However, in the laboratory, the number of measurement points is limited to the capability of the data acquisition system. Additionally, installing a large number of thermocouples in the model cell could create other adverse effects, such as increasing the risk of fluids fingering or channelling along the thermocouples, and conduction of heat along the thermocouple rods.

The temperature at the location of thermocouple #93 (Figure 3-7) was obviously lower than the surrounding area, which resulted in a big chasm on the temperature contour in Figures 5-28, 5-29, 5-30, 5-31, and 5-32. All the temperature readings on the rod T\_W\_120 or point thermocouple #93 (Figure 3-7) were checked to insure temperature increased gradually from the very beginning to the end. It is reasonable to believe that the thermocouple itself was in good condition and worked well during the test. One possible cause might be that insufficient thermocouple distribution resulted in inadequate temperature representation in the local region. However, this abnormal behaviour would disappear when the temperature gradient was reduced, which can be seen in the Figures 5-39 and 5-40. In fact, this irregular behaviour can not be distinguished in the temperature readings in Figures 4-8, 4-9, and 4-10, which show temperatures growing smoothly and gradually. The other possibility is that one patch of oil residing in the region around that point did not drain as fast as the adjacent oil, and hence the steam entered more slowly into this area than into the adjacent area.

The temperature in the regions near both side walls of the model increased very slowly. Even after the two chambers had connected for a while, the temperatures in areas near both side walls were still relatively low. This can be explained by means of heat balance between heat loss and gain. Initially, the vertical heat loss (upward and downward) was very little since the area for heat to be conducted away was small. With steam progressing and chambers expanding vertically and sideward, heat is lost by vertical and sideway conduction, both upwards and downwards from chamber regions. The interfacial area between chambers and adjacent cold region got bigger as the chamber grew. The rate of heat loss increased, especially toward both sides. Such loss had the effects of reducing the heat available to advance the chamber front toward both side walls and reducing the quality of the steam that was flowing. The rate of heat gain from steam to drive the steam front sideways was slightly greater than the rate of heat loss. The fraction of the injected heat available to advance the front laterally toward both side walls became smaller as the front advanced. However, in the middle region of the test model, the heat loss accumulated to warm the oil sands in the transition region.

The high temperature zone at the right side well pair started to shrink after 285 minutes when the right injector was shut-in, while the high temperature zone in the left side well

pair and the middle part between the two well pairs continued to grow (comparing the temperature profiles at different stages between the 300<sup>th</sup> and 528<sup>th</sup> minute). These observations suggested that the steam injected from the left injector moved to the right producer, thus resulting in high oil production between the two well pairs; on the other hand, the steam injected from the left injector did not reach the upper right side of the right well pair steam chamber; therefore, oil drainage from the right side of the right well pair should be expected to be low.

In this experiment, two branches of steam injected into the two well pairs were flowing separately through two independent orifices installed in the steam tubing. However, the flow rates from the two sides were very similar for each point of measurement during the experiment. Moreover, it was found the left chamber grew much slower than the right side chamber. Some doubt and concern about the steam measurement accuracy was raised. In reality, these two branches of steam were originally split from one steam pipe which was supplied by the same boiler. Before the test, the steam measurement was also calibrated by comparing the weight for the collection of condensed water and the computer calculation that was based on the differential pressure between entrance to the orifice and exit from the orifice. The cause for these uneven chambers is unclear. One possible reason that has been considered is that the heat gain from the left injector was less than that from the right one. In less than 120 minutes, the temperature at the top on the right side had reached as high as 218 °C. It took the left side about 180 minutes to reach 219 °C. The steam heated up the cold bitumen in the sand pack by means of convection heat, and then condensed to water with low temperature. The mobilized bitumen was then produced from the two producing wells along with solution gas and condensed water. The producing fluid would carry much heat out from the sand pack. Driven to some extent by differential pressure between the two steam chambers, the left side well produced more fluids and carried more energy than that of the right side. Therefore, the left steam chamber grew more slowly than the opposite one.

### ***5.8 Main Mechanisms in Dual Well Pair SAGD***

SAGD operation was such a complicated process with multiple phase flow involved in the porous media. The cold crude oil could not flow at low temperature. The oil was warmed by hot steam, it turned hot. The hot oil and condensed water flowed downward

while the steam and exsolved gas from the live oil traveled upward. Solution gas, with lower viscosity than steam, traveled upward in advance of the injected steam and had an impact on the steam rising and chamber growth. The steam chamber was expected to be impeded by solution gas. Therefore, exsolved gas should be removed from the wells by adjusting the pressure gradient at an earlier stage of the process. Solution gas would eventually stay at the top of the formation if it was not removed from the producing wells on time, and could be considered a natural insulation zone, reducing heat loss to the overburden.

When the steam chambers were mainly going upwards, they also kept spreading sideways slowly. The temperature profiles indicated that the steam front preferentially advanced upwards in the early stage of SAGD process. Then the top boundary limited the continuous growth of the chambers and forced them to grow laterally. The heat loss near the side walls reduced the tendency for the steam front developing sideways. The two steam chambers started to merge at the top middle of the test model at the 280<sup>th</sup> minute of running time. After steam injection was stopped in the right well pair and continued in the left side, the existing warm areas associated to this right pair (the chamber) could be maintained and production continued for an extended period. This was mainly because the area adjacent to the hot chamber was warmed by continuous steam injection from the adjacent well pair.

Comparing the vertical and horizontal steam growth, vertical growth rate was obviously greater than the horizontal. This observation was in agreement with the steam chamber profiles predicted by the analytical and numerical simulation models. As to steam in the porous media, the rate of chamber growth was determined by steam growing in the porous media. The vertical permeability was viewed to be much more critical than the horizontal. Steam was driven upwards with a buoyant force which was associated with the density differential between the steam and the liquid mixture. The high permeability formation provided a greater possibility for allowing faster steam development upwards than in the relatively lower permeability formation.

When the oil in the transition area was warmed up, the oil viscosity in the local area dropped sharply and the oil mobility increased dramatically. With a small pressure differential between the two sides, oil at the top middle of transition region could be

driven from one side to the other. In this physical experiment, it could be seen that the oil at the top middle of transition region was driven from side to side. At around 285<sup>th</sup> minute of running time, communication between two steam chambers was achieved. Once two chambers were connected, the hot steam traveled this top middle area easily. After the right injector was shut in at the 285<sup>th</sup> minute, oil production from the right producer continued until the end of the experiment. Oil production from right producer continued for an extended period due to continuous steam injection from left injector. It was indicative that a portion of the steam injected from the left injector drove oil in the top transition area moving to the right side and produced it through the right producer. This observation demonstrated that the operation strategy of one injection well and two production wells works properly.

Based on the experimental observation in terms of temperature profiles, oil residual profiles and other related data, some main mechanisms were involved in this experiment. Firstly, steam with high temperature was injection into injectors, which reduced oil viscosity dramatically. The oil mobility thus increased greatly. Secondly, movement of oil to the production well was mainly determined by gravity. Based on the fact that the two steam chambers maintained shapes as expected during most of the experiment, it was believed that gravity dominated in the whole recovery process. In spite of the different behaviours of the chamber growth in the early stage of the test, there was no significant impact from testing the lateral drive effect on moving oil from the region between the well pairs before the chambers were connected. Moreover, the tendency of steam was determined by the lateral force which was associated with the differential pressure between the two adjacent wells. The mechanism of steam flooding was considered to be involved to drive the oil from one side to another in a short period just before the two steam chambers communicated.

### ***5.9 Summary of Experimental Approach***

In this experimental approach, an experimentation on a dual well pair model was designed and set up to be able to demonstrate the behaviour and performance of SAGD process through the growth and interference of steam chambers, oil recovery in transition area, and fluid production including oil production, water production, and gas production. The purpose of this experiment was to examine operating strategies and thus improve

SAGD process performance. In the two-dimension lab scale experiment, two operating strategies were tested in the dual well pair model. One was that the production pressure kept variable and some differential pressure existed during the whole experiment; and another one was that one injection well and two production wells after the two steam chambers communicated.

The experiment began with steam initialization between wells, and then regular steam injection into the injection wells. Frequent tuning of the back pressures was done during the experiment to maintain continuous production from both producers. The differential pressure across two well pairs maintained viable. At the 285<sup>th</sup> minute running time, the right side injector was shut-in and the left injector continued. The steam rate for the left side injector was then doubled and was kept steady until the end of the experiment. The whole test was run for 528 minutes. At the end of the test, all the wells of the test model were shut-in immediately. The pressure vessel with the test model was then turned 90° to reduce further vertical movement of the remaining fluid in the test model.

The temperature profiles indicated that the steam front preferentially advanced upwards in the early stage of SAGD process. Then the top boundary limited the continuous growth of the chambers and forced them to grow laterally. In this physical experiment, it could be seen that the oil at the top middle of transition region was driven from one side to another. The two steam chambers started to merge at the top middle of the test model at the 280<sup>th</sup> minute of running time. Comparing the vertical and horizontal steam growth, vertical growth rate was obviously greater than the horizontal. After the right injector was shut in at the 285<sup>th</sup> minute, oil production from the right producer continued until the end of the experiment. The existing warm areas in the right chamber maintained and oil production from right producer continued for an extended period due to continuous steam injection from left injector. It was indicative that a portion of the steam injected from the left injector drove oil in the top transition area moving to the right side and produced it through the right producer. This observation demonstrated that the operation strategy of one injection well and two production wells works properly.

Based on the information and data in the experiment, it was noted that control of differential pressure was a challenge in operating this type of experiment. In this study, the phenomenon that showed the production rate was sensitive to the differential pressure

was obvious. Meanwhile, the fluid production from both producers occasionally experienced choking during the whole experiment. It suggested that more sophisticated pressure control systems/devices and modifications to the test facility should be in need to allow better tuning of back pressures.

The experimental results indicated that residual oil saturation in the region between the well pairs was lower than in the offset regions, suggesting that the operation strategy of sweeping the oil between the two well pairs worked properly.

SAGD operation was such a complicated process with multiple phase flow involved in the porous media. The hot oil and condensed water flowed downward while the steam and exsolved gas traveled upward. Based on the experimental observation in terms of temperature profiles, oil residual profiles and other related data, some main mechanisms involved in this experiment were summarized as the following. Hot steam injection reduced oil viscosity and increased oil mobility dramatically. Gravity mainly dominated the movement of oil to the production well in the whole recovery process. The differential pressure between the two adjacent wells determined the tendency of steam at the top transition region. The mechanism of steam flooding was considered to be involved to drive the oil at the top transition region from one side to another.

## 6 NUMERICAL SIMULATION

Traditional methods of estimating of reservoir performance can be divided into three categories: analogical methods, experimental methods, and mathematical methods. Mathematical models are probably the methods most commonly used by modern petroleum engineers. In numerical models using high speed computers, the mathematical equations solved describe the physical behaviour of the processes in a reservoir used to obtain a numerical solution to reservoir behaviour in the field. In the research and development of reservoir engineering, many models have been used to assist reservoir engineers in understanding the oil world underground and to forecast reservoir performance. Both physical models and mathematical models play a vital role in petroleum engineering.

The main advantage of a reservoir simulator is the ability to inexpensively forecast reservoir performance under a variety of different operating conditions. Reservoir simulation uses physics, mathematics, reservoir engineering, and computer programming to develop a tool for predicting hydrocarbon reservoir performance under various operating conditions. Thus, the optimum strategy for producing the reservoir can be determined without equipment investment and without actually producing any oil.

The two-dimension lab scale experiment investigated the impact of operating strategies on the dual well pair SAGD model and demonstrated the behaviour and performance of SAGD process through the growth and interference of steam chambers, oil recovery in transition area, and fluid production such as oil production and gas production. However,

the advantages of the behaviour and performance of the SAGD process operated with these strategies over the conventional ones have not examined and determined yet. There are two options that can be chosen from. The conventional operating strategies can be run and tested either in another lab scale experiment with the similar parametrical conditions or in a verified numerical model which matched the historical results in the experiment. An economical choice and solution definitely goes to the numerical simulation. History matching the experiment conducted will help generalize the dual well pairs SAGD behaviour and performance to test the conventional operating strategies in the simulation model. Moreover, the impact of the interference from adjacent chambers, solution gas and other operating variables on the SAGD performance can be investigated as well to understand the key mechanisms of oil recovery in multiple well pair SAGD process.

Better understanding the key mechanisms of heavy oil recovery is a step towards maximizing productivity with a minimum level of steam injection and a minimum number of infill wells drilled. Numerical simulation will be carried out for the two 2-D lab-scale experiment that has been conducted to investigate the operating strategy on multiple well pair SAGD process.

The objective of the numerical simulation is to identify the mechanisms involved in the multiple well pair SAGD process and thus investigate the impact of different operating strategies on SAGD performance. In this study, a verified numerical model is used to predict and assess the performance of a dual well pair SAGD process under a variety of operating.

### ***6.1 Model Initialization***

Numerical history matching of the dual well pair SAGD lab test results was conducted to validate the numerical model and to study the mechanisms and performance of the multiple well pairs SAGD process. The STARS simulator, by Computer Modeling Group, was used in this study. Before the numerical simulation began, some parametric factors were initialized. This included grid block set up, initial sand packing conditions, and assumptions.

### 6.1.1 Grid Block

A two dimension Cartesian grid was built for simulating the experimental test in the test cell. A grid system of  $160 \times 1 \times 24$  as shown in Figure 6-1 was used in the numerical model to represent the test model 160 cm in length, 24 cm in height, and 10 cm thick, which results in a two dimensional grid block. There are a total of 3,840 grid blocks with 24 vertical layers in this simulation. The total 3840 blocks were distributed in 160 blocks in the 'i' direction, 1 block in the 'j' direction and 24 blocks in the 'k' direction. Each block has a length of 1 cm in 'i' and 'k' directions, and 10 cm in 'j' direction.

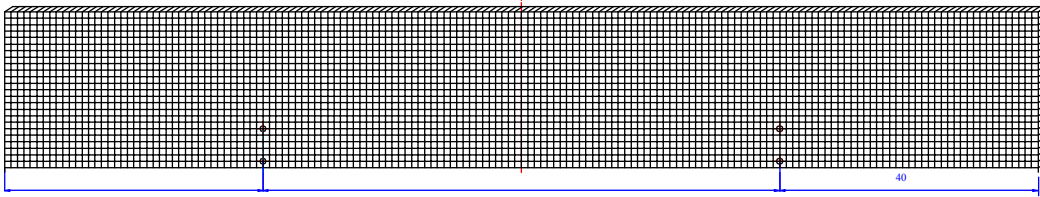


**FIGURE 6-1 GRID BLOCK SETTING IN THE NUMERICAL SIMULATION**

Eight SAGD wells located in the blocks are showed in Table 6-1. The block number in 'i' direction went from left to right, and in 'k' direction went downward. The wells 2, 3, 6, and 7 were shut in after the steam initialization period; however it is necessary to simulate the recirculation steam at the beginning of the test.

**TABLE 6-1 WELL NAME AND LOCATION IN THE GRID**

Well (#)	Well Name	Blocks		
		<i>i</i>	<i>j</i>	<i>k</i>
1	Injector_Left	40	1	18
2	Injector_Left as Producer	40	1	18
3	Producer_Left as Injector	40	1	23
4	Producer_Left	40	1	23
5	Injector_Right	120	1	18
6	Injector_Right as Producer	120	1	18
7	Producer_Right as Injector	120	1	23
8	Producer_Right	120	1	23

### 6.1.2 Initial Condition and Fluid Properties

The key initial conditions of the sand packing are listed in [Table 6-2](#). The numerical model was mainly based on these conditions.

**TABLE 6-2 INITIAL CONDITION IN  
EXPERIMENTAL AND  
NUMERICAL SIMULATION**

Oil: Burnt Lake Bitumen	
Temperature (°C)	21.0
Pressure, (kPa)	2236
Initial Water Saturation, $S_{wi}$ (%)	10.4
Initial Oil Saturation, $S_{oi}$ (%)	89.6
GOR (std m <sup>3</sup> / m <sup>3</sup> )	6.45
Pore Volume, $V_p$ (cm <sup>3</sup> )	13,751
Porosity, $\Phi$ (%)	33.3
Horizontal Permeability, $K_H$ (Darcy)	80
Vertical Permeability, $K_V$ (Darcy)	80

The viscosity of dead bitumen was measured and shown as a function of temperature in [Figure 6-2](#). As the sand used had high permeability, capillary pressure was expected to be insignificant and, hence, was neglected. The relative permeability curves of the water-oil system and gas-liquid system used in the numerical simulation model are shown in [Figure 6-3](#) and [Figure 6-4](#), respectively. The properties of rock and fluid are summarized in [Table 6-3](#) and [Table 6-4](#). All these data are based on previous experimental tests carried out in a single SAGD well pair model at the HOOS laboratory in the Alberta Research Council.

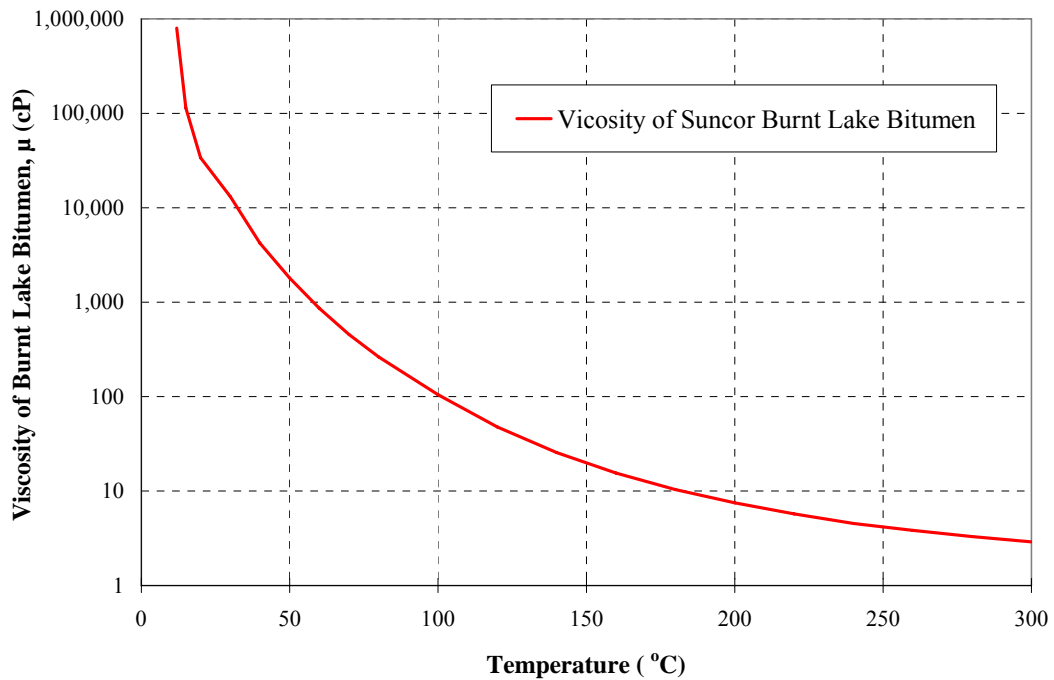


**FIGURE 6-2 OIL VISCOSITIES VERUS TEMPERATURE**

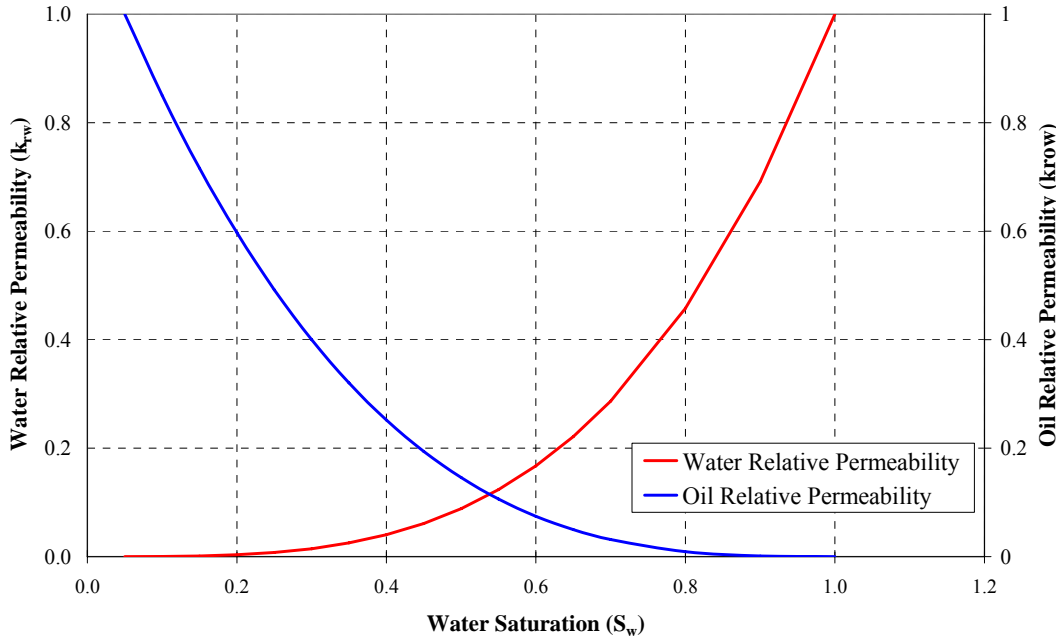


**FIGURE 6-3 WATER AND OIL RELATIVE PERMEABILITY FOR NUMERICAL SIMULATION**

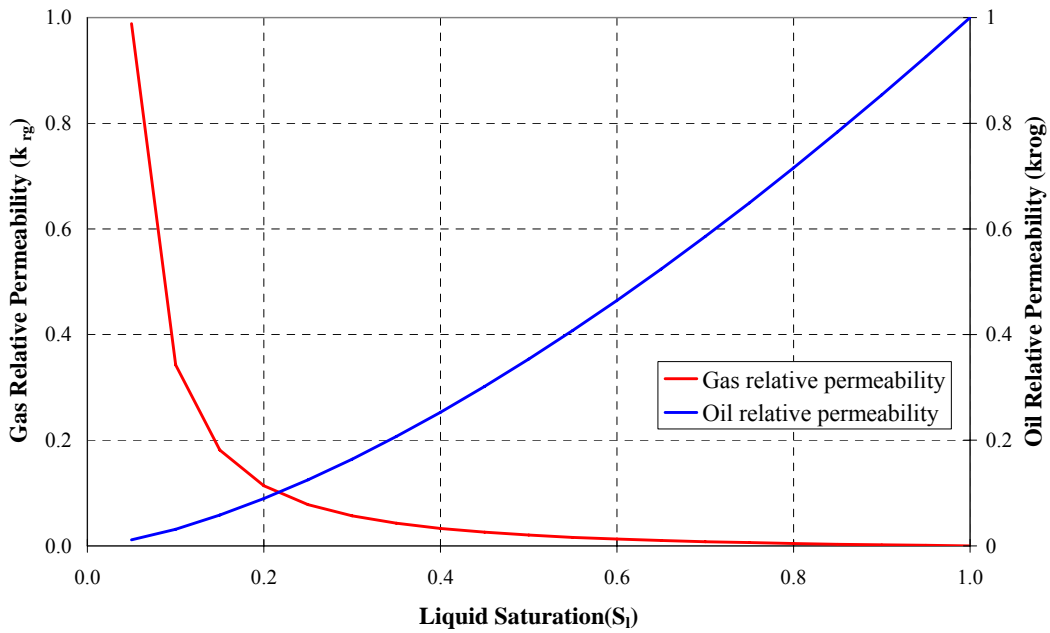


**FIGURE 6-4 GAS-OIL RELATIVE PERMEABILITY FOR NUMERICAL SIMULATION**

**TABLE 6-3 THERMAL CONDUCTIVITIES USED IN THE NUMERICAL MODEL**

Property	Units	Value
Volumetric Heat Capacity Of Solid Formation (Rock)	J/cm <sup>3</sup> -C	2.35
Thermal Conductivity Of Reservoir Rock	J/cm-min-C	2.5833
Thermal Conductivity Of The Water Phase	J/cm-min-C	0.3715
Thermal Conductivity Of The Oil Phase	J/cm-min-C	0.07986
Thermal Conductivity Of The Gas Phase	J/cm-min-C	9.72×10 <sup>-04</sup>

**TABLE 6-4 FLUID PROPERTIES USED IN THE NUMERICAL MODEL**

Property	Units	Water	Dead Oil	Methane
Molecular Weight	kg/gmol	CMG STARS Default Setting	0.52334	0.01604
Liquid Molecular Density @ 101.3 kPa, 20 <sup>0</sup> C	gmol/cm <sup>3</sup>		1.903×10 <sup>-3</sup>	61.93×10 <sup>-3</sup>
Critical Pressure	kPa		1360.0	4596
Critical Temperature	<sup>0</sup> C		624.65	-82.7
Thermal Expansion Coefficient	1/ <sup>0</sup> C	CMG STARS Default Setting	8.0×10 <sup>-4</sup>	0
Coefficients In Liquid Heat Capacity Correlation	J/gmol- <sup>0</sup> C	76.21	1060	29.2
Reference Pressure	kPa	101.325		
Reference Temperature	<sup>0</sup> C	20.0		
Coefficient In The Correlation For Gas-Liquid K Value	kPa	CMG STARS Default Setting	0	3.96×10 <sup>5</sup>
	<sup>0</sup> C		0	-879.84
	<sup>0</sup> C		0	-265.99

### **6.1.3 Assumptions**

The following assumptions were made in the numerical simulation model.

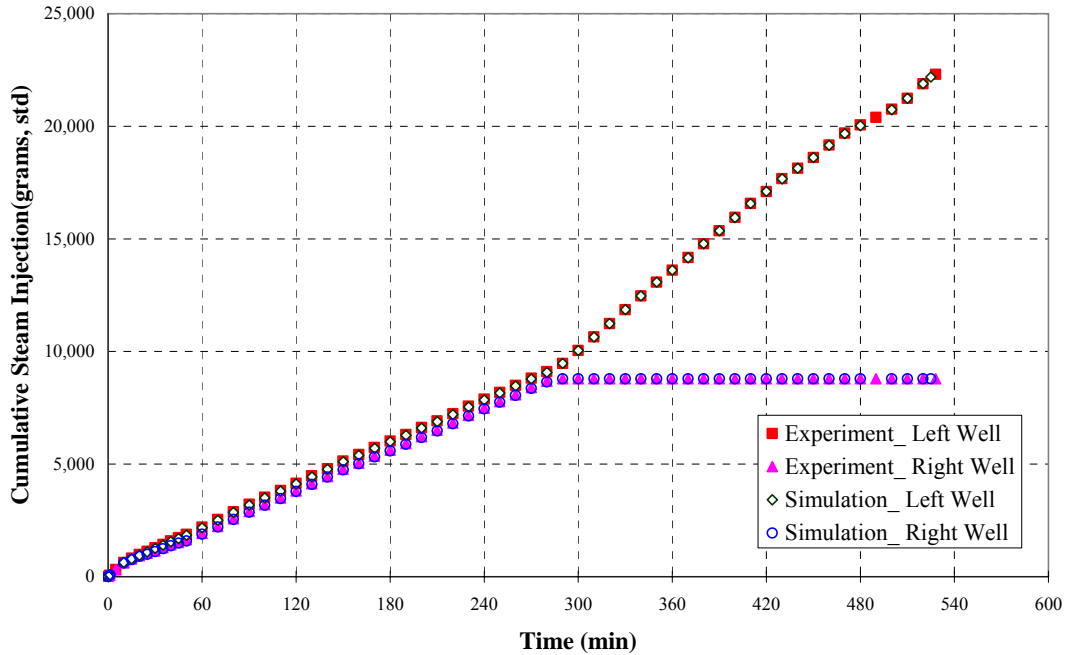
- Homogenous porosity distribution
- Uniform initial water saturation distribution
- Uniform initial oil saturation distribution
- Capillary pressure neglected

### ***6.2 Tuning Parameters***

History matching parameters in this study were fluids production, including cumulative oil, gas, and water production, and steam chamber patterns. Since the experiment was completed under a controlled steam injection rate and controlled bottom hole pressure at the producer wells, these two parameters were treated as input variables for history matching simulation.

Steam injection rates are the average experimental values over a five minute period and are shown in the [Figure 6-5](#), which illustrates that the input steam injection rates are a perfect match to the experimental rates. In other words, the amount of steam injection into both injectors in the experiment was equal to that in the numerical model.

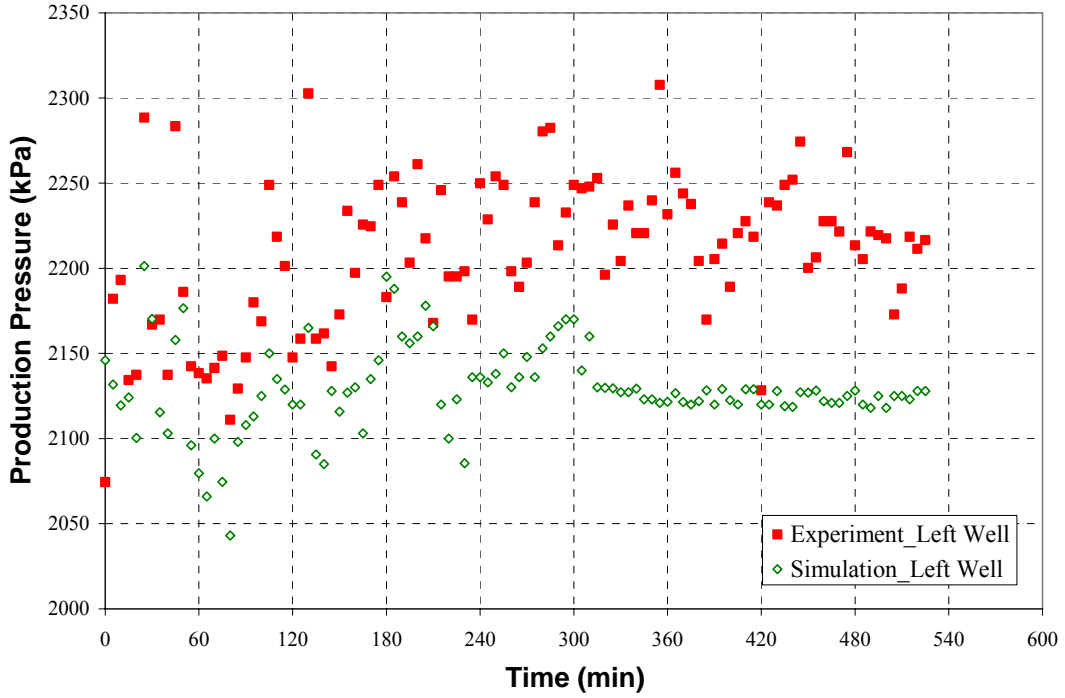
To achieve the history match, various parameters were modified including production pressures of both producers, and heat loss. The pressure transducers were located some distance away from the production and injection wells. Therefore, the pressure readings are believed to not exactly reflect what happened in the wells. In fact, there was some pressure drop from the production well to the pressure transducer, especially in the case when multiple phase fluids existed in the system. Adjustments on both sides were made to achieve a successful history match.



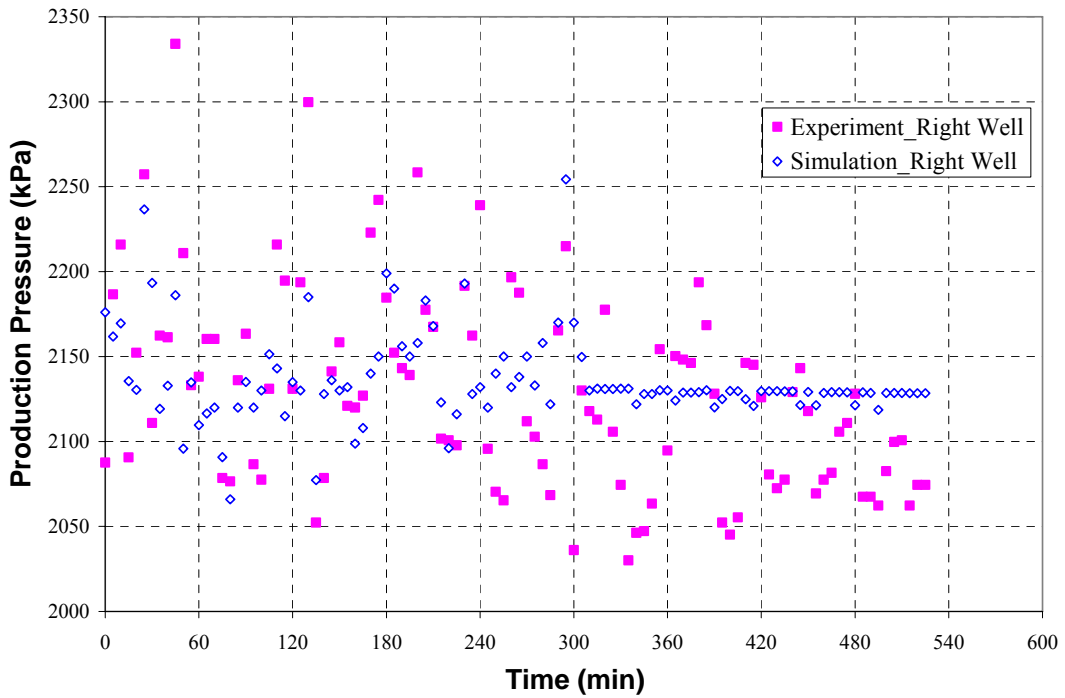
**FIGURE 6-5 CUMULATIVE STEAM INJECTION IN THE EXPERIMENT AND NUMERICAL SIMULATION**

Figure 6-6 and 6-7 compare the production pressure in the experiment with one in the simulation model in the left producer well and right producer well, respectively. Both figures show some difference between the measured pressures in the experiment and the input parameters in the simulation. However, it can be noted that the input pressures reasonably followed the trend of the measured production pressures.

As described above, there were many deliberate insulation blankets and plywood pieces covering the model during the test. Even so, big heat loss could not be avoided. Figure 6-8 displays the temperature change during the whole experiment. In this numerical simulation the heat loss was calculated according to the heat transfer coefficients and the exposed area. The multiplier can be treated as an overall convective heat transfer coefficient to represent heat loss. The heat loss in one grid block was associated with the ambient temperature, and it decreased with the rising ambient temperature. However, the overall heat loss in the whole test model was still quite big due to the increasing exposed size with the growth of steam chamber. The adjustment of this overall multiplier was determined based on trial and experience.



**FIGURE 6-6 BOTTOM HOLE PRESSURES IN THE LEFT SIDE OF THE EXPERIMENT AND NUMERICAL SIMULATION**



**FIGURE 6-7 BOTTOM HOLE PRESSURES IN THE RIGHT SIDE OF THE EXPERIMENT AND NUMERICAL SIMULATION**

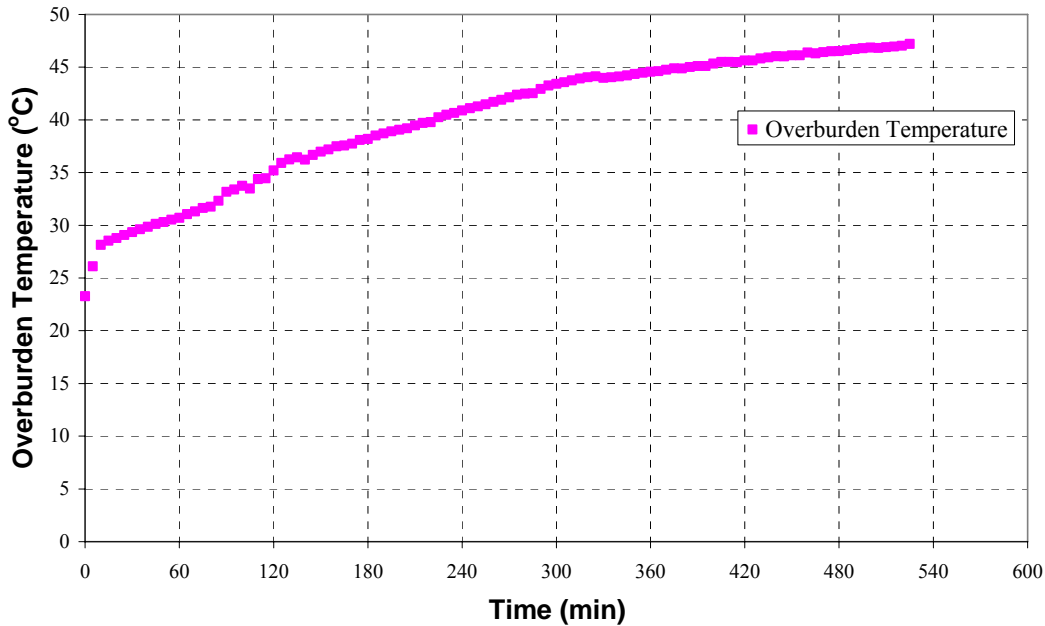


**FIGURE 6-8 AMBIENT TEMPERATURE IN THE EXPERIMENT AND NUMERICAL SIMULATION**

### ***6.3 Numerical History Matching Results***

A successful history match was obtained. The numerically generated fluids production curves including cumulative oil, water, and gas production are shown in [Figures 6-9, 6-10, and 6-11](#) respectively. There was reasonable agreement between the numerical simulation and the historical data from the experiment. The amount of oil from the left producer in the simulation was slightly more than that after the 360<sup>th</sup> running minute in the experiment. The left production well produced a bit less water in the simulation than that in the experiment after the 240<sup>th</sup> running time; however, the other producer generated greater amounts of water in the simulation than that of the experiment.

Compared with water and oil, gas had lower viscosity at the same temperature, which resulted in being more sensitive to the variation of operating pressures and differential pressures across both well pairs. It is surprising that the gas production fluctuated both in the experiment and in the history match shown in the [Figure 6-11](#).

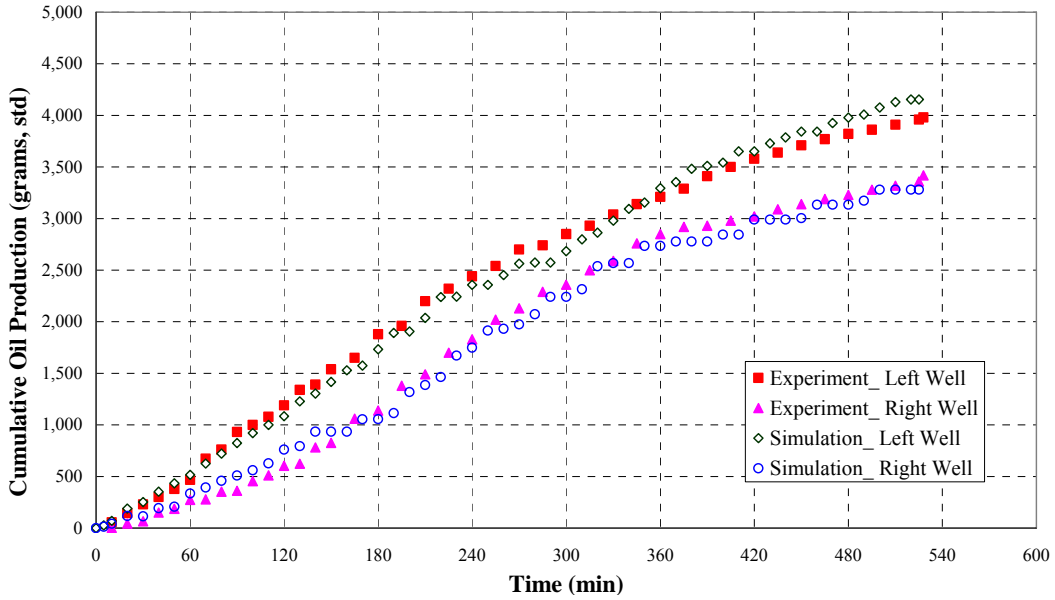


**FIGURE 6-9 SIMULATION RESULT: COMPARISON OF CUMULATIVE OIL PRODUCTION IN THE EXPERIMENT AND NUMERICAL SIMULATION**

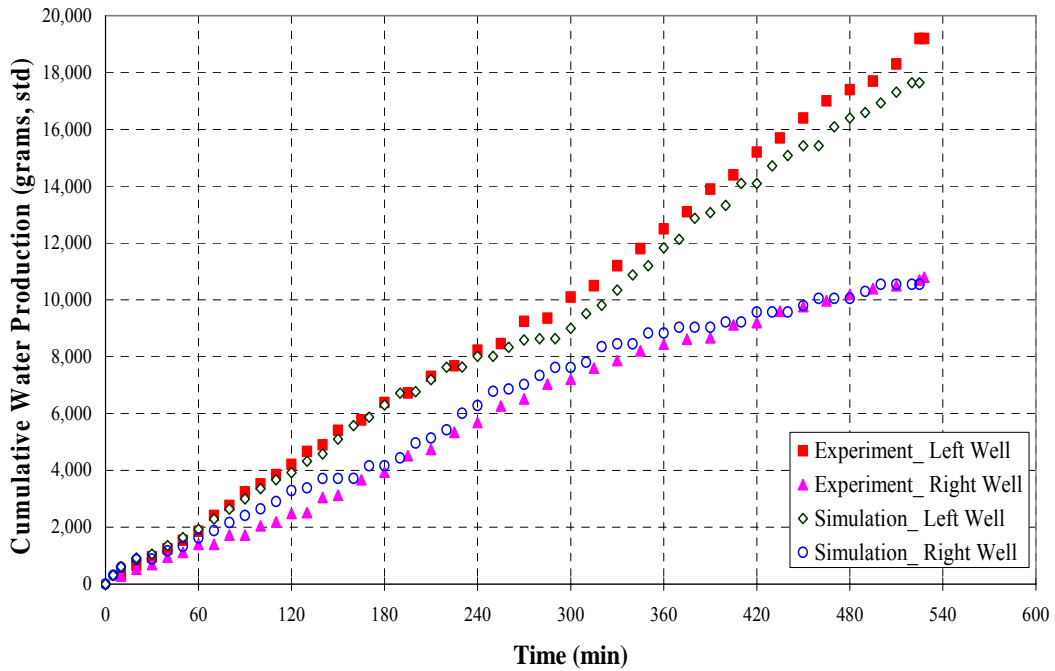


**FIGURE 6-10 SIMULATION RESULT: COMPARISON OF CUMULATIVE WATER PRODUCTION IN THE EXPERIMENT AND NUMERICAL SIMULATION**

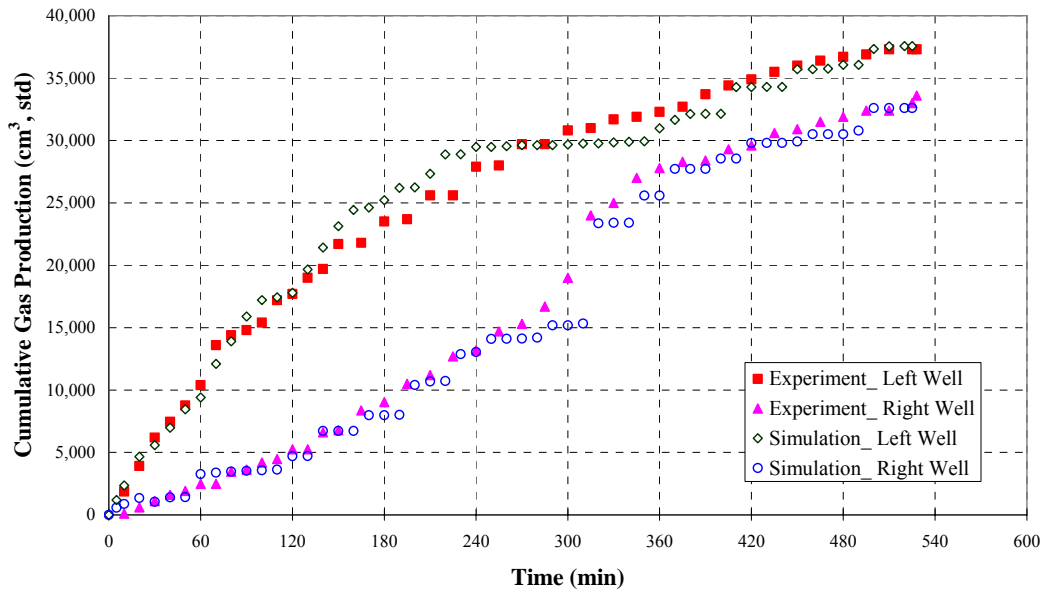


**FIGURE 6-11 SIMULATION RESULT: COMPARISON OF CUMULATIVE GAS PRODUCTION IN THE EXPERIMENT AND NUMERICAL SIMULATION**

An attempt to match steam chamber patterns was made. Figures 6-12 to 6-20 show the comparison of the simulated and the measured temperature contour in the dual-well-pair SAGD test with Burnt Lake bitumen at the 60<sup>th</sup>, 120<sup>th</sup>, 240<sup>th</sup>, 300<sup>th</sup>, 360<sup>th</sup>, 420<sup>th</sup>, 480<sup>th</sup>, and 527<sup>th</sup> minute, respectively. It is noted from these comparisons that the test results were reasonably matched well by the numerical simulation, although some deviation between simulation and real results for the steam chamber still existed.

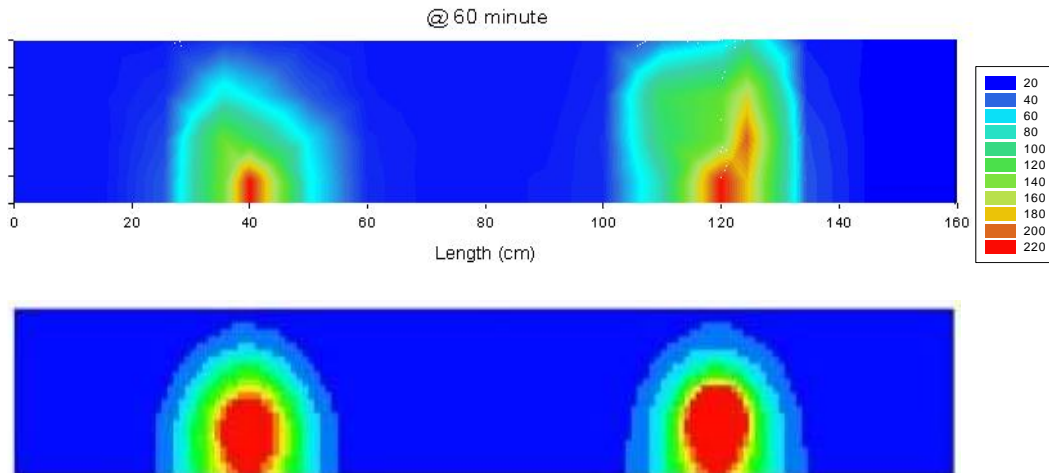


**FIGURE 6-12 SIMULATION RESULT: COMPARISON OF STEAM CHAMBER IN THE EXPERIMENT (TOP) AND NUMERICAL SIMULATION (BOTTOM) AT THE 60<sup>TH</sup> MINUTE**

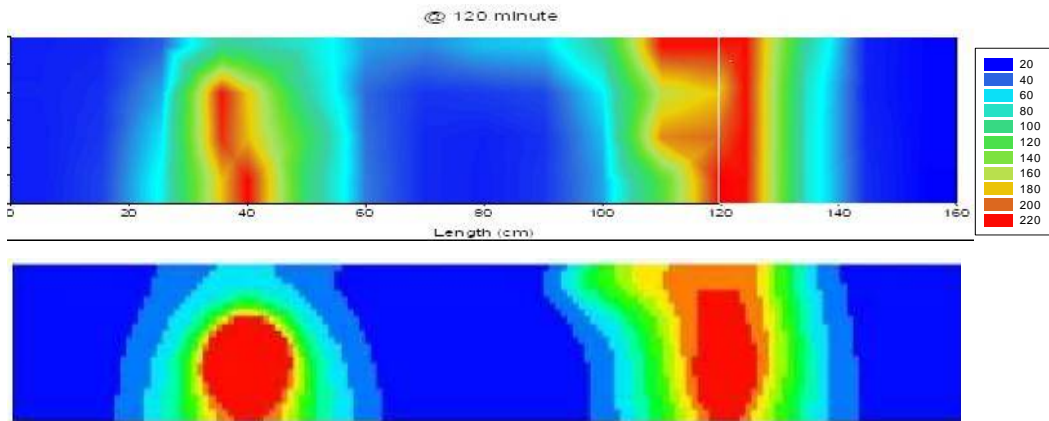


**FIGURE 6-13 SIMULATION RESULT: COMPARISON OF STEAM CHAMBER IN THE EXPERIMENT (TOP) AND NUMERICAL SIMULATION (BOTTOM) AT THE 120<sup>TH</sup> MINUTE**

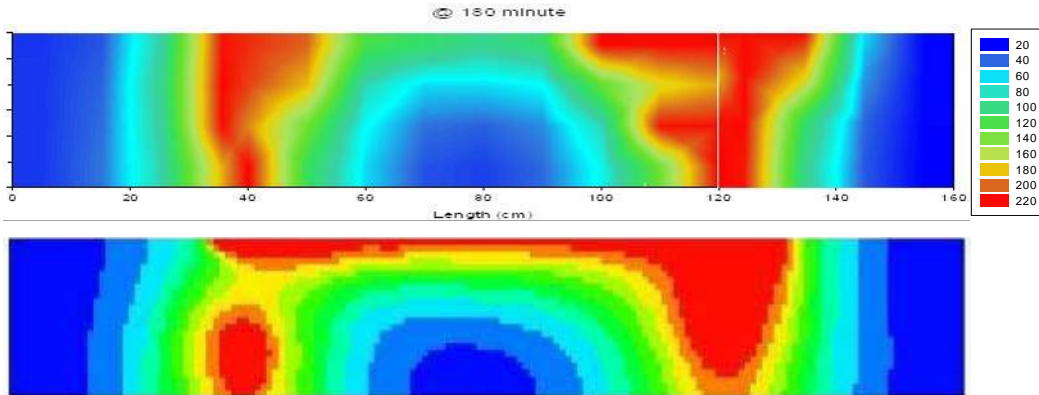


**FIGURE 6-14 SIMULATION RESULT: COMPARISON OF STEAM CHAMBER IN THE EXPERIMENT (TOP) AND NUMERICAL SIMULATION (BOTTOM) AT THE 180<sup>TH</sup> MINUTE**

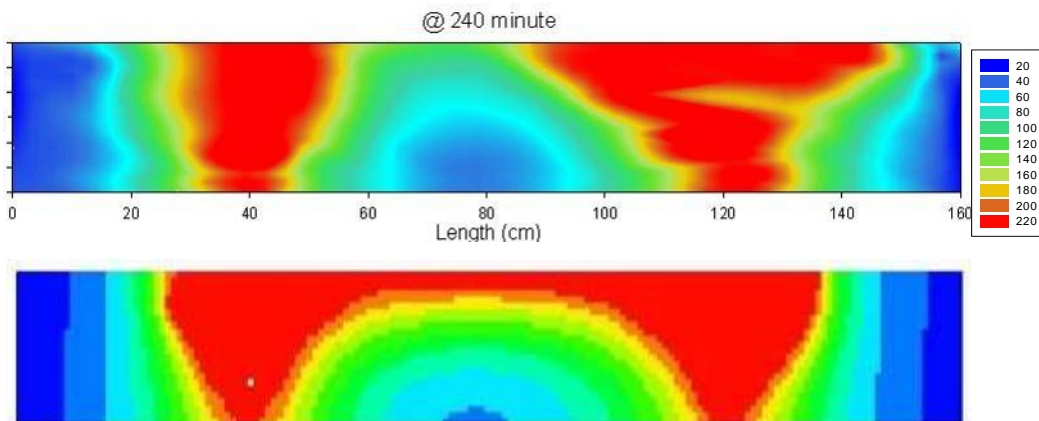


**FIGURE 6-15 SIMULATION RESULT: COMPARISON OF STEAM CHAMBER IN THE EXPERIMENT (TOP) AND NUMERICAL SIMULATION (BOTTOM) AT THE 240<sup>TH</sup> MINUTE**

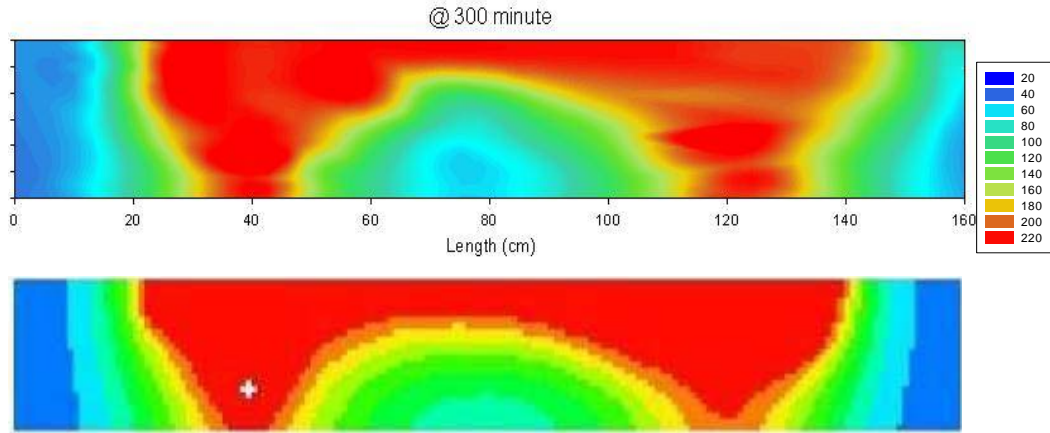


**FIGURE 6-16 SIMULATION RESULT: COMPARISON OF STEAM CHAMBER IN THE EXPERIMENT (TOP) AND NUMERICAL SIMULATION (BOTTOM) AT THE 300<sup>TH</sup> MINUTE**

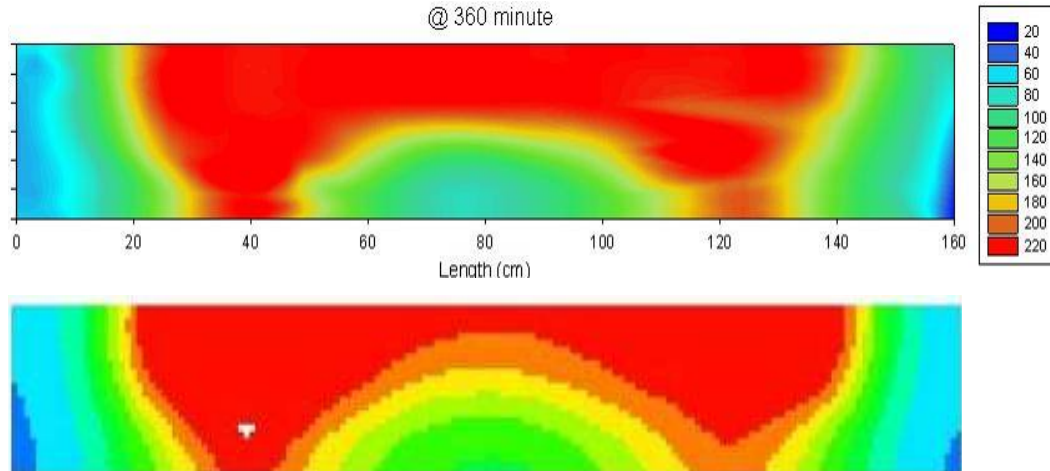


**FIGURE 6-17 SIMULATION RESULT: COMPARISON OF STEAM CHAMBER IN THE EXPERIMENT (TOP) AND NUMERICAL SIMULATION (BOTTOM) AT THE 360<sup>TH</sup> MINUTE**

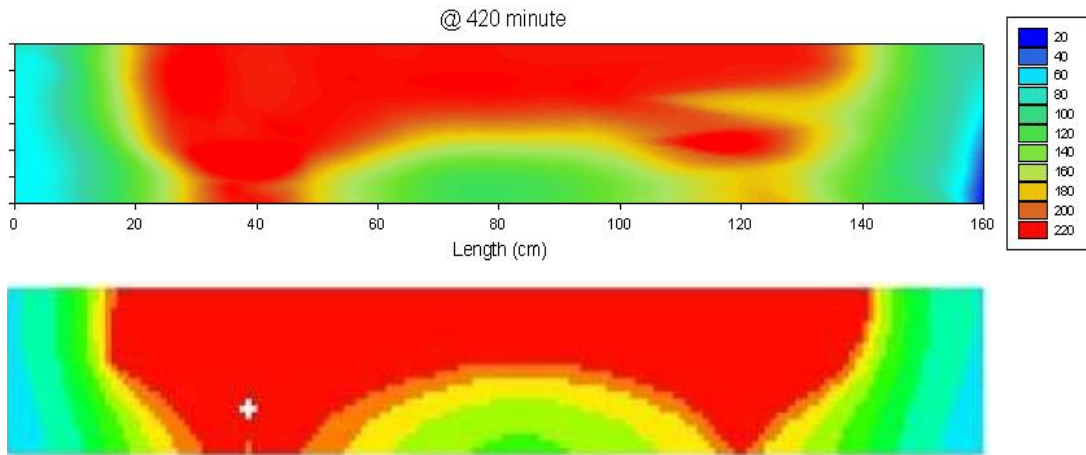


**FIGURE 6-18 SIMULATION RESULT: COMPARISON OF STEAM CHAMBER IN THE EXPERIMENT (TOP) AND NUMERICAL SIMULATION (BOTTOM) AT THE 420<sup>TH</sup> MINUTE**

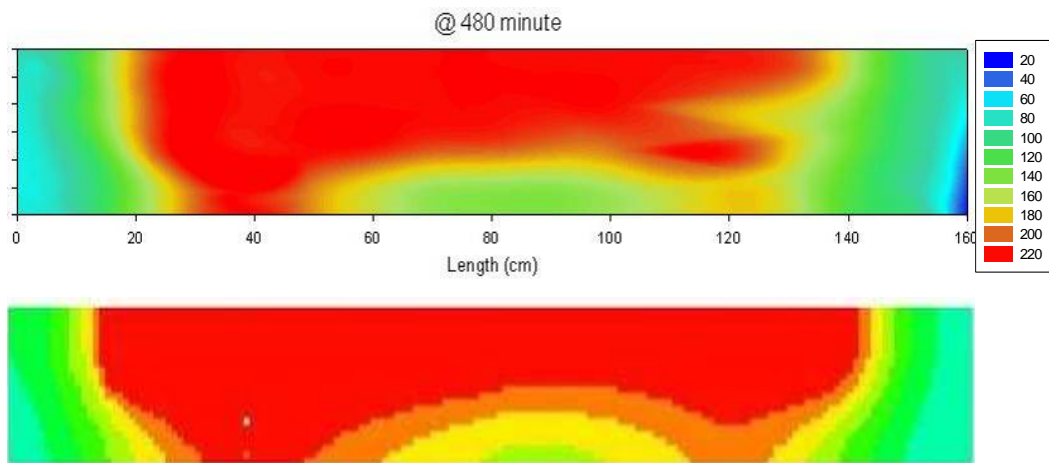


**FIGURE 6-19 SIMULATION RESULT: COMPARISON OF STEAM CHAMBER IN THE EXPERIMENT (TOP) AND NUMERICAL SIMULATION (BOTTOM) AT THE 480<sup>TH</sup> MINUTE**

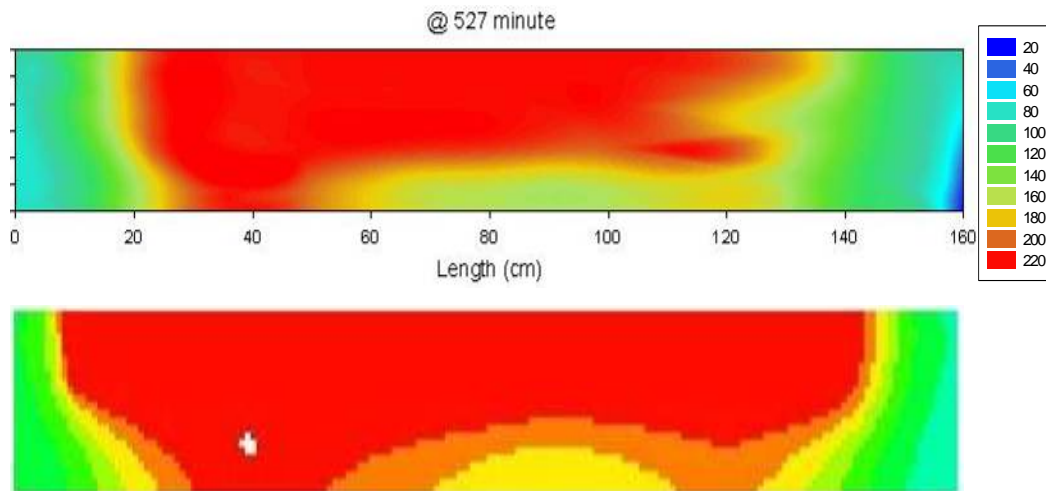


**FIGURE 6-20 SIMULATION RESULT: COMPARISON OF STEAM CHAMBER IN THE EXPERIMENT (TOP) AND NUMERICAL SIMULATION (BOTTOM) AT THE 527<sup>TH</sup> MINUTE**

The steam chamber growth in the simulation was slightly faster than that in the real physical experiment due to an over prediction in temperatures at both wells. The temperatures from the simulation at the right side of the sand pack were rising faster than that from the left side. Therefore, the left side of steam chamber was slowly growing upwards and moving further away. A large amount of energy gained from the injected steam might be pushed back from the left side. Large amounts of fluids production from the left side producer brought large amounts of energy back to the producer. Bitumen was cooled and plugged the flow paths when it flowed into a cold zone.

It can be noted that through matching the historical production (oil, water, and gas) and steam chamber patterns, the experimental results were matched reasonably well. With this verified numerical model, the performance and behaviour of dual well pair SAGD can be evaluated through investigating the impact of differential pressure between steam chambers and the impact of different steam injection scheme on fluid production and steam chamber profiles.

## 6.4 Operating Strategy Analysis

Based on the numerical model verified from the history match, the operating strategy on SAGD performance can be examined. In the following study, three operating strategies shown in Table 6-5 were investigated.

**TABLE 6-5 STRATEGY STUDY - THREE CASES OF OPERATING STRATEGIES**

Case	Operating Strategy		
	Production	Steam Injection	
	Bottom Hole Pressure	Injection Scheme	Quantity
A	Variable pressure: ~ 2130kPa; and $\Delta P \sim 7.3$ kPa	0~285min: same steam injection rate for both injectors; After 285min: right injector shut-in and double steam injection rate for left injector	Left:22,305g Right:8,791g
B	Fixed production pressure 2130kPa; and $\Delta P=0$ kPa	0~528min: Continuous steam injection from both injector at same rate	Left:15,548g Right:15,548g
C	Fixed production pressure 2130kPa; and $\Delta P=0$ kPa	0~285min: same steam injection rate for both injectors; After 285min: right injector shut-in and double steam injection rate for left injector	Left:22,305g Right:8,791g

### **6.4.1 Description of Operating Strategies**

Case A represented the scenario of the numerical simulation results which reasonably well matched the historical production and steam chamber patterns in the experiment. The production pressure was varying during the whole 528 minutes running time with averaged operating production pressure of 2130kPa. The differential pressure across both well pairs was fluctuating as well. In the first 285 minutes, same steam injection rate was for both injectors. However, the right injector was shut in and double steam injection rate was for left injector after 285 minutes. Totally, 31,096 grams of steam were injected into both injection wells in 528 minutes running time, which averaged as around 29.5 grams of steam per minute injected from each individual injector.

Case B represented the scenario operated at a fixed operating production pressure of 2130kPa and averaged steam injection rate of 29.5 grams per minute from the beginning of the run to the end of the run. Therefore, totally 31,096 grams of steam were uniformly injected into both injection wells in 528 minutes running time, of which 15,548 grams of steam were injected from the left injector and right injector respectively.

Case C represented the scenario operated at a fixed operating production pressure of 2130kPa. Therefore, the differential pressure across both well pairs was zero in the whole 528 minutes running time. The same steam injection strategy as Case A was executed in this scenario. Therefore, 31,096 grams of steam were injected into both injection, of which 22,305 grams of steam was injected from the left side injected in 528 minutes and 8,791 grams from the right side in the first 285 minutes.

### **6.4.2 Comparison of Process Performance**

Figure 6-21 shows the simulated profiles of cumulative oil productions under three operating strategies including the physical experimental results.

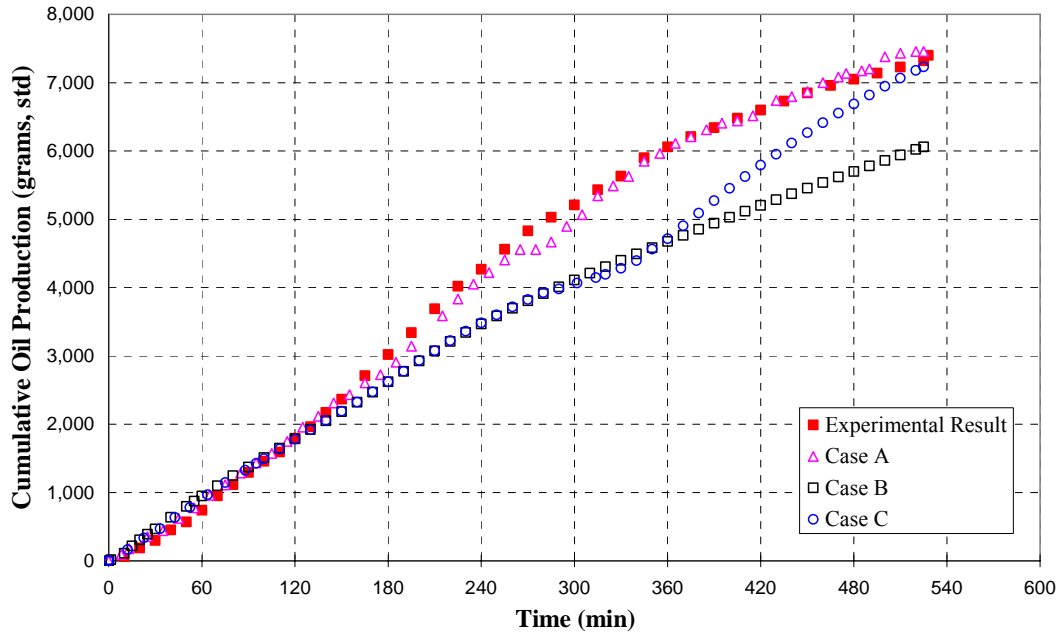


**FIGURE 6-21 SIMULATION RESULT: COMPARISON OF CUMULATIVE OIL PRODUCTION BASED ON NUMERICAL MODEL**

It is noticeable that sand pack produced more cumulative oil in Case A during the SAGD operation after the 150<sup>th</sup> minute with the operating strategy used in the physical experiment. The final cumulative oil production by the strategies of Case C was approaching the historical result at the end of experiment. However, the final oil recovery under the Case B was quite lower than that of the previous two cases. It is obvious that the operating strategy with Case A recovered oil faster and had a shorter pay back period than the other two.

Figure 6-22 shows the simulated profiles of cumulative gas production under the same circumstance except for different operation strategies. It is obvious that the sand pack would produce less cumulative gas if the production pressure was maintained unchanged in Case C during the whole process than in the historical match Case A, which was under the variable production pressure and differential pressure. There was significant gas production on the right producer due to steam injection from the left injector, which resulted in a big jump on the cumulative production at the 285<sup>th</sup> of running time in the Case C. Even so, Case A still produced quite more gas than the other two cases did by the end of operating process. Operated with the similar operating strategy as the

conventional one used in current commercial SAGD operation, Case B produced the least gas in these three operating strategies.

Figure 6-23 indicates that the cumulative steam amount injected into both left and right injectors were almost the same in three cases and in the experiment.

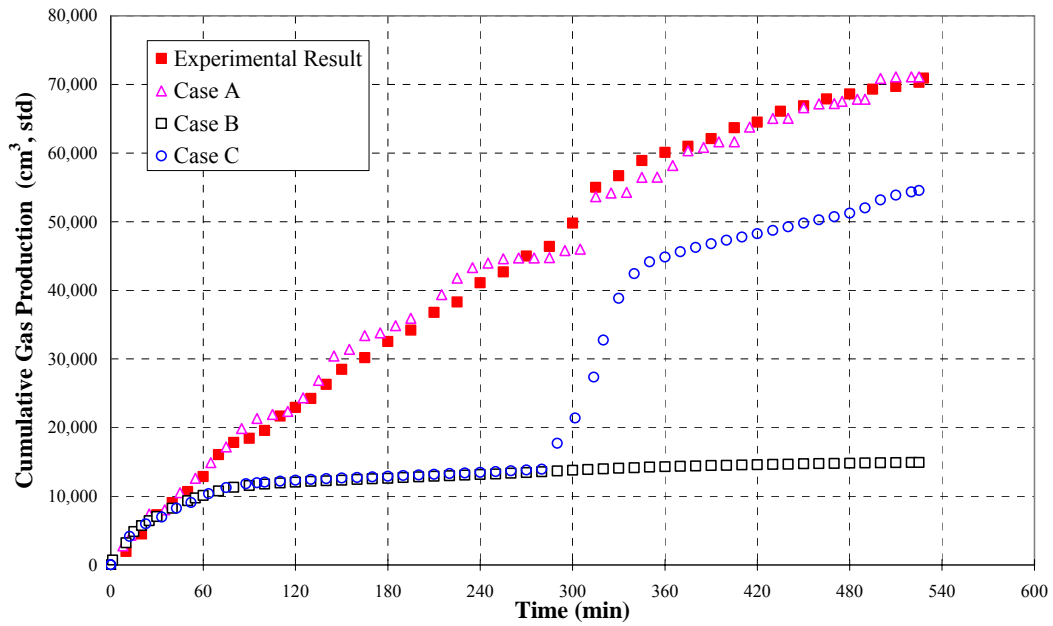


**FIGURE 6-22 SIMULATION RESULT: COMPARISON OF CUMULATIVE GAS PRODUCTION BASED ON NUMERICAL MODEL**

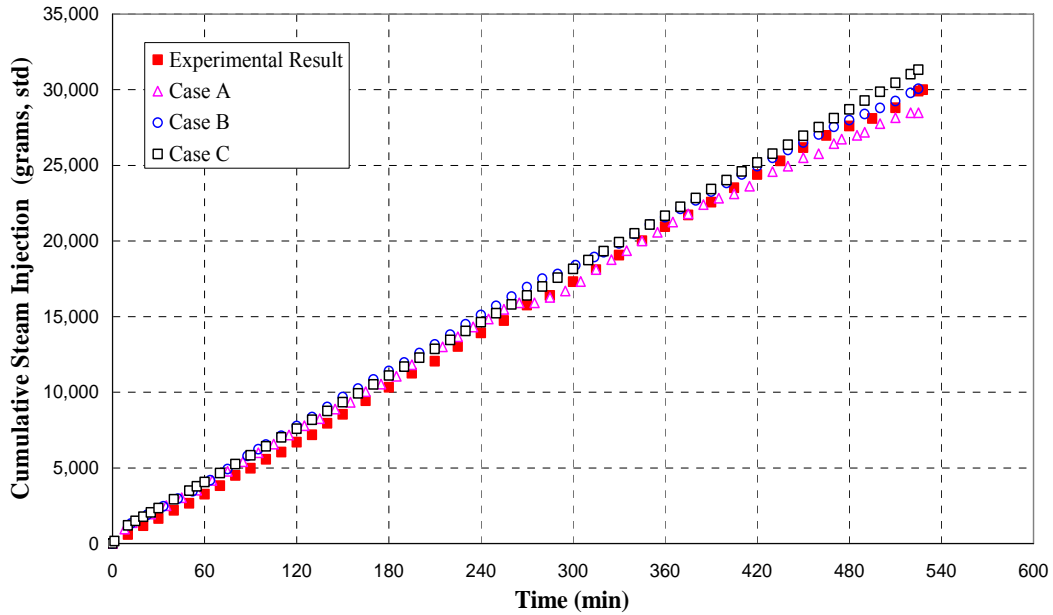
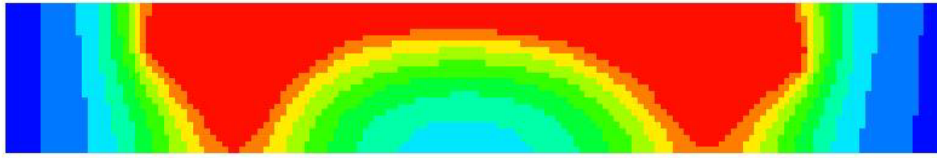


**FIGURE 6-23 SIMULATION RESULT: COMPARISON OF CUMULATIVE STEAM INJECTION**

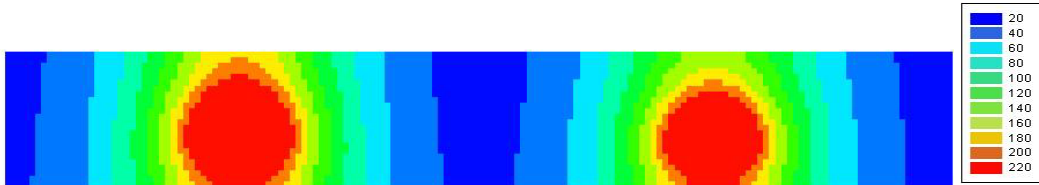
### 6.4.3 Analysis and Discussion

The cause for so much difference in the oil production has been considered to be due to the variation of production pressure, existing of differential pressure across the well pairs, and the role of solution gas in the sand pack.

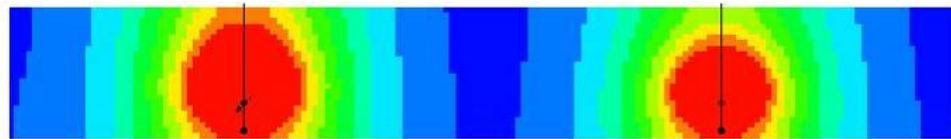
With varied production pressure and certain differential pressure across both well pairs in Case A, steam chamber was developed much faster than with a fixed production pressure and zero differential pressure. Figure 6-24 compare three steam chambers at the time of 270<sup>th</sup> minute. Compared with the temperature, both the left and right steam chambers in Case B and C are much smaller and grow slower than in Case A at the 270<sup>th</sup> minute. It can be noted that the oil sands in the top-middle area had been quite hot in Case A, however it was still very cold in both Case B and Case C.



Case A



Case B



Case C

**FIGURE 6-24 COMPARISON OF EMERGING STEAM CHAMBERS AT THE 270<sup>TH</sup> MINUTE OF RUNING TIME**

In case A, driven by differential pressure across both well pairs, the left steam chamber and the right steam chamber had merged for some period of time. However, it would take a long time to get the left chamber to communicate with the right one in Case B and C as Figure 6-24 predicted. The accumulated gas, which could not be produced in time, would affect the chamber growth and eventually result in less oil production. The exsolved gas would move in front of the steam and stay at the top of the sand pack might reduce heat loss to the overburden; however, the impact on the energy saving could not override the energy loss carried by the production fluids from the wells.

In the experiment carried out in the test cell, the production wells were operated through back pressure regulators which adjusted and controlled production fluids. Solution gas could be produced more from either the left side or the right side, and hence the steam chambers could grow smoothly. When the production pressure in the sand pack declined below the live oil saturation pressure or the temperature in the reservoir rose over the

saturation temperature due to steam, the solution gas dissolved from the live oil and rose to the top of the sand pack. The solution gas couldn't be produced from the producer resulting from a lack of pressure gradient in the sand pack.

To further illustrate the effect of solution gas on oil production, a cross-sectional distribution of properties was plotted. The rising gas moved in front of the steam chamber and impeded chamber growth. [Figure 6-25](#) show the simulated profiles of gas saturation at the 270<sup>th</sup> minute based on the matched numerical model.

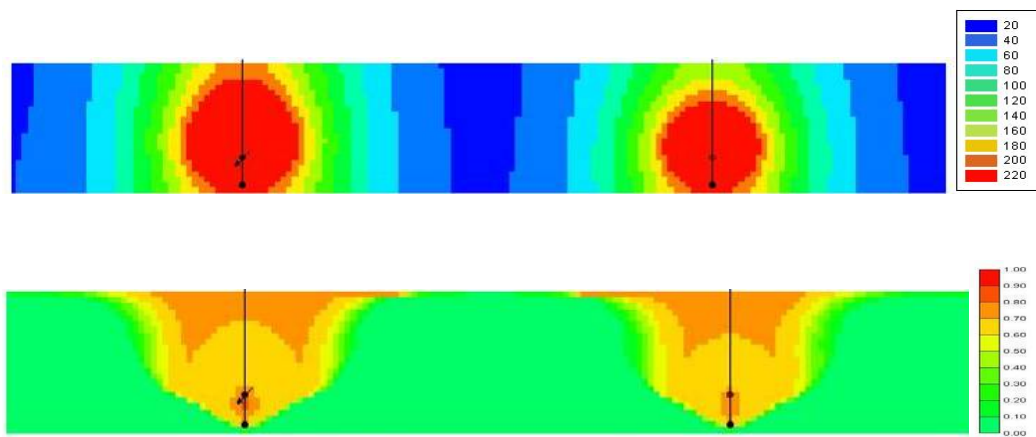


**FIGURE 6-25 TOP: STEAM CHAMBER AT THE 270TH MINUTE IN CASE C; BOTTOM: GAS SATURATION PROFILE AT THE 270TH MINUTE IN CASE C**

## ***6.5 Summary of Numerical Simulation Study***

In this numerical simulation study, a numerical model was verified through history matching with a thermal simulator CMG STARS. The numerical model with a grid block of  $160 \times 24 \times 1$ , represented the test model 160 cm in length, 24 cm in height, and 10cm in width. The steam injection rates were treated as input variables for history matching simulation. Tuning parameters include production pressures of both producers, and heat loss.

The numerical simulation matched reasonably well experimental results, including the oil production, gas production, water production, and steam chamber patterns. Therefore, the numerical model captured main and key mechanisms of the dual well pairs experiment.

In the numerical simulation study, three cases of operating strategies were examined for the behaviour and performance of each process. Case A represented the scenario of the numerical simulation results which matched the experimental history. The production pressure and the differential pressure were varying during the whole 528 minutes of running time. In the first 285 minutes, same steam injection rate was for both injectors. However, the right injector was shut in and double steam injection rate was for the left injector after 285 minutes. Case B represented the process operated at a fixed production pressure and steam injection rate during the whole experiment. Case C represented the scenario operated at a fixed production pressure and the differential pressure across both well pairs being zero in the whole experiment. The same steam injection strategy as Case A was executed in this scenario.

The numerical simulation results showed that the SAGD process operated with strategies of Case A performed the best. In Case A, steam chamber communication was accelerated; gas production was enhanced; and oil production was improved. Two operating strategies were involved in Case A: one was that the production pressure kept variable and some differential pressure existed during the whole experiment; and another one was that one injection well and two production wells after the two steam chambers communicated.

Based on the verified numerical model, the study showed that the amount of gas produced from the wells was mainly determined from the pressure gradient between the core pressure of the sand packing and production well pressure. It was essential that the production pressure was adjusted to keep viable to generate some differential pressure across the two well pairs, and gas was encouraged to be removed on time. The study of operating strategy indicated that the same amount of steam injection resulted in quite different oil production from one case to another; the cause most likely came from the operating strategies. It is obvious that such operating strategy as steam injection into one injector while producing from both producers could sweep the oil in the transition region. This operating strategy could not only recover oil fast comparing with the conventional operating strategy, but also improve ultimate oil recovery.

## 7 SUMMARY

SAGD performance is directly tied to natural conditions such as formation characteristics, and imposed conditions such as well configuration, initialization strategies, and operational strategies. This research study included experimental approach and numerical approach on the multiple well pairs SAGD to improve process performance. Operating strategies were investigated in the dual well pair model and in a verified numerical model, respectively.

In this experimental approach, an experimentation on a dual well pair model was designed and set up to be able to demonstrate the behaviour and performance of SAGD process through the growth and interference of steam chambers, oil recovery in transition area, and fluid production. The purpose of this two-dimension lab scale experiment was to examine the impact of operating strategies on multiple well pairs and thus explore proper operating strategies to improve SAGD process performance. In the experiment, two operating schemes were tested in the dual well pair model. One was that the production pressure kept variable and some differential pressure existed during the whole experiment; and another one was that one injection well and two production wells after the two steam chambers communicated.

The temperature profiles indicated that the steam front preferentially advanced upwards in the early stage of SAGD process. Then the top boundary limited the continuous growth of the chambers and forced them to grow laterally. The two steam chambers started to merge at the top middle of the test model at around the 280<sup>th</sup> minute of running time.

Comparing the vertical and horizontal steam growth, vertical growth rate was obviously greater than the horizontal. After the right injector was shut in at the 285<sup>th</sup> minute, oil production from the right producer continued until the end of the experiment. The existing warm areas in the right chamber maintained and oil production from right producer continued for an extended period due to continuous steam injection from the left injector. It was indicative that a portion of the steam injected from the left injector drove oil in the top transition area moving to the right side and produced it through the right producer. This observation demonstrated that the operation strategy of one injection well and two production wells works properly.

The experimental results indicated that residual oil saturation in the region between the well pairs was lower than in the offset regions, suggesting that the operation strategy of sweeping the oil between the two well pairs worked well by tuning the production pressure. It was indicative that the oil in the transition region could be swept with high oil recovery by applying these operating strategies after the adjacent steam chambers merged.

Through the observation from the experiment, it can be concluded that SAGD was such a complicated process with multiple phase flow involved in the porous media, and with many mechanisms involved in the oil recovery process. The hot oil and condensed water flowed downward while the steam and exsolved gas traveled upward. Hot steam injection reduced oil viscosity and increased oil mobility dramatically. Gravity mainly dominated the movement of oil to the production well in the whole recovery process. The differential pressure between the two adjacent wells determined the tendency of steam at the top transition region. The mechanism of steam flooding was considered to be involved to drive the oil at the top transition region from one side to another.

A numerical model was verified through matching the historical experimental results. The numerical simulation matched reasonably well experimental results, including the oil production, gas production, water production, and steam chamber patterns. Therefore, the numerical model captured main mechanisms of the dual well pairs experiment.

Based on the verified numerical model, the study of the impact of operating strategies on the behaviour and performance of dual well pair SAGD process was completed. The study showed that the negative impact of solution gas on the chamber growth could be

reduced. Local solution gas could be produced either from the nearest production well or from the adjacent one. The study also indicated that the existence of differential pressure between adjacent well pairs could enhance gas production after the steam chambers were in communication.

The numerical simulation study suggested that more oil could be produced with the same amount of steam injected in the same specific time span if proper operation strategies were applied to the dual well pair SAGD process. The numerical simulation study showed that communication between two well pairs could be accelerated by applying differential pressure across two well pairs; and gas production could be enhanced. In the meanwhile, oil production enhancement was accompanied with the increasing gas production. The overall process performance was therefore improved. These operating strategies included that the production pressure kept variable and some differential pressure existed during the whole experiment; and one injection well and two production wells after the two steam chambers communicated.

## 8 BIBLIOGRAPHY

Alberta Energy and Utilities Board, “*EUB ST98-2007: Alberta’s Energy Reserves 2006 and Supply/Demand Outlook 2007-2016*,” June 2007, p.2-2.

Albahlani, A.M. and Babadagli, T.: (2008), “*A Critical Review of the Status of SAGD: Where Are We and What is Next?*” SPE113283.

Asquez H, A R. et al.: (1999), “*Mechanical and Thermal Properties of Unconsolidated Sands and Its Applications to the Heavy Oil SAGD Project in the Tia Juana Field, Venezuela*,” SPE54009.

Bagci, A.S., Olushola, S. and Mackay, E.: (2008), “*Performance Analysis of SAGD Wind-Down Process with CO<sub>2</sub> Injection*,” SPE113234.

Belgrave, J.D.M., Nzekwu, B. and Chhina, H.S.: (2007), “*SAGD Optimization with Air Injection*,” SPE 106901.

Birrell, G.: (2003), “*Heat Transfer Ahead of a SAGD Steam Chamber: A Study of Thermocouple Data from Phase B of the Underground Test Facility (Dover Project)*,” JCPT Vol.42, No.3, p.40-47.

Birrel, G.E.: (2005), "*Cyclic SAGD-Economic Implications of Manipulating Steam Injection Rates in SAGD Projects – Re-Examination of the Dover Project*," JCPT Vol.34, No 4, p54-58.

Butler, R., Stephens, D.J.: (1981), "*The Gravity Drainage of Steam –heated Heavy Oil to Parallel Horizontal Wells*," JCPT 1981-02-01.

Butler, R.: (1982), "*Method for Continuously Producing Viscous Hydrocarbons by Gravity Drainage While Injecting Heated Fluids*," Patent CA 1130201, Issued: 1982-08-24 (22), Filed: 1979-07-10.

Butler, R.: (1987), "*Rise of Interfering Steam Chambers*," JCPT May-June 1987.

Butler, R. M.: (1991), "*Thermal Recovery of Oil and Bitumen*," Prentice Hall Inc., New Jersey: Prentice Hall, pp.528.

Butter, R.: (1997), "*The Steam and Gas Push (SAGP)*," Petroleum Society of CIM Paper No.97-137.

Butler, R., (1998), "*SAGD Comes of AGE*," JCPT V37, No.7, p.9-12.

Butler, R.: (2001), "*Some Recent Developments in SAGD*," JCPT Vol. 40, No. 1, p.18-22.

Butler, R., Yee, C.T.: (2002), "*Progress in the in Situ Recovery of Heavy Oils and Bitumen*," JCPT Vol.41, No.1, p.31-40.

Canbolat, S., Akin, S. and Polikar, M.: (2004), "*Evaluation of SAGD Performance in the Presence of Non-Condensable Gases*," CIPC Paper No.2004-222.

Cardwell Jr., W.T. and Parsons, R.L.: (1949), "*Gravity Drainage Theory*," AIME, Vol.179, 1949, p.199-215.

Chan, M Y S. Fong, J. and Leshchyshyn, T.: (1997), "*Effects of Well Placement and Critical Operating Conditions on the Performance of Dual-Well-Pair SAGD Well Pairs in Heavy Oil Reservoir*," SPE-39082.

Chhina, Harbir Singh: (1998), “*Convective Heating Startup for Heavy Oil Recovery*,” [Patent] CA 2241478, Issued: 1999-12-23, Filed: 1999-06-23.

Cyr, T. Coates, R. and Polikar, M.: (1999), “*Steam-Assisted Gravity Drainage Heavy Oil Recovery Process*,” [Patent] Can. 2,277,378, C.9/24/2002, F.7/8/1999 (Appl.2, 277,378).

Deng, X., Escobar, E., Heck, G., Beaulieu, G., Yuan, J., Huang, H. and Makarowski, K.: (2007), “*Multiple Well Strategies for Improving SAGD Performance – Dual-Well-Pair SAGD Experiments Part I: Baseline Test with MacKay River Oil*,” AACI Report #0708-3, April, 2007.

Ding, M. and Whale, L. A.: (2006), “*History Match of the 1993 ESAGD Pilot Performance in the Peace River Reservoir*,” 1st Petroleum Society CIM World Heavy Oil Conference (Beijing, China, 11/12-15/2006), Paper No.2006-552.

Donnelly, J.K.: (1998), “*Who Invented Gravity?*” JCPT Vol.37, No.9, p.19-21.

Dykstra, H., (1978), “*The Prediction of Oil Recovery by Gravity Drainage*,” SPE 6548.

Edmunds, N., Haston, J. A. and Cordell, G.M.: (1989), “*Alberta Science and Research Authority*,” Patent CA 1304287, Issued: 1992-06-30 (22), Filed: 1989-06-28.

Edmunds, N.: (1994), “*Review of Phase A SAGD Test*,” SPE 21529.

Edmunds, N.R., Suggett, J.C.: (1995), “*Design of a Commercial SAGD Heavy Oil Project*,” SPE30277.

Farouq-Ali, S M.: (1997), “*Is There Life after SAGD?*” JCPT Vol.36, No.6, p.20-24.

Gates, I.D., Kenny, J., Hernandez, I.L. and Bunio, G.L.: (2005), “*Steam-Injection Strategy and Energetics of Steam-Assisted Gravity Drainage*,” SPE 97742.

Goobie, L M A., Good, W K.: (1994), "*Peace River Horizontal Well Demonstration Project - A Test of the Enhanced Steam Assisted Gravity Drainage Process,*" Petroleum Society of CIM Paper No.1994-41.

Hamm, R.A. and Ong, T.S.: (1995), "*Enhanced Steam-Assisted Gravity Drainage: A New Horizontal Well Recovery Process for Peace River, Canada,*" JCPT Vol.44, No.1, p.33-40.

Hang, F., Zhang, L., Han, B., and Yu, L.: (2006) "*Test of the Application of Steam Assisted Gravity Drainage in the Super Heavy-Oil Development in Liaohe Oilfield,*" 1st Petroleum Society CIM World Heavy Oil Conference (Beijing, China, 11/12-15/2006), Paper No.2006-643.

Ito, Y., Hirata, T. and Ichikawa, M.: (2004), "*The Effect of Operating Pressure on the Growth of the Steam Chamber Detected at the Hangingstone SAGD Project,*" JCPT Vol.43, No.1, p.47-53.

Ito, Y. and Ipek, G.: (2005), "*Steam-Fingering Phenomenon during SAGD Process,*" SPE 97729.

Ito, Y. Ipek: (2006), "*Field Observation of Steam Fingering Phenomenon,*" 1st Petroleum Society CIM World Heavy Oil Conference (Beijing, China, 11/12-15/2006, Paper No.2006-421.

Jespersen, P.J. and Fontaine, T.J.C.: (1993), "*The Tangleflags North Pilot--- A Horizontal Well Steamflood,*" JCPT 93-05-05, p.52-57.

Jiang, Q., Butler, R. and Yee, C.-T.: (1998), "*The Steam and Gas Push (SAGP)-2: Mechanism Analysis and Physical Model Testing,*" Petroleum Society of CIM Paper No. 98-43.

Kisman, K. E. and Yeung, K. C.: (1995), "*Numerical Study of the SAGD Process in the Burnt Lake Oil Sands Lease,*" SPE 30276.

Komery, D P. Good, W K. Luhning, R W. and Pearce, J V., (1998), "*Pilot Testing of Post-Steam Bitumen Recovery from Mature SAGD Wells in Canada*," 7th UNITAR Heavy Crude & Tar Sands Int. Conf. (Beijing, China, 10/27-30/1998), Proc., Paper No.1998-214.

Miller, K.A. and Xiao, Y.: (2008), "*Improving the Performance of Classic SAGD with Offsetting Vertical Producers*," JCPT Vol.47, No.2, p.22-27.

Mukherjee, N J. Gittins, S D. Edmunds, N R. and Kisman, K E A.: (1995), "*Comparison of Field Versus Forecast Performance for Phase B Of the UTF SAGD Project in the Athabasca Oil Sands*," 6th Unitar Et Al. Heavy Crude & Tar Sands Int. Conf. (Houston, 2/12-17/95) Proc. Vol.1, p.581-595.

Nasr, T.N., Golbeck, H., Korpany, G. and Pierce, G.: (1998), "*SAGD Operating Strategies*," SPE 50411.

O'Rourke, J.C.: (1997), "*UTF Project Status Update May 1997*," CIM Paper No.1997-08.

Polikar, M., Cyr, T.J. and Coates, R.M.: (2000), "*Fast-SAGD: Half the Wells and 30% Less Steam*," SPE 65509.

Pujol L. and Boberg T.C.: (1972), "*Scaling Accuracy of Laboratory Steam Flooding Models*," SPE 4191.

Puttagunta, V.R., Singh, B. and Miadonye, A.: (1993), "*Correlation of Bitumen Viscosity with Temperature and Pressure*," Canadian Journal of Chemical Engineering, 71, June p.447-450.

Rose, P E. and Deo, M.D.: (1994), "*New Algorithms for Steam Assisted Gravity Drainage Using Combinations of Vertical and Horizontal Wells*," Kentucky Univ. & US Doe East. Oil Shale Symp. (Lexington, Ky, 11/16-19/93) Proc., p.232-240.

Sadler, K. and Davis, P.: (2005), "*In-Situ Bitumen Overview and Activity Update in the Province of Alberta*," SPE 97800.

Sasaki, K., Akibayashi, S. Kato, K. and Ono, K.: (1998), “*A New Concept of Enhanced SAGD Process by Adding Intermittent Steam-Stimulation on Lower Horizontal Production-Well (SAGD-Isstw)*,” 15th World Petrol. Congr. (Beijing, China, 10/12-16/1997) Proc. Vol.2, p.511-513.

Sedae Sola, B. and Rashidi, F.: (2006), “*Application of the SAGD to an Iranian Carbonate Heavy-Oil Reservoir*,” SPE-100533.

Shamila, A., Shirif, E., Dong, M. and Henni, A.: (2005), “*A Chamber Volume/Size Estimation for SAGD Process from Horizontal Well Testing*,” CIPC Paper No. 2005-075.

Shin, H. and Polikar, M.: (2005), “*Optimizing the SAGD Process in Three Major Canadian Oil-Sands Areas*,” SPE 95754.

Shin, H. and Polikar, M.: (2007), “*Review of Reservoir Parameters to Optimize SAGD and Fast-SAGD Operating Conditions*,” JCPT Vol.46, No.1, Pp.35-41.

Stalder, J. L.: (2005), “*Cross SAGD (XSAGD)—an Accelerated Bitumen Recovery Alternative*,” SPE-97647.

Vanegas Prada, J.W. and Cunha, L.B. and Alhanati, F.J.S.: (2005), “*Impact of Operational Parameters and Reservoir Variables during the Start-up Phase of a SAGD Process*,” SPE 97918.

Yang, C. Card, C. Nghiem, L.: (2007), “*Economic Optimization and Uncertainty Assessment of Commercial SAGD Operations*,” CIPC Paper No. 2007-029.

Yang, G. and Butler, R.: (1992), “*Effects of Reservoir Heterogeneities on Heavy Oil Recovery by Steam Assisted Gravity Drainage*,” JCPT Vol.31, No.8, p.37-43.

Yee, C. T. and Spargo, R., (2001), “*Wind-Down of A Mature SAGD Steam Chamber at the Dover Project (Formerly UTF)*,” 8th SPE/Cim Petrol. Soc. Horizontal Well Technol. Conf. (Calgary, Alberta, 11/7/2001).

Yee, C T. and STROICH, A.: (2004), "*Flue Gas Injection into a Mature SAGD Steam Chamber at the Dover Project (Formerly UTF)*," JCPT Vol.43, No.1, p.54-61.

Yuan, J.-Y., Huang, H., Mintz, R., Wang, X., Jossy, C. and Tunny, C.: (2004), "*Wet Electric Heating for Starting Up SAGD/VAPEX*," CIPC Paper No.2004-130.

Zhao, L. and Law, D.H.-S., Nasr, T.N., Coates, R., Golbeck, H., Beaulieu, G., Heck, G.: (2005), "*SAGD Wind-Down: Lab Test and Simulation*," JCPT Vol.44, No.1, p.49-53.